Assessing the role of arousal state in sensorimotor gating and memory consolidation

Dissertation

zur Erlangung des Grades eines
Doktors der Naturwissenschaften

der Mathematisch-Naturwissenschaftlichen Fakultät
und
der Medizinischen Fakultät
der Eberhard-Karls-Universität Tübingen

vorgelegt
von

Mingyu Yang
aus Hebei, China

2020

Tag der mündlichen Prüfung: 29.November.2021

Dekan der Math.-Nat. Fakultät: Prof. Dr. Thilo Stehle
Dekan der Medizinischen Fakultät: Prof. Dr. Bernd Pichler

1. Berichterstatter: Prof. Dr. Nikos Logothetis

2. Berichterstatter: Prof. Dr. Steffen Gais

Prüfungskommission: Prof. Dr. Nikos Logothetis

Prof. Dr. Steffen Gais

Prof. Dr. Andrea Burgalossi

Prof. Dr. Markus Siegel

Erklärung / Declaration:

Ich erkläre, dass ich die zur Promotion eingereichte Arbeit mit dem Titel:

„ Assessing the role of arousal state in sensorimotor gating and memory consolidation “

selbständig verfasst, nur die angegebenen Quellen und Hilfsmittel benutzt und wörtlich oder inhaltlich übernommene Stellen als solche gekennzeichnet habe. Ich versichere an Eides statt, dass diese Angaben wahr sind und dass ich nichts verschwiegen habe. Mir ist be- kannt, dass die falsche Abgabe einer Versicherung an Eides statt mit Freiheitsstrafe bis zu drei Jahren oder mit Geldstrafe bestraft wird.

I hereby declare that I have produced the work entitled "Assessing the role of arousal state in sensorimotor gating and memory consolidation" , submitted for the award of a doctorate, on my own (without external help), have used only the sources and aids indicated and have marked passages included from other works, whether verbatim or in content, as such. I swear upon oath that these statements are true and that I have not concealed anything. I am aware that making a false declaration under oath is punishable by a term of imprisonment of up to three years or by a fine.

Tübingen, den ....

Datum / Date Unterschrift /Signature

Contents

Abbreviations 4
Keywords 4
Acknowledgments 5
1. Summary/ Abstract 7
2. Synopsis 9
2.1 Introduction 9
2.1.1 General Remarks 9
2.1.2 Neural oscillations underlying different brain states 10
2.1.2.1 Slow oscillation 11
2.1.2.2 Sleep spindles 12
2.1.2.3 Sharp wave-ripple 13
2.1.2.6 Neural oscillation coupling for information transfer 14
2.1.3 LC-NA system 15
2.1.3.1. Role of the LC in tuning arousal 15
2.1.3.2. Modulatory action of the LC on sensory processing 16
2.1.3.3. Modulatory action of the LC on synaptic plasticity and memory formation in the hippocampus 17
2.1.4 Mediodorsal thalamus 18
2.1.4.1 Role of the MD in working memory 19
2.1.4.2 Role of the MD in memory consolidation 20
2.2 Introduction to manuscripts 21
2.2.1 Manuscript 1: Phasic activation of the locus coeruleus attenuates the acoustic startle response via increasing cortical arousal 21
2.2.2 Manuscript 2: The locus coeruleus activity during hippocampal-cortical communication 23
2.2.3 Manuscript 3: Occurrence of hippocampal ripples is associated with activity suppression in the mediodorsal thalamic nucleus 25
2.3 Discussions 27
2.3.1 Modulation of sensorimotor gating via an increased cortical arousal 27
2.3.2 Coordinated neuronal activity during awake and sleep SPW-Rs 28
2.3.3 Limitations and future investigations 30

2.4 References 32

2.5 List of manuscripts/papers and statement of contributions 44

Abbreviations

ACC	Anterior cingulate cortex
ASR	Acoustic startle response
BOLD	Blood oxygen-level dependent
CA1	Cornu ammonis field 1
CA3	Cornu ammonis field 3
CNS	Central nervous system
CRN	Cochlear root neuron
EEG	Electroencephalogram
EMG	Electromyography
GABA	Gamma-aminobutyric acid
IC	Inferior colliculus
LC	Locus coeruleus
LDTg	Lateral dorsal tegmental nucleus
LFP	Local field potential
LTD	Long-term depression
LTP	Long-term potentiation
MD	Mediodorsal thalamus
mPFC	Medial prefrontal cortex
MUA	Multi-unit activity
NA	Noradrenaline
NREM	Non-rapid eye movement
REM	Rapid eye movement
SPW-R	Sharp wave-ripple
TRN	Thalamic reticular nucleus
PFC	Prefrontal cortex
PnC	Caudal pontine reticular nucleus
PPI	Prepulse inhibition
PPTg	Pedunculopontine tegmental nucleus
SC	Superior Colliculus
SO	Slow oscillation

Keywords

Arousal, Memory consolidation, Prepulse inhibition, Locus coeruleus, Sharp-wave ripple, Sleep spindle, Mediodorsal thalamus

Acknowledgments

First and foremost, I would like to thank my parents for their endless love and care. Thank you for always supporting my chosen path, understanding me, and cheering me up in difficult situations. You powered me with the confidence and courage to go through all the ups and downs in my life. I would also like to thank my brother for always being there for me, sharing life, and giving enlightening advice on life and career.

I want to thank my mentors, Oxana Eschenko and Nikos Logothetis, for their guidance, support, and encouragement, as well as for their intellectual contributions to my Ph.D. work and development as a scientist. Both have taught me how to design and conduct a research project and the presentation and communication of scientific work. Their wisdom and guidance helped me a lot through this long journey.

I sincerely thank my committee members, Steffen Gais and Andrea Burgalossi, for their encouragement, time, and valuable critiques in the previous advisory board meetings.

I would like to thank my previous lab members, Silvia and Ricardo, who helped with the experimental skills when I started my Ph.D. I also want to send my special thanks to the colleagues and friends in the department for the scientific discussions, random discussions, jokes, food, drinks, and many other things. Thank you, Alireza, Anna, Elena, Ernesto, Hao, Kaidi, Leonid, Masa, Rui, Ryo, and Shervin. I would also like to thank Ryo Iwai, Kaidi Shao, and Jiexiu Zhai for proofreading my thesis.

The staff from the fine mechanical workshop and electronic workshop were being supportive the whole time. Thank you all for moving and building my recording setup again, again and again; also, for immediate help whenever something was needed. I would also like to thank Eduard Krampe for helping me build electrodes from scratch; Axel Oeltermann, for everything related to electronics and delicate mechanical design; and Joachim Werner for all the help one can get from a system administrator and much more beyond.

My sincere thanks go to my friends, with whom I shared laughers, tears, and life details! Thank you, Yun, Yi, Yiling, Yan (Dawang), Cen (Dacencen), Lina (Jiejie), Wenyun. Without your support, life would be colorless.

Last but not least, I would like to thank all the rats used in my Ph.D. projects for their irreplaceable sacrifice. Without them, nothing would be possible.

1. Summary/ Abstract

The brain state is a recurring, temporally enduring constellation of neural activity. It varies with or without external stimuli to both spatial and temporal extent. Brain state can be characterized in various dimensions, such as arousal, affective, cognitive, exploratory, and many others. Among them, the arousal state is the most well-studied one. Neural activities that support sensory processing, motor control, decision making, mnemonic function are all influenced by the ongoing arousal level. However, the modulation of arousal state on different aspects of brain functions and behavioral outputs remains largely unexplored. In my Ph.D. work, I investigated the sensorimotor gating and memory consolidation across different arousal states, measured by the frontal electroencephalogram (EEG) and concurrently recorded animals' movements. Acoustic startle response (ASR) and prepulse inhibition (PPI) were used to assess the sensorimotor function (Manuscript 1). To manipulate the arousal level, we delivered electrical micro-stimulation pulses to the locus coeruleus (LC), the nucleus that sends brain-wide projections and regulates arousal via releasing noradrenaline (NA) in the target brain regions. We observed that the magnitude of the startle response was significantly reduced by increasing cortical arousal effectively with phasic LC activation.

Next, by examining startle response across spontaneous fluctuations of arousal levels, we found that the smallest startle response during the active awake state, further suggesting that arousal states modulated ASR amplitudes. To study memory consolidation, we selected a well-studied hippocampal neural event, sharp wave-ripple (SPW-R), which is essential for various memory functions. We characterized neuronal activity in the LC (Manuscript 2) and mediodorsal thalamus (MD, Manuscript 3) through multi-site electrophysiological recordings around SPW-Rs during quiet awake state and slow wave sleep. Overall, we observed suppressions of both LC and MD spiking activity around SPW-Rs. The

SPW-R-associated suppression in both structures differed across arousal states, being strongest and the most consistent during awake ripples. Taken together, these results showed that the fluctuation of the arousal state could modulate neural activity and behavioral output, including both the basic motor reflex and higher cognitive function, in this case, memory consolidation. The engagement of neural circuits and cross-regional communications in the same behavioral context highly depends on the ongoing background brain activity.

2. Synopsis

2.1 Introduction

2.1.1 General Remarks

Brain state is a recurring, temporally enduring constellation of neural activity in single or multiple brain regions [1]. It varies at multiple temporal resolutions: from hundreds of milliseconds to hours, both with and without external stimuli [2-4]. One way to simplify such complexity is to characterize the brain state by a number of indicator variables that measure brain and behavioral activity [1, 5]. For example, awake and sleep states can be identified by two variables: amplitudes of low-frequency oscillations derived from electroencephalogram (EEG) signals and amplitudes of muscle activity recorded by electromyography (EMG) [6, 7]. Brain state can be characterized in various dimensions, such as arousal, affective, cognitive, exploratory, and others [2].

The arousal state is probably the most well-studied brain state, as it recurs very often and strongly influences neural activity and behavior [5]. The arousal state fluctuates from deep sleepiness/sedation to high-arousal stress- or fear-related conditions with many sub-states in between, such as drowsiness or attentive state [8, 9]. It is commonly measured by EEG/cortical local field potential (LFP), EMG, and pupillometry [10, 11]. The level of arousal is regulated by both cortico-cortical/ thalamo-cortical circuits and ascending neuromodulatory systems, which are typically localized in the brainstem and hypothalamic nuclei that send broad projections through the thalamus and cortex [12-19]. Neural activities that support sensory processing [20-22], motor control [23, 24], decision making [25, 26], memory [27-29] are all influenced by the ongoing arousal state. However, the modulation of arousal state on different aspects of brain functions and behavioral outputs remains largely unexplored.

In my Ph.D. work, I investigated how arousal state influences the basic sensorimotor reflex and memory consolidation. We monitored arousal levels by frontal EEG and concurrently recorded animal movement. Behavioral paradigms such as acoustic startle response (ASR) and prepulse inhibition (PPI) were used to assess the sensorimotor function during spontaneous fluctuations of arousal levels. To reveal a causal link between arousal states and sensorimotor gating, we delivered electrical micro-stimulation pulses to the locus coeruleus (LC) , the nucleus that sends brain-wide projections and regulates arousal via releasing noradrenaline (NA) in the target brain regions [30]. To study memory consolidation, we selected a well-studied hippocampal neural event, sharp wave-ripple (SPW-R), which plays a critical role in various memory functions [31]. We examined the state-dependency of cross-regional interactions associated with memory consolidation through multi-site electrophysiological recordings in freely behaving rats. In the following chapters, I will first summarize neural oscillations across different arousal states and the brain structures we studied: the LC and mediodorsal thalamus (MD). Subsequently, I will briefly introduce and discuss the findings in each manuscript, limitations, and directions for future investigations.

2.1.2 Neural oscillations underlying different brain states

The specific organization of interconnectivity in neuronal networks, together with intrinsic properties of individual neurons, give rise to various oscillatory patterns, which can be observed at the level of scalp EEG and intracranial LFP [32, 33]. Oscillatory frequencies range from infraslow (< 0.01Hz) to ultrafast (>200Hz) rhythms [34]. Distinct frequency bands of oscillatory patterns displayed in a given brain structure are highly dependent on the arousal state [32, 35]. One example is that theta oscillations (4 -10 Hz) in the hippocampus are mainly present during active behavior and rapid eye movement (REM) sleep but not when the animals stay awake immobility or in non-rapid eye movement (NREM) sleep [36, 37]. Another example is cortical gamma oscillations (30 – 90Hz) that are most prominent during attentive state [38, 39].

Furthermore, frequency-specific oscillations among widely distributed brain regions offer temporal and spatial frames for grouping neuronal activities to effectively exchange information and synaptic plasticity, e.g., mechanisms that support numerous cognitive functions, such as attention, decision making, and memory consolidation [33, 40-42]. Neural oscillations thus can be used to characterize the arousal state and the state-associated brain functions. Below, we will review several selected thalamocortical and hippocampal oscillations that define the offline state and interactions among the oscillations.

2.1.2.1 Slow oscillation

Slow oscillation (SO; < 1Hz) is one of the most prominent features of NREM sleep. It consists of periods of prolonged depolarization (UP state), interspersed with periods of hyperpolarization (DOWN state) [43]. SOs in the cortex survived after extensive thalamic lesions and were present in the cortical slice in vitro, suggesting the cortical origin of this rhythm [44, 45]. Nevertheless, subsequent studies demonstrated an active role of the thalamus in mediating large-scale synchronization of SOs and regulating properties such as the frequency and DOWN state duration of SOs [46-49].

Rhythmic shifts between synchronous activation and silence states during the widespread SOs across cortical and subcortical structures provide a temporal frame for synaptic plasticity and cross-regional interactions, supporting memory formation [50-52]. Growing evidence has linked SOs with memory processing. For example, during post-learning sleep, amplitudes of SOs are increased locally in the cortical areas involved in the previous motor learning experience in humans [53] and decreased when subjects' arms were immobilized after motor learning, thus the encoding of information was blocked [54]. Enhancing SOs by transcranial electric or auditory stimuli facilitates memory consolidation [55-57], while disruption of SOs interferes with sleep-associated memory formation [58]. Moreover, a replay of multicell firing sequences during the awake experience is organized during UP states of SOs, and perturbing spiking activity during UP states by optogenetic simulations impaired memory consolidation [59, 60]. Overall, these data suggest a causal role of SO in memory formation.

2.1.2.2 Sleep spindles

Another prominent feature of NREM sleep is sleep spindles [61]. Sleep spindles are waxing-and-waning field potentials, oscillating in a frequency range of 12 to 16 Hz and with a duration of 0.5-3 seconds [62, 63]. Spindles are generated in the intrathalamic circuits through the interplay between the glutamatergic thalamocortical neurons and GABAergic neurons in the thalamic reticular nucleus (TRN), the pacemaker of spindle oscillations [64, 65]. Despite its thalamic origin, synchronization and near-simultaneity of spindles across thalamocortical circuits are mediated by corticothalamic projections [66, 67].

What are the functions of spindle oscillations? First, NREM sleep is associated with a loss of behavioral responses to external stimuli, which has been hypothesized to be controlled by the gating mechanism of the thalamus [68]. Consistent with this idea, sleep spindles have been shown to play a key role in reducing the transmission of incoming sensory signals from the thalamus to the cortex [69-72]. Another critical function of sleep spindles that has attracted high attention in recent years is its role in synaptic plasticity and memory consolidation [73, 74]. Spindles are associated with coherent neural activity and massive calcium entry into cortical pyramidal neurons, a situation that favors plasticity [74, 75]. It has been shown that by applying a firing pattern recorded *in vivo* during sleep spindles, it is possible to trigger long-term potentiation (LTP) through stimulating cortical pyramidal cells *in vitro* [76].

Regarding the role of spindles in memory consolidation, previous studies in both humans and rats showed that spindle density during NREM sleep after learning was increased [77-79] and correlated with the subsequent task performance [80-82]. Furthermore, a causal role of spindles in memory consolidation has been established by manipulating spindle oscillations. For example, inducing spindles in phase with SOs by optogenetic stimulation of the TRN boosts fear memory consolidation in mice [83].

2.1.2.3 Sharp wave-ripple

Sharp wave-ripple (SPW-R), which is driven by the synchronous CA3 excitatory output, consists of a transient high-frequency (140-250 Hz) oscillation in the CA1 pyramidal layer and a large-amplitude negative deflection in the CA1 *stratum radiatum* [84, 85]. SPW-Rs mainly occur during an offline state when theta oscillation is absent and subcortical neuromodulators are reduced, such as during immobility, grooming, or NREM sleep [31]. In the time window of SPW-R, population synchrony of spiking activity in the CA1 increases several fold and produces strong depolarizations in its downstream targets, such as entorhinal-neocortical areas [31, 86, 87].

Reactivations of neural activity in the hippocampus and other brain regions that represent previous experience coincide with SPW-Rs during both awake state and NREM sleep [59, 88-93]. The SPW-R-associated reactivation of memory traces thus makes it a possible physiological mechanism underlying memory processing [94]. This idea continuously receives further experimental support. Indeed, SPW-Rs occur more frequently after a learning experience [95, 96]. Disruption of SPW-Rs during learning and post-learning sleep results in spatial memory impairment [97-99], while prolongation of SPW-R increases memory performance during maze learning [100].

In recent years, it has become evident that SPW-Rs reflect not only synchronization within the hippocampus but also coordination of activity in the large-scale networks [101, 102]. The SPW-R-associated cross-regional communication may occur through synchronized up/down-regulation of neural activity across cortical and subcortical structures, including activity in the anterior cingulate cortex (ACC) [103], ventral tegmental area (VTA) [104], median raphe [105], and thalamus [106-109].

2.1.2.6 Neural oscillation coupling for information transfer

Neural oscillations of different frequencies occurring during the same state often temporally coordinate within the same or across different brain regions [34, 110]. Simultaneous interactions of oscillations in various frequencies and brain regions are essential for encoding, communications, integration, and storage of information [111, 112]. Oscillation coupling is organized in a hierarchical way by synchronizing fast oscillations to slower oscillations through relations between their amplitudes and phases [113, 114]. One of the best-studied examples is that the phase of theta oscillation modulates the power of gamma oscillation during wakefulness across species [115-118].

In the past two decades, accumulating evidence has shown a fine-tuned temporal coupling among SOs, spindles, and SPW-Rs during NREM sleep [65, 102, 119]. SOs exert a grouping influence on spindles and SPW-Rs; both oscillations are phase-locked to the depolarizing UP state of SOs [120-127].

Furthermore, SPW-Rs tend to precede spindles [128, 129], but they can also occur during spindles and are nested in the excitable troughs of spindle oscillations [120, 123, 130].

A causal role of SO-spindle-ripple coupling in coordinating information transfer among the hippocampus, thalamus, and cortex, as well as in mediating memory consolidation, has been demonstrated in rodents: increasing the SO-spindle-ripple coupling improves memory consolidation [83, 131] while decreasing spindle-ripple coupling results in impaired performance in spatial memory tasks [132, 133]

2.1.3 LC-NA system

The LC, located adjacent to the fourth ventricle in the rostral pons, contains a small cluster of noradrenergic neurons (~3000 in rats) [134, 135]. Afferents that drive LC neurons originate from more than 100 brain regions, including the nucleus paragigantocellularis, nucleus prepositus hypoglossus and dorsal raphe in the brain stem, deep cerebellar nuclei, and cerebellar Purkinje cells, and a variety of forebrain regions, including the central amygdala, lateral hypothalamus, and prefrontal cortex (PFC) [136-138]. The LC sends wide projections to almost the whole brain and spinal cord, sometimes with individual LC cells simultaneously innervating multiple brain regions [139, 140]. The convergent input and broadly-projecting output organization of the LC enable regulation of diverse behavioral and cognitive functions, including arousal, attention, sensory processing, synaptic plasticity, and memory consolidation [30, 134, 135].

2.1.3.1. Role of the LC in tuning arousal

The LC is a part of the ascending arousal system [141]. Early studies have shown that the firing rate of LC neurons co-varies with the arousal states, being highest during active exploration, slowly decreasing during self-directed behavior such as drinking and grooming, lower during NREM sleep, and virtually absent during REM sleep [142-144]. Also, an increase in firing rate in the LC preceding transition from sleep to awake state was observed [143, 144]. In the past few years, it has been reported that activities of LC neurons and noradrenergic axons in the cortex reflected changes in pupil diameter, further indicating a tight positive link between LC activity and moment-to-moment arousal fluctuations during awake state [145, 146].

However, it was only until recently that the causal role of the LC in tuning arousal was demonstrated using optogenetic methods [147-149]. Specifically, optogenetic activation of LC neurons induces sleep-to-awake transition and a large increase in pupil size, while inhibition of the LC causes pupil constriction and reduces wakefulness.

2.1.3.2. Modulatory action of the LC on sensory processing

Local administration of NA or LC stimulation has been shown to lead to a net increase in the signal-to-noise ratio in both anesthetized and awake animals by suppressing the spontaneous activity and relatively sparing the evoked responses in many thalamic and cortical regions, including visual, auditory, olfactory, and somatosensory [150-158]. In addition to enhancing threshold-level sensory-evoked responses, applying NA iontophoretically often shifts neurons to respond robustly to otherwise sub-threshold stimuli, a phenomenon is referred to as "sensory gating" [30, 159]. Moreover, activation of the LC can enhance the fidelity in neuronal responses to sensory stimuli by reducing response latency and suppressing trial-to-trial jitters [156, 160].

Notably, NA-mediated actions can also alter specific receptive field properties of neurons in the visual cortex [161, 162] and increase feature selectivity in the somatosensory thalamus [163]. Also, presenting sound together with LC stimulation can shift the peak of the frequency tuning curve of auditory cortex neurons to the frequency paired with LC stimulation [164, 165]. Later studies have demonstrated that the NA-induced selective tuning can enhance performance in a discrimination task when comparing tones with tuned frequencies and other tones in neighboring frequencies [166, 167]. Furthermore, recent studies showed that elevation of NA can improve signal detection/discrimination tasks performance both in humans [168] and animals [163].

However, the sensory response does not increase monotonically with NA concentration. NA effects follow an inverted-U function, that is, the facilitating effects rise to a maximum as NA level increases from a relatively low level and then gradually decreases with further increases in NA concentrations [30, 134, 159].

2.1.3.3. Modulatory action of the LC on synaptic plasticity and memory formation in the hippocampus

In the 1970s, Kety proposed a functional role of the LC-NA system in inducing persistent facilitation in all synapses activated by a common input and promoting memory consolidation [169]. A decade later, the hypothesis was first supported by experimental evidence demonstrating that NA produces LTP of glutamatergic perforant-path input to the dentate gyrus in the rodent hippocampus [170, 171]. Later studies in behaving animals showed that novelty induces hippocampal LTP and burst firing in LC neurons, leading to increased extracellular NA concentration in the hippocampus. The novelty-elicited LTP can be blocked by the beta-noradrenergic antagonist propranolol, suggesting it is NA-dependent [172, 173]. Furthermore, the LC can also modulate place cell plasticity, e.g., optogenetic activation of LC-CA1 axons near the reward site induces place cell overrepresentation [174]. These findings suggest that the LC-NA system contributes to hippocampal plasticity, which is considered a cellular mechanism of memory consolidation [175].

Previous pharmacological studies suggest that the LC-NA system's engagement occurs at a late stage of memory consolidation: rats who received injections of beta-receptor antagonists 2h after learning showed amnesia, while immediate injection after learning had no effect [176, 177]. Consistently, subsequent electrophysiological recordings in the LC showed an increase of firing rate during NREM sleep 2h after learning [178]. Later, by applying tonic [133] or SPW-R triggered phasic [132] stimulation in the LC during the whole post-learning sleep, memory performance in spatial tasks was impaired, further suggesting the timing of the LC activation/suppression during memory consolidation is critical. Interestingly, recent studies reported that LC neurons could mediate memory enhancement through co-releasing dopamine in the hippocampus [179-181]. Taken together, although numerous pieces of evidence have confirmed the involvement of the LC in synaptic plasticity and memory consolidation, the exact mechanisms seem to be more complicated and depend on multiple factors such as the degree of the LC activation, the concentration of the NA, the timing of the activation, and the neuromodulator type released from LC terminals.

2.1.4 Mediodorsal thalamus

The mediodorsal thalamus (MD) is the largest nucleus in the medial thalamus, and it has dense reciprocal connections with the PFC via glutamatergic projections [182, 183]. In addition to the primary excitatory input from the deep layers of the PFC, the MD receives afferents from the lateral entorhinal and perirhinal cortices, which send projections to the hippocampus [184, 185]. It also receives many inputs from the TRN, amygdala, basal ganglia, and brain stem nuclei, including the LC [184, 186-189]. The MD is a higher thalamic relay nucleus supporting diverse cognitive functions, including learning, working memory, behavioral flexibility, and memory consolidation [183, 190].

2.1.4.1 Role of the MD in working memory

Because of its dense reciprocal projections with the PFC, the MD has long been hypothesized to play a role in tasks that require sustaining cortical representations, such as working memory [183, 191-193]. Almost fifty years ago, Fuster and Alexander [194] first reported that in monkeys, the MD neurons showed a sustained elevation of discharge during the delay period in a delayed response task, suggesting a functional role of the MD in working memory. However, the results from the following lesion studies were inconsistent; some of them showed impairment in working memory after ablating the MD while others did not have such effects [195-199]. The controversy might result from the imprecise and irreversible nature of brain lesions. Specifically, the lesion might not be circumscribed to the MD but extend to other nearby nuclei, or the brain could develop an alternative pathway to compensate for the function of the MD after permanent damage.

Recently, by employing a chemogenetic approach to selectively and reversibly decrease the MD activity, Parnaudeau and his colleagues [200] showed that a small decrease in MD activity is sufficient to impair working memory in mice. A subsequent study [201] delivered pathway-specific inhibition optogenetically during different phases of a working memory task. On top of providing more evidence for the impairment of working memory after silencing the MD-PFC pathway, their results revealed directional interactions between the MD and PFC, where MD-to-PFC supports the maintenance of the information and PFC-to-MD supports subsequent choices. In addition, enhancing neuronal activity in the MD has been shown to improve working memory performance [201, 202].

Meanwhile, multi-site recordings in the MD and PFC further uncovered the interactions at the physiological level between these two structures. MD-PFC beta-range synchrony increased during a working memory task, and the degree of this synchrony is positively correlated with the behavioral performance [200]. Furthermore, it has been shown that spiking activity in the MD does not represent task-relevant information, such as task rule or spatial location, but is more likely to be driven by the PFC at the initial phase of the delay period when performing working memory tasks. Then its activity is elevated to support the maintenance of information in the PFC [201, 202].

2.1.4.2 Role of the MD in memory consolidation

Clinical studies repeatedly showed that human patients suffer severe amnesia (diencephalic amnesia) after damage in the medial diencephalon, e.g., after stroke, traumatic injury, hemorrhage, or Korsakoff's syndrome [203, 204]. The damage is usually diffuse and extends to several adjacent structures in the diencephalon, including the anterior thalamus, mammillary body, and MD [205-207].

Subsequent lesion studies in animals then focused on identifying the contribution of each structure in the diencephalon amnesia. Since not much convincing evidence was found for the involvement of the MD in long-term memory [208-212], the memory consolidation function of the MD has long been overlooked. Moreover, unlike the reuniens nucleus of the thalamus that has direct projections to the hippocampus [213], the MD is only connected with hippocampal input and output structures: perirhinal and entorhinal cortices [184, 214, 215]. Nevertheless, the lack of direct projections does not mean that the MD cannot be a node in the thalamo-cortico-hippocampal circuit supporting memory formation. For example, one study [216] showed that the MD could inhibit hippocampal-evoked firing in the PFC. The relative timing of inputs from the MD determines their impact on PFC neurons' responsiveness to hippocampal inputs. This finding suggests that MD inputs to the PFC are important for heterosynaptic coincidence detection, inhibiting the PFC processing inputs from the hippocampus unless they arrive synchronously with inputs from the MD.

2.2 Introduction to manuscripts

2.2.1 Manuscript 1: Phasic activation of the locus coeruleus attenuates the acoustic startle response via increasing cortical arousal

Introduction: The acoustic startle response (ASR) is a motor response caused by a sudden and loud sound [217]. Pre-exposure to a weaker sound (prepulse) could reduce the amplitude of the startle response. This phenomenon is called prepulse inhibition (PPI). The ASR and PPI are consistent across mammals and are commonly used as diagnostic tools for many psychiatric disorders [218, 219]. The neural circuit of the ASR consists of a simple pathway linking the cochlear root neurons (CRN) with the spinal motor neurons through the caudal pontine reticular nucleus (PnC) [220-222]. On the contrary, the neuromodulatory circuit of PPI is still equivocal [223, 224]. It has been shown that during PPI, inhibitory inputs from forebrain regions and neuromodulatory nuclei in the brainstem converge on the PnC to reduce the subsequent contraction of muscles [217]. For example, one long-standing hypothesis is that prepulse activates the pedunculopontine tegmental nucleus (PPTg), which sends cholinergic projections to inhibit PnC neurons, resulting in the attenuation of startle response [223, 224]. However, this hypothesis has recently been challenged [225-227].

The LC is involved in orienting response and attention reorienting [228]. The LC-NA system responds to salient sensory stimuli [144, 229] and modulates sensory processing [164, 166, 167, 230, 231]. Surprisingly, the role of the LC has not yet been examined in the context of the ASR or PPI, and the auditory-evoked LC responses have not been documented using the ASR/PPI paradigm. The present study aimed to study the modulation of the ASR by activating the LC through a brief train of mild electric pulses to the LC cell bodies and pairing the LC stimulation with the startling sound.

Materials and Methods: Rats were first habituated to a sound-attenuated chamber. The motor activity level was assessed by motion sensors measuring the deflection amplitude of the floor. After habituation, rats with microstimulation electrodes within (n = 7) and outside (n = 4) the LC were exposed to acoustic, microstimulation, and mixed (microstimulation preceded by startle sound) trials in each session. The acoustic trials included a non-starting auditory tone (prepulse), startle tone alone, or preceded by prepulse. The microstimulation trials included delivering a mild (0.05mA) electric current at different frequencies for 100ms without pairing with auditory stimuli. During mixed trials, microstimulation was preceded with a startling sound. Each trial type was repeated 40 times and presented in random order with inter-trial intervals varied between 10 to 20 s to avoid habituation. The auditory PPI group (n = 7) without microstimulation was exposed to 40 to 80 repetitions of acoustic trials. The frontal EEG was continuously monitored.

Results: We observed a significant reduction of the ASR amplitude when the startle tone was preceded by phasic LC activation. The magnitude of the attenuation was scaled with the frequency of LC stimulation. LC stimulation at 100Hz decreased the startle response to a similar level as acoustic prepulse. Meanwhile, the LC stimulation changed the EEG spectral components. It led to transient cortical desynchronization (higher arousal), namely, an increase in the high-frequency power band while a decrease in the low-frequency power band. The degree of this cortical desynchronization was also frequency-dependent, being highest with 100Hz LC stimulation. Moreover, in the microstimulation-free group, the ASR amplitude was the lowest during the most alert state (active awake).

Conclusions: The attenuation of ASR amplitudes by LC stimulation was positively correlated with the degree of cortical desynchronization. Besides, the ASR became lower when the arousal level fluctuated to a higher level spontaneously. Overall, our findings suggest the LC plays a role in regulating the ASR, possibly through its diffuse ascending projections to the forebrain arousal network. However, alternative mechanisms, including the LC directly affecting the three nodes on the ASR circuits, could not be ruled out.

2.2.2 Manuscript 2: The locus coeruleus activity during hippocampal-cortical communication

Introduction: During states of awake immobility or NREM sleep, the hippocampal neural activity is characterized by irregular transient synchronization reflected in the extracellular potential as hippocampal ripples [85]. In recent years, it has become evident that ripple is not only a local event within the hippocampus but indicates a time window of cross-regional communication, such as information transfer between the hippocampus and cortex [106, 232].

The LC, is critical for learning, synaptic plasticity, and memory consolidation [134]. The noradrenergic neurotransmission has been long suggested to play a crucial role during the late memory phase [176-178], which may coincide with the protein-dependent phase of synaptic consolidation [233, 234]. However, the direct relationship between the LC activity and hippocampal ripples has not yet been demonstrated, whereas indirect evidence is controversial.

Materials and Methods: Electrophysiology activities (0.1Hz - 8kHz) were recorded simultaneously in the CA1 area of the dorsal hippocampus and LC in four rats. Microwire brush electrodes or silicon probes were mounted on a microdrive to optimize the spiking activity in the LC. An EEG screw was placed in the frontal cortex for monitoring cortical states. Recordings were performed when the animals were quiet awake or sleeping in a sleeping box. Animals' movement was monitored by video tracking the LEDs attached to the headstage.

Results: We reported a consistent suppression of LC population activity around hippocampal ripple occurrence. LC activity started decreasing several seconds earlier before ripple onset, but the early decreasing was most likely due to the ripple-related cortical state transition. Interestingly, the LC exhibited a brief suppression before ripple onset, and the degree of LC MUA suppression around ripples greatly varied across the subsets of ripples. Yet, no systematic relations were found with the ripple amplitude or inter-ripple frequency. Notably, ripples that occurred during distinct brain states correlated with different degrees of modulation of LC activity. Suppression of LC activity was more consistent and much stronger around awake ripples compared to sleep ripples. Furthermore, during NREM sleep, LC activity showed earlier decreasing around spindle-coupled ripples than spindle-uncoupled ones.

Conclusions: This study characterized the precise temporal relationship between hippocampal ripples and LC activity across different brain states. It provides new evidence for the engagement of the LC in ripple-associated memory processing. It raises further questions about the role of the LC in mediating ripple generation and synergistic interactions across multiple cortical and subcortical brain structures during ripples.

2.2.3 Manuscript 3: Occurrence of hippocampal ripples is associated with activity suppression in the mediodorsal thalamic nucleus

Introduction: Memory consolidation during the offline state could be mediated by high-frequency (140-250 Hz) oscillations in the hippocampal CA1, or ripples, produced by the synchronized discharge of the CA3 neurons [85, 235]. Simultaneous reactivations of experience-related firing patterns in the hippocampus and other brain structures during ripples have been shown to facilitate selective synaptic plasticity and cross-regional information transfer [94, 236, 237]. Moreover, ripple-triggered fMRI-based mapping of the whole brain activity in macaques revealed a characteristic pattern, with positive BOLD responses in many cortical and limbic regions and negative BOLD responses in a subset of subcortical areas, including the thalamus [232].

The MD has dense reciprocal connections with the mPFC [238]. Thus, the MD is involved in a variety of higher cognitive functions that the mPFC participates [190], including mnemonic processes [239, 240]. It has been postulated that the MD could modulate the hippocampal- cortical and cortico-cortical interactions relevant to declarative memory [199, 241]. However, the exact role of the MD in memory formation has been largely unexplored. We chose hippocampal ripple as the biomarker for offline memory consolidation and sought to characterize the temporal relationship between the MD spiking activity and hippocampal ripples.

Materials and Methods: Electrophysiology activities (0.1Hz - 8kHz) were recorded simultaneously in the CA1 area of the dorsal hippocampus and MD in eight rats. Twisted wires or tube tetrodes were mounted on a microdrive to optimize ripples in the CA1 and spike activity in the MD. An EEG screw was placed in the frontal cortex for monitoring cortical states. Recordings were performed during animals being quiet awake or sleeping. Animals' movement was monitored by video tracking with LEDs attached to the headstage.

Results: MD firing rate decreased around hippocampal ripples, and the decrease preceded the ripple onsets systematically. A substantial fraction of ripples was accompanied by a transient increase of power in the high gamma range. Therefore, we first separated ripples into high-gamma-coupled and -uncoupled ripples. We observed that the magnitude of MD suppression was weaker around high-gamma-coupled ripples, and thus, only “pure” ripples uncoupled with high gamma were further analyzed.

Next, we found that the ripple-associated MD suppression was not homogeneous across all ripples. The degree of MD suppression was correlated with ripple amplitudes but not intra-ripple frequencies. Moreover, the MD suppression was state-dependent, being more consistent and robust during the awake state. Strikingly, peri-ripple MD modulation was fine-tuned to the thalamocortical activity such that the MD suppression was only observed around spindle-uncoupled ripples. In contrast, no MD suppression was present during spindle-coupled ripples, and in about half of cases, MD firing rate increased.

Conclusion: Our study showed that the MD was engaged differently when the hippocampal-cortical communication was accompanied with or without thalamocortical interaction, suggesting a possible competitive relationship between these two pathways. Suppression of MD activity around spindle-uncoupled ripples might contribute to memory replay by reducing interferences from peripheral sensory input. In contrast, activation of MD activity around spindle-coupled ripples may be beneficial for selectivity and reliability of information transfer.

2.3 Discussions

2.3.1 Modulation of sensorimotor gating via an increased cortical arousal

Although reflexive in nature, the behavioral response to a sudden alerting stimulus is an integrative result of the excitatory and inhibitory processes and depends on the organism's state [242]. However, the state-dependency of the ASR is inconsistent. For example, one study in cats showed that ASR was maximal during quiet awake and greatly suppressed during REM sleep [242], while another study in rats reported that ASR did not differ across sleep-awake states [243]. By classifying arousal levels at a finer time scale, we observed that ASR amplitudes were arousal-dependent and were higher when the cortical arousal level was lower.

Cortical arousal can be manipulated by activating cholinergic neurons in the PPTg and lateral dorsal tegmental nucleus (LDTg), which sends excitatory projections to almost all thalamic nuclei [244]. Meanwhile, PPTg and LDTg neurons have been shown to exert an inhibitory influence on the primary startle pathway [245]. The role of PPTg and LDTg neurons in reducing startle response could be mediated through their main role in increasing cortical arousal [224].

In addition to the cholinergic system, the LC-NA system has also long been posited to play a role in modulating arousal states and sensory processing by alternating its discharge rates and patterns [30]. LC neurons exhibit both tonic and phasic firing patterns. The tonic firing of the LC neuron co-varies consistently with the sleep-waking cycle: high firing rate during awake, much lower during slow wave sleep, and virtually silent during REM sleep. Phasic firing can contribute to the sleep-to-awake transition. Therefore, it is possible that the LC indirectly influences ASR through the ascending pathways involved in regulating the arousal state [246].

In our study, phasic activation of the LC increased arousal. The ASR amplitude was reduced when the LC stimulation was applied before the startle-eliciting acoustic stimulus in spontaneously behaving rats. The behavioral effect depended on the LC stimulation frequency and was comparable to the effect of acoustic prepulse at 100Hz. Moreover, the ASR amplitude was the lowest during the most alert state. Thus, the role of LC stimulation on the ASR attenuation could be mediated by activation of the arousal network; however, it is also possible that the startle-inhibiting effect of the LC was achieved by affecting the brainstem ASR circuit directly.

2.3.2 Coordinated neuronal activity during awake and sleep SPW-Rs

Awake and sleep SPW-Rs are both involved in memory processing, but further examination suggests the underlying mechanism and the mnemonic function they serve are different [101, 247]. Compared to sleep SPW-Rs, awake SPW-Rs are associated with stronger and more structured reactivation of previous awake experience, and the reactivation is more correlated with the recent memory [248]. Moreover, the up-/down-regulations in other brain regions, such as the ACC, VTA, and thalamus, are stronger around awake SPW-Rs [103, 104, 109]. Our study also found a larger suppression of the MD and LC activity around the awake SPW-Rs. One possibility is, the firing rate in the MD and LC is higher during the awake state and thus requires to be lowered more to reach the optimal level needed for SPW-R generation. Another possibility could be that more information must be processed during the awake state. Stronger MD and LC suppression might contribute to the inhibition of irrelevant or remote information for reactivation of recently encoded memory traces with high signal-to-noise ratios.

Unlike the awake SPW-Rs, sleep SPW-Rs are coordinated with cortical SOs and spindles [102]. The precise temporal correlation between SPW-Rs and spindles has been causally linked to memory consolidation involving transferring newly encoded information from the hippocampus to the cortex for storage [83, 131].]. Consistently, we observed coupling between sleep SPW-R and spindle in our recordings. Interestingly, in the MD, a different engagement of the MD during spindle-coupled versus spindle-uncoupled SPW-Rs was observed. The MD suppression was only present around SPW-Rs occurring outside sleep spindles. In contrast, during spindle-coupled SPW-Rs, the MD firing rate was increased in about half of the cases. Hippocampal ripples tend to precede sleep spindles [128]; therefore, memory trace reactivation during ripples might trigger synaptic modifications in the cortex during subsequent spindles [249]. It was hypothesized that the hippocampal output during SPW-R-associated replay might selectively recruit thalamocortical cells during spindles [129]. Thus, spindle-uncoupled ripples combined with thalamic activity suppression might present a brain state that is favorable for information transfer from the hippocampus to the cortex, while the thalamic input at the time of hippocampal-cortical communication, indicated by spindle-ripple coupling, may contribute to the neural assembly selection for promoting synaptic plasticity in the cortex.

2.3.3 Limitations and future investigations

In our study, we showed that sensorimotor gating was arousal-dependent. However, we cannot rule out the possibility that the LC modulates startle response via its direct projections on the ASR circuit. To get a clearer picture about how the LC modulates the ASR, it would be necessary to examine the effect of LC stimulation on the CRN, PnC, and motor neurons in the spinal cord, and also compare the auditory-evoked responses in neurons within the ASR circuit when auditory stimuli are presented with and without LC stimulation. It would also be interesting to correlate neuronal activity with the behavioral properties of the ASR. Moreover, it is necessary to record LC spiking activity in the ASR and PPI paradigm. By examining the prepulse and startle sound-elicited response in the LC neurons across different arousal states, we can better understand LC's role in mediating startle responses.

SPW-R-associated suppression was observed in both the LC and MD, and the suppression varied across subsets of SPW-Rs. We identified one main factor underlying the heterogeneity of the modulation around SPW-Rs: fluctuations in the arousal level. However, SPW-Rs can be classified in many other dimensions, such as the phase of the sharp waves that ripples are locked to [250], or the sequence of place cells firing during each SPW-R [104]. As we only recorded LFPs in the pyramidal layer of the dorsal CA1, it is impossible to extract all the information about each SPW-R. Thus, to better characterize SPW-Rs, it would be good to record simultaneously: 1) LFPs from *stratum oriens*, *pyramidal layer*, and *stratum radiatum* in the CA1 to have a detailed description of the SPW-Rs profiles in spatial and temporal domains; 2) SPW-Rs from multi-sites in the CA1 (e.g., ventral and dorsal hippocampus) to examine whether the SPW-Rs are locally generated or synchronized through the whole hippocampus; 3) large-scale spiking activities in the hippocampus to specify the reactivation contents.

Another limitation in our study on SPW-R-associated long-range modulation is that we did not record many single-unit activities in the MD and LC due to the technical difficulties in targeting deep brain structures and maintaining high-quality signals in chronic-implanted animals. It would be interesting to record a large population of single-neuron activities from these structures and examine their activity pattern and cross-regional information transfer during behavioral tasks, which measures memory encoding, consolidation, and retrieval.

2.4 References

1. McCarley, R.W., *Mechanisms and Models of Behavioral State Control* in *The Reticular Formation Revisited: Specifying function for a nonspecific system* J.A.B. Hobson, M. A., Editor. 1980, Raven Press: New York, New York. p. 375-403.
2. McCormick, D.A., D.B. Nestvogel, and B.J. He, *Neuromodulation of Brain State and Behavior.* Annu Rev Neurosci, 2020. **43**: p. 391-415.
3. Siclari, F. and G. Tononi, *Local aspects of sleep and wakefulness.* Current Opinion in Neurobiology, 2017. **44**: p. 222-227.
4. Zagha, E. and D.A. McCormick, *Neural control of brain state.* Current Opinion in Neurobiology, 2014. **29**: p. 178-186.
5. McGinley, M.J., et al., *Waking State: Rapid Variations Modulate Neural and Behavioral Responses.* Neuron, 2015. **87**(6): p. 1143-1161.
6. Brown, R.E., et al., *Control of Sleep and Wakefulness.* Physiological Reviews, 2012. **92**(3): p. 1087-1187.
7. Kohn, A., A. Zandvakili, and M.A. Smith, *Correlations and brain states: from electrophysiology to functional imaging.* Current Opinion in Neurobiology, 2009. **19**(4): p. 434-438.
8. Berridge, C.W., *Noradrenergic modulation of arousal.* Brain Research Reviews, 2008. **58**(1): p. 1-17.
9. Berridge, C.W., B.E. Schmeichel, and R.A. Espana, *Noradrenergic modulation of wakefulness/arousal.* Sleep Medicine Reviews, 2012. **16**(2): p. 187-197.
10. Poulet, J.F.A. and C.C.H. Petersen, *Internal brain state regulates membrane potential synchrony in barrel cortex of behaving mice.* Nature, 2008. **454**(7206): p. 881-U36.
11. Reimer, J., et al., *Pupil Fluctuations Track Fast Switching of Cortical States during Quiet Wakefulness.* Neuron, 2014. **84**(2): p. 355-362.
12. McCormick, D.A. and T. Bal, *Sleep and arousal: Thalamocortical mechanisms.* Annual Review of Neuroscience, 1997. **20**: p. 185-215.
13. Ren, S.C., et al., *The paraventricular thalamus is a critical thalamic area for wakefulness.* Science, 2018. **362**(6413): p. 429-+.
14. Herrera, C.G., et al., *Hypothalamic feedforward inhibition of thalamocortical network controls arousal and consciousness.* Nat Neurosci, 2016. **19**(2): p. 290-8.
15. Gent, T.C., et al., *Thalamic dual control of sleep and wakefulness.* Nat Neurosci, 2018. **21**(7): p. 974-984.
16. Lewis, L.D., et al., *Thalamic reticular nucleus induces fast and local modulation of arousal state.* Elife, 2015. **4**: p. e08760.
17. Poulet, J.F., et al., *Thalamic control of cortical states.* Nat Neurosci, 2012. **15**(3): p. 370-2.
18. Li, C.Y., M.M. Poo, and Y. Dan, *Burst spiking of a single cortical neuron modifies global brain state.* Science, 2009. **324**(5927): p. 643-6.
19. Lee, S.H. and Y. Dan, *Neuromodulation of brain states.* Neuron, 2012. **76**(1): p. 209-22.
20. Marguet, S.L. and K.D. Harris, *State-Dependent Representation of Amplitude-Modulated Noise Stimuli in Rat Auditory Cortex.* Journal of Neuroscience, 2011. **31**(17): p. 6414-6420.
21. McGinley, M.J., S.V. David, and D.A. McCormick, *Cortical Membrane Potential Signature of Optimal States for Sensory Signal Detection.* Neuron, 2015. **87**(1): p. 179-192.
22. Vinck, M., et al., *Arousal and Locomotion Make Distinct Contributions to Cortical Activity Patterns and Visual Encoding.* Neuron, 2015. **86**(3): p. 740-754.
23. Burgess, C.R. and J.H. Peever, *A Noradrenergic Mechanism Functions to Couple Motor Behavior with Arousal State.* Current Biology, 2013. **23**(18): p. 1719-1725.

24. Cho, J.Y. and P.W. Sternberg, *Multilevel Modulation of a Sensory Motor Circuit during C. elegans Sleep and Arousal.* Cell, 2014. **156**(1-2): p. 249-260.
25. Murphy, P.R., J. Vandekerckhove, and S. Nieuwenhuis, *Pupil-Linked Arousal Determines Variability in Perceptual Decision Making.* Plos Computational Biology, 2014. **10**(9).
26. de Gee, J.W., et al., *Dynamic modulation of decision biases by brainstem arousal systems.* Elife, 2017. **6**.
27. Kay, K. and L.M. Frank, *Three brain states in the hippocampus and cortex.* Hippocampus, 2019. **29**(3): p. 184-238.
28. Buzsaki, G., *Neural Syntax: Cell Assemblies, Synapsembles, and Readers.* Neuron, 2010. **68**(3): p. 362-385.
29. Klinzing, J.G., N. Niethard, and J. Born, *Mechanisms of systems memory consolidation during sleep (vol 22, pg 1598, 2019).* Nature Neuroscience, 2019. **22**(10): p. 1743-1744.
30. Berridge, C.W. and B.D. Waterhouse, *The locus coeruleus-noradrenergic system: modulation of behavioral state and state-dependent cognitive processes.* Brain Res Brain Res Rev, 2003. **42**(1): p. 33-84.
31. Buzsaki, G., *Hippocampal Sharp Wave-Ripple: A Cognitive Biomarker for Episodic Memory and Planning.* Hippocampus, 2015. **25**(10): p. 1073-1188.
32. McCormick, D.A., M.J. McGinley, and D.B. Salkoff, *Brain state dependent activity in the cortex and thalamus.* Curr Opin Neurobiol, 2015. **31**: p. 133-40.
33. Singer, W., *Neuronal oscillations: unavoidable and useful?* European Journal of Neuroscience, 2018. **48**(7): p. 2389-2398.
34. Buzsaki, G., N. Logothetis, and W. Singer, *Scaling Brain Size, Keeping Timing: Evolutionary Preservation of Brain Rhythms.* Neuron, 2013. **80**(3): p. 751-764.
35. Buzsáki, G., *Rhythms of the brain*. 2006, Oxford ; New York: Oxford University Press. xiv, 448 p.
36. Colgin, L.L., *Mechanisms and Functions of Theta Rhythms.* Annual Review of Neuroscience, Vol 36, 2013. **36**: p. 295-312.
37. Buzsaki, G., *Theta oscillations in the hippocampus.* Neuron, 2002. **33**(3): p. 325-340.
38. Engel, A.K., P. Fries, and W. Singer, *Dynamic predictions: Oscillations and synchrony in top-down processing.* Nature Reviews Neuroscience, 2001. **2**(10): p. 704-716.
39. Harris, K.D. and A. Thiele, *Cortical state and attention.* Nature Reviews Neuroscience, 2011. **12**(9): p. 509-523.
40. Buzsaki, G. and A. Draguhn, *Neuronal oscillations in cortical networks.* Science, 2004. **304**(5679): p. 1926-1929.
41. Siegel, M., T.H. Donner, and A.K. Engel, *Spectral fingerprints of large-scale neuronal interactions.* Nature Reviews Neuroscience, 2012. **13**(2): p. 121-134.
42. Steriade, M., *Grouping of brain rhythms in corticothalamic systems.* Neuroscience, 2006. **137**(4): p. 1087-1106.
43. Steriade, M., A. Nunez, and F. Amzica, *A novel slow (< 1 Hz) oscillation of neocortical neurons in vivo: depolarizing and hyperpolarizing components.* J Neurosci, 1993. **13**(8): p. 3252-65.
44. Sanchez-Vives, M.V. and D.A. McCormick, *Cellular and network mechanisms of rhythmic recurrent activity in neocortex.* Nature Neuroscience, 2000. **3**(10): p. 1027-1034.
45. Steriade, M., A. Nunez, and F. Amzica, *Intracellular Analysis of Relations between the Slow (Less-Than-1 Hz) Neocortical Oscillation and Other Sleep Rhythms of the Electroencephalogram.* Journal of Neuroscience, 1993. **13**(8): p. 3266-3283.
46. David, F., et al., *Essential Thalamic Contribution to Slow Waves of Natural Sleep.* Journal of Neuroscience, 2013. **33**(50): p. 19599-19610.

47. Lemieux, M., S. Chauvette, and I. Timofeev, *Neocortical inhibitory activities and long-range afferents contribute to the synchronous onset of silent states of the neocortical slow oscillation.* Journal of Neurophysiology, 2015. **113**(3): p. 768-779.
48. Lemieux, M., et al., *The Impact of Cortical Deafferentation on the Neocortical Slow Oscillation.* Journal of Neuroscience, 2014. **34**(16): p. 5689-5703.
49. Zucca, S., et al., *Thalamic Drive of Cortical Parvalbumin-Positive Interneurons during Down States in Anesthetized Mice.* Current Biology, 2019. **29**(9): p. 1481-+.
50. Hoffman, K.L., et al., *The upshot of up states in the neocortex: From slow oscillations to memory formation.* Journal of Neuroscience, 2007. **27**(44): p. 11838-11841.
51. Neske, G.T., *The Slow Oscillation in Cortical and Thalamic Networks: Mechanisms and Functions.* Frontiers in Neural Circuits, 2016. **9**.
52. Puentes-Mestril, C., et al., *How rhythms of the sleeping brain tune memory and synaptic plasticity.* Sleep, 2019. **42**(7).
53. Huber, R., et al., *Local sleep and learning.* Nature, 2004. **430**(6995): p. 78-81.
54. Huber, R., et al., *Arm immobilization causes cortical plastic changes and locally decreases sleep slow wave activity.* Nature Neuroscience, 2006. **9**(9): p. 1169-1176.
55. Binder, S., et al., *Transcranial Slow Oscillation Stimulation During Sleep Enhances Memory Consolidation in Rats.* Brain Stimulation, 2014. **7**(4): p. 508-515.
56. Marshall, L., et al., *Boosting slow oscillations during sleep potentiates memory.* Nature, 2006. **444**(7119): p. 610-613.
57. Ngo, H.V.V., et al., *Auditory Closed-Loop Stimulation of the Sleep Slow Oscillation Enhances Memory.* Neuron, 2013. **78**(3): p. 545-553.
58. Garside, P., et al., *Cross-hemispheric Alternating Current Stimulation During a Nap Disrupts Slow Wave Activity and Associated Memory Consolidation.* Brain Stimulation, 2015. **8**(3): p. 520-527.
59. Ji, D.Y. and M.A. Wilson, *Coordinated memory replay in the visual cortex and hippocampus during sleep.* Nature Neuroscience, 2007. **10**(1): p. 100-107.
60. Kim, J., T. Gulati, and K. Ganguly, *Competing Roles of Slow Oscillations and Delta Waves in Memory Consolidation versus Forgetting.* Cell, 2019. **179**(2): p. 514-+.
61. Steriade, M., D.A. Mccormick, and T.J. Sejnowski, *Thalamocortical Oscillations in the Sleeping and Aroused Brain.* Science, 1993. **262**(5134): p. 679-685.
62. Astori, S., R.D. Wimmer, and A. Luthi, *Manipulating sleep spindles - expanding views on sleep, memory, and disease.* Trends in Neurosciences, 2013. **36**(12): p. 738-748.
63. Fernandez, L.M.J. and A. Luthi, *Sleep Spindles: Mechanisms and Functions.* Physiological Reviews, 2020. **100**(2): p. 805-868.
64. Halassa, M.M., et al., *Selective optical drive of thalamic reticular nucleus generates thalamic bursts and cortical spindles.* Nature Neuroscience, 2011. **14**(9): p. 1118-1120.
65. Steriade, M., *The corticothalamic system in sleep.* Frontiers in Bioscience-Landmark, 2003. **8**: p. D878-D899.
66. Contreras, D., et al., *Spatiotemporal patterns of spindle oscillations in cortex and thalamus.* Journal of Neuroscience, 1997. **17**(3): p. 1179-1196.
67. Contreras, D. and M. Steriade, *Spindle oscillation in cats - The role of corticothalamic feedback in a thalamically generated rhythm (vol 490, pg 159, 1996).* Journal of Physiology-London, 1996. **491**(3): p. 889-889.
68. McCormick, D.A. and T. Bal, *Sensory gating mechanisms of the thalamus.* Curr Opin Neurobiol, 1994. **4**(4): p. 550-6.
69. Elton, M., et al., *Event-related potentials to tones in the absence and presence of sleep spindles.* Journal of Sleep Research, 1997. **6**(2): p. 78-83.

70. Wimmer, R.D., et al., *Sustaining Sleep Spindles through Enhanced SK2-Channel Activity Consolidates Sleep and Elevates Arousal Threshold.* Journal of Neuroscience, 2012. **32**(40): p. 13917-13928.
71. Cote, K.A., T.M. Epps, and K.B. Campbell, *The role of the spindle in human information processing of high-intensity stimuli during sleep.* Journal of Sleep Research, 2000. **9**(1): p. 19-26.
72. Yamadori, A., *Role of the spindles in the onset of sleep.* Kobe J Med Sci, 1971. **17**(3): p. 97-111.
73. Ulrich, D., *Sleep Spindles as Facilitators of Memory Formation and Learning.* Neural Plasticity, 2016. **2016**.
74. Peyrache, A. and J. Seibt, *A mechanism for learning with sleep spindles.* Philosophical Transactions of the Royal Society B-Biological Sciences, 2020. **375**(1799).
75. Timofeev, I., et al., *Short- and medium-term plasticity associated with augmenting responses in cortical slabs and spindles in intact cortex of cats in vivo.* Journal of Physiology-London, 2002. **542**(2): p. 583-598.
76. Rosanova, M. and D. Ulrich, *Pattern-specific associative long-term potentiation induced by a sleep spindle-related spike train.* Journal of Neuroscience, 2005. **25**(41): p. 9398-9405.
77. Morin, A., et al., *Motor sequence learning increases sleep spindles and fast frequencies in post-training sleep.* Sleep, 2008. **31**(8): p. 1149-1156.
78. Eschenko, O., et al., *Elevated sleep spindle density after learning or after retrieval in rats.* Journal of Neuroscience, 2006. **26**(50): p. 12914-12920.
79. Molle, M., et al., *The influence of learning on sleep slow oscillations and associated spindles and ripples in humans and rats.* European Journal of Neuroscience, 2009. **29**(5): p. 1071-1081.
80. Cox, R., W.F. Hofman, and L.M. Talamini, *Involvement of spindles in memory consolidation is slow wave sleep-specific.* Learning & Memory, 2012. **19**(7): p. 264-267.
81. Schabus, M., et al., *Sleep spindles and their significance for declarative memory consolidation.* Sleep, 2004. **27**(8): p. 1479-1485.
82. Gais, S., et al., *Learning-dependent increases in sleep spindle density.* Journal of Neuroscience, 2002. **22**(15): p. 6830-6834.
83. Latchoumane, C.F.V., et al., *Thalamic Spindles Promote Memory Formation during Sleep through Triple Phase-Locking of Cortical, Thalamic, and Hippocampal Rhythms.* Neuron, 2017. **95**(2): p. 424-+.
84. Csicsvari, J., et al., *Ensemble patterns of hippocampal CA3-CA1 neurons during sharp wave-associated population events.* Neuron, 2000. **28**(2): p. 585-594.
85. Ylinen, A., et al., *Sharp Wave-Associated High-Frequency Oscillation (200-Hz) in the Intact Hippocampus - Network and Intracellular Mechanisms.* Journal of Neuroscience, 1995. **15**(1): p. 30-46.
86. Buzsaki, G., et al., *High-Frequency Network Oscillation in the Hippocampus.* Science, 1992. **256**(5059): p. 1025-1027.
87. Csicsvari, J., et al., *Reliability and state dependence of pyramidal cell-interneuron synapses in the hippocampus: an ensemble approach in the behaving rat.* Neuron, 1998. **21**(1): p. 179-189.
88. Foster, D.J. and M.A. Wilson, *Reverse replay of behavioural sequences in hippocampal place cells during the awake state.* Nature, 2006. **440**(7084): p. 680-683.
89. Girardeau, G., I. Inema, and G. Buzsaki, *Reactivations of emotional memory in the hippocampus-amygdala system during sleep.* Nature Neuroscience, 2017. **20**(11): p. 1634-+.
90. Lansink, C.S., et al., *Hippocampus Leads Ventral Striatum in Replay of Place-Reward Information.* Plos Biology, 2009. **7**(8).
91. Lee, A.K. and M.A. Wilson, *Memory of sequential experience in the hippocampus during slow wave sleep.* Neuron, 2002. **36**(6): p. 1183-1194.

92. Nadasdy, Z., et al., *Replay and time compression of recurring spike sequences in the hippocampus.* Journal of Neuroscience, 1999. **19**(21): p. 9497-9507.
93. Peyrache, A., et al., *Replay of rule-learning related neural patterns in the prefrontal cortex during sleep.* Nature Neuroscience, 2009. **12**(7): p. 919-U143.
94. Buzsaki, G., *Two-stage model of memory trace formation: a role for "noisy" brain states.* Neuroscience, 1989. **31**(3): p. 551-70.
95. Eschenko, O., et al., *Sustained increase in hippocampal sharp-wave ripple activity during slow-wave sleep after learning.* Learning & Memory, 2008. **15**(4): p. 222-228.
96. Ramadan, W., O. Eschenko, and S.J. Sara, *Hippocampal Sharp Wave/Ripples during Sleep for Consolidation of Associative Memory.* Plos One, 2009. **4**(8).
97. Ego-Stengel, V. and M.A. Wilson, *Disruption of Ripple-Associated Hippocampal Activity During Rest Impairs Spatial Learning in the Rat.* Hippocampus, 2010. **20**(1): p. 1-10.
98. Girardeau, G., et al., *Selective suppression of hippocampal ripples impairs spatial memory.* Nature Neuroscience, 2009. **12**(10): p. 1222-1223.
99. Jadhav, S.P., et al., *Awake hippocampal sharp-wave ripples support spatial memory.* Science, 2012. **336**(6087): p. 1454-8.
100. Fernandez-Ruiz, A., et al., *Long-duration hippocampal sharp wave ripples improve memory.* Science, 2019. **364**(6445): p. 1082-1086.
101. Tang, W.B. and S.P. Jadhav, *Sharp-wave ripples as a signature of hippocampal-prefrontal reactivation for memory during sleep and waking states.* Neurobiology of Learning and Memory, 2019. **160**: p. 11-20.
102. Todorova, R. and M. Zugaro, *Hippocampal ripples as a mode of communication with cortical and subcortical areas.* Hippocampus, 2020. **30**(1): p. 39-49.
103. Wang, D.V. and S. Ikemoto, *Coordinated Interaction between Hippocampal Sharp-Wave Ripples and Anterior Cingulate Unit Activity.* Journal of Neuroscience, 2016. **36**(41): p. 10663-10672.
104. Gomperts, S.N., F. Kloosterman, and M.A. Wilson, *VTA neurons coordinate with the hippocampal reactivation of spatial experience.* Elife, 2015. **4**.
105. Wang, D.V., et al., *Mesopontine median raphe regulates hippocampal ripple oscillation and memory consolidation.* Nature Neuroscience, 2015. **18**(5): p. 728-+.
106. Logothetis, N.K., *Neural-Event-Triggered fMRI of large-scale neural networks.* Current Opinion in Neurobiology, 2015. **31**: p. 214-222.
107. Varela, C. and M.A. Wilson, *mPFC spindle cycles organize sparse thalamic activation and recently active CA1 cells during non-REM sleep.* Elife, 2020. **9**.
108. Viejo, G. and A. Peyrache, *Precise coupling of the thalamic head-direction system to hippocampal ripples.* Nature Communications, 2020. **11**(1).
109. Yang, M.Y., N.K. Logothetis, and O. Eschenko, *Occurrence of Hippocampal Ripples is Associated with Activity Suppression in the Mediodorsal Thalamic Nucleus.* Journal of Neuroscience, 2019. **39**(3): p. 434-444.
110. Jensen, O. and L.L. Colgin, *Cross-frequency coupling between neuronal oscillations.* Trends in Cognitive Sciences, 2007. **11**(7): p. 267-269.
111. Wilson, M.A., C. Varela, and M. Remondes, *Phase organization of network computations.* Current Opinion in Neurobiology, 2015. **31**: p. 250-253.
112. Canolty, R.T. and R.T. Knight, *The functional role of cross-frequency coupling.* Trends in Cognitive Sciences, 2010. **14**(11): p. 506-515.
113. Hyafil, A., et al., *Neural Cross-Frequency Coupling: Connecting Architectures, Mechanisms, and Functions.* Trends in Neurosciences, 2015. **38**(11): p. 725-740.
114. Aru, J., et al., *Untangling cross-frequency coupling in neuroscience.* Current Opinion in Neurobiology, 2015. **31**: p. 51-61.

115. Canolty, R.T., et al., *High gamma power is phase-locked to theta oscillations in human neocortex.* Science, 2006. **313**(5793): p. 1626-1628.
116. Sirota, A., et al., *Entrainment of Neocortical Neurons and Gamma Oscillations by the Hippocampal Theta Rhythm.* Neuron, 2008. **60**(4): p. 683-697.
117. Colgin, L.L., *Theta-gamma coupling in the entorhinal-hippocampal system.* Current Opinion in Neurobiology, 2015. **31**: p. 45-50.
118. Spyropoulos, G., C.A. Bosman, and P. Fries, *A theta rhythm in macaque visual cortex and its attentional modulation.* Proceedings of the National Academy of Sciences of the United States of America, 2018. **115**(24): p. E5614-E5623.
119. Molle, M. and J. Born, *Slow oscillations orchestrating fast oscillations and memory consolidation.* Slow Brain Oscillations of Sleep, Resting State and Vigilance, 2011. **193**: p. 93-110.
120. Sirota, A., et al., *Communication between neocortex and hippocampus during sleep in rodents.* Proceedings of the National Academy of Sciences of the United States of America, 2003. **100**(4): p. 2065-2069.
121. Molle, M., et al., *Grouping of spindle activity during slow oscillations in human non-rapid eye movement sleep.* Journal of Neuroscience, 2002. **22**(24): p. 10941-10947.
122. Niethard, N., et al., *Cortical circuit activity underlying sleep slow oscillations and spindles.* Proceedings of the National Academy of Sciences of the United States of America, 2018. **115**(39): p. E9220-E9229.
123. Staresina, B.P., et al., *Hierarchical nesting of slow oscillations, spindles and ripples in the human hippocampus during sleep.* Nature Neuroscience, 2015. **18**(11): p. 1679-1686.
124. Molle, M., et al., *Hippocampal sharp wave-ripples linked to slow oscillations in rat slow-wave sleep.* Journal of Neurophysiology, 2006. **96**(1): p. 62-70.
125. Klinzing, J.G., et al., *Spindle activity phase-locked to sleep slow oscillations.* Neuroimage, 2016. **134**: p. 607-616.
126. Battaglia, F.P., G.R. Sutherland, and B.L. McNaughton, *Hippocampal sharp wave bursts coincide with neocortical "up-state" transitions.* Learning & Memory, 2004. **11**(6): p. 697-704.
127. Sanda, P., et al., *Bidirectional Interaction of Hippocampal Ripples and Cortical Slow Waves Leads to Coordinated Spiking Activity During NREM Sleep.* Cereb Cortex, 2020.
128. Siapas, A.G. and M.A. Wilson, *Coordinated interactions between hippocampal ripples and cortical spindles during slow-wave sleep.* Neuron, 1998. **21**(5): p. 1123-1128.
129. Peyrache, A., F.P. Battaglia, and A. Destexhe, *Inhibition recruitment in prefrontal cortex during sleep spindles and gating of hippocampal inputs.* Proceedings of the National Academy of Sciences of the United States of America, 2011. **108**(41): p. 17207-17212.
130. Zsofia, C., et al., *Fine-tuned coupling between human parahippocampal ripples and sleep spindles.* European Journal of Neuroscience, 2011. **33**(3): p. 511-520.
131. Maingret, N., et al., *Hippocampo-cortical coupling mediates memory consolidation during sleep.* Nature Neuroscience, 2016. **19**(7): p. 959-964.
132. Novitskaya, Y., et al., *Ripple-triggered stimulation of the locus coeruleus during post-learning sleep disrupts ripple/spindle coupling and impairs memory consolidation.* Learning & Memory, 2016. **23**(5): p. 238-248.
133. Swift, K.M., et al., *Abnormal Locus Coeruleus Sleep Activity Alters Sleep Signatures of Memory Consolidation and Impairs Place Cell Stability and Spatial Memory.* Current Biology, 2018. **28**(22): p. 3599-+.
134. Poe, G.R., et al., *Locus coeruleus: a new look at the blue spot.* Nature Reviews Neuroscience, 2020.
135. Schwarz, L.A. and L.Q. Luo, *Organization of the Locus Coeruleus-Norepinephrine System.* Current Biology, 2015. **25**(21): p. R1051-R1056.

136. Schwarz, L.A., et al., *Viral-genetic tracing of the input-output organization of a central noradrenaline circuit.* Nature, 2015. **524**(7563): p. 88-U180.
137. Luppi, P.H., et al., *Afferent-Projections to the Rat Locus-Coeruleus Demonstrated by Retrograde and Anterograde Tracing with Cholera-Toxin-B Subunit and Phaseolus-Vulgaris-Leukoagglutinin.* Neuroscience, 1995. **65**(1): p. 119-160.
138. Astonjones, G., et al., *The Brain Nucleus Locus-Coeruleus - Restricted Afferent Control of a Broad Efferent Network.* Science, 1986. **234**(4777): p. 734-737.
139. Loughlin, S.E., S.L. Foote, and J.H. Fallon, *Locus Coeruleus Projections to Cortex - Topography, Morphology and Collateralization.* Brain Research Bulletin, 1982. **9**(1-6): p. 287-294.
140. Sara, S.J., *The locus coeruleus and noradrenergic modulation of cognition.* Nature Reviews Neuroscience, 2009. **10**(3): p. 211-223.
141. Moruzzi, G. and H.W. Magoun, *Brain Stem Reticular Formation and Activation of the Eeg.* Electroencephalography and Clinical Neurophysiology, 1949. **1**(4): p. 455-473.
142. McCarley, R.W. and J.A. Hobson, *Neuronal excitability modulation over the sleep cycle: a structural and mathematical model.* Science, 1975. **189**(4196): p. 58-60.
143. Astonjones, G. and F.E. Bloom, *Activity of Norepinephrine-Containing Locus Coeruleus Neurons in Behaving Rats Anticipates Fluctuations in the Sleep-Waking Cycle.* Journal of Neuroscience, 1981. **1**(8): p. 876-886.
144. Foote, S.L., G. Astonjones, and F.E. Bloom, *Impulse Activity of Locus Coeruleus Neurons in Awake Rats and Monkeys Is a Function of Sensory Stimulation and Arousal.* Proceedings of the National Academy of Sciences of the United States of America-Biological Sciences, 1980. **77**(5): p. 3033-3037.
145. Reimer, J., et al., *Pupil fluctuations track rapid changes in adrenergic and cholinergic activity in cortex.* Nature Communications, 2016. **7**.
146. Joshi, S., et al., *Relationships between Pupil Diameter and Neuronal Activity in the Locus Coeruleus, Colliculi, and Cingulate Cortex.* Neuron, 2016. **89**(1): p. 221-234.
147. Li, Y., et al., *Retrograde optogenetic characterization of the pontospinal module of the locus coeruleus with a canine adenoviral vector.* Brain Research, 2016. **1641**: p. 274-290.
148. Hayat, H., et al., *Locus coeruleus norepinephrine activity mediates sensory-evoked awakenings from sleep.* Science Advances, 2020. **6**(15).
149. Carter, M.E., et al., *Tuning arousal with optogenetic modulation of locus coeruleus neurons.* Nature Neuroscience, 2010. **13**(12): p. 1526-U117.
150. Bouret, S. and S.J. Sara, *Locus coeruleus activation modulates firing rate and temporal organization of odour-induced single-cell responses in rat piriform cortex.* European Journal of Neuroscience, 2002. **16**(12): p. 2371-2382.
151. Mccormick, D.A., H.C. Pape, and A. Williamson, *Actions of Norepinephrine in the Cerebral-Cortex and Thalamus - Implications for Function of the Central Noradrenergic System.* Neurobiology of the Locus Coeruleus, 1991. **88**: p. 293-305.
152. Videen, T.O., N.W. Daw, and R.K. Rader, *The Effect of Norepinephrine on Visual Cortical-Neurons in Kittens and Adult Cats.* Journal of Neuroscience, 1984. **4**(6): p. 1607-1617.
153. Rogawski, M.A. and G.K. Aghajanian, *Norepinephrine and Serotonin - Opposite Effects on the Activity of Lateral Geniculate Neurons Evoked by Optic Pathway Stimulation.* Experimental Neurology, 1980. **69**(3): p. 678-694.
154. Armstrong-James, M. and K. Fox, *Effects of ionophoresed noradrenaline on the spontaneous activity of neurones in rat primary somatosensory cortex.* J Physiol, 1983. **335**: p. 427-47.
155. Kasamatsu, T. and P. Heggelund, *Single cell responses in cat visual cortex to visual stimulation during iontophoresis of noradrenaline.* Exp Brain Res, 1982. **45**(3): p. 317-27.

156. Devilbiss, D.M. and B.D. Waterhouse, *The effects of tonic locus ceruleus output on sensory-evoked responses of ventral posterior medial thalamic and barrel field cortical neurons in the awake rat.* J Neurosci, 2004. **24**(48): p. 10773-85.
157. Waterhouse, B.D., H.C. Moises, and D.J. Woodward, *Noradrenergic modulation of somatosensory cortical neuronal responses to iontophoretically applied putative neurotransmitters.* Exp Neurol, 1980. **69**(1): p. 30-49.
158. Foote, S.L., R. Freedman, and A.P. Oliver, *Effects of Putative Neurotransmitters on Neuronal-Activity in Monkey Auditory-Cortex.* Brain Research, 1975. **86**(2): p. 229-242.
159. Waterhouse, B.D. and R.L. Navarra, *The locus coeruleus-norepinephrine system and sensory signal processing: A historical review and current perspectives.* Brain Research, 2019. **1709**: p. 1-15.
160. Lecas, J.C., *Locus coeruleus activation shortens synaptic drive while decreasing spike latency and jitter in sensorimotor cortex. Implications for neuronal integration.* European Journal of Neuroscience, 2004. **19**(9): p. 2519-2530.
161. Mclean, J. and B.D. Waterhouse, *Noradrenergic Modulation of Cat Area-17 Neuronal Responses to Moving Visual-Stimuli.* Brain Research, 1994. **667**(1): p. 83-97.
162. Waterhouse, B.D., et al., *Modulation of Rat Cortical Area-17 Neuronal Responses to Moving Visual-Stimuli during Norepinephrine and Serotonin Microiontophoresis.* Brain Research, 1990. **514**(2): p. 276-292.
163. Rodenkirch, C., et al., *Locus coeruleus activation enhances thalamic feature selectivity via norepinephrine regulation of intrathalamic circuit dynamics.* Nature Neuroscience, 2019. **22**(1): p. 120-+.
164. Edeline, J.M., Y. Manunta, and E. Hennevin, *Induction of selective plasticity in the frequency tuning of auditory cortex and auditory thalamus neurons by locus coeruleus stimulation.* Hearing Research, 2011. **274**(1-2): p. 75-84.
165. Manunta, Y. and J.M. Edeline, *Noradrenergic induction of selective plasticity in the frequency tuning of auditory cortex neurons.* Journal of Neurophysiology, 2004. **92**(3): p. 1445-1463.
166. Martins, A.R.O. and R.C. Froemke, *Coordinated forms of noradrenergic plasticity in the locus coeruleus and primary auditory cortex.* Nature Neuroscience, 2015. **18**(10): p. 1483-+.
167. Glennon, E., et al., *Locus coeruleus activation accelerates perceptual learning.* Brain Research, 2019. **1709**: p. 39-49.
168. Navarra, R.L., et al., *Methylphenidate Enhances Early-Stage Sensory Processing and Rodent Performance of a Visual Signal Detection Task.* Neuropsychopharmacology, 2017. **42**(6): p. 1326-1337.
169. Kety, S.S., *The possible role of the adrenergic systems of the cortex in learning.* Res Publ Assoc Res Nerv Ment Dis, 1972. **50**: p. 376-89.
170. Neuman, R.S. and C.W. Harley, *Long-Lasting Potentiation of the Dentate Gyrus Population Spike by Norepinephrine.* Brain Research, 1983. **273**(1): p. 162-165.
171. Stanton, P.K. and J.M. Sarvey, *Norepinephrine Regulates Long-Term Potentiation of Both the Population Spike and Dendritic Epsp in Hippocampal Dentate Gyrus.* Brain Research Bulletin, 1987. **18**(1): p. 115-119.
172. Vankov, A., A. Herveminvielle, and S.J. Sara, *Response to Novelty and Its Rapid Habituation in Locus-Coeruleus Neurons of the Freely Exploring Rat.* European Journal of Neuroscience, 1995. **7**(6): p. 1180-1187.
173. Kitchigina, V., et al., *Novelty-elicited, noradrenaline-dependent enhancement of excitability in the dentate gyrus.* European Journal of Neuroscience, 1997. **9**(1): p. 41-47.
174. Kaufman, A.M., T. Geiller, and A. Losonczy, *A Role for the Locus Coeruleus in Hippocampal CA1 Place Cell Reorganization during Spatial Reward Learning.* Neuron, 2020. **105**(6): p. 1018-+.

175. Bliss, T.V.P. and G.L. Collingridge, *A Synaptic Model of Memory - Long-Term Potentiation in the Hippocampus.* Nature, 1993. **361**(6407): p. 31-39.
176. Roullet, P. and S. Sara, *Consolidation of memory after its reactivation: Involvement of beta noradrenergic receptors in the late phase.* Neural Plasticity, 1998. **6**(3): p. 63-68.
177. Tronel, S., M.G.P. Feenstra, and S.J. Sara, *Noradrenergic action in prefrontal cortex in the late stage of memory consolidation.* Learning & Memory, 2004. **11**(4): p. 453-458.
178. Eschenko, O. and S.J. Sara, *Learning-Dependent, Transient Increase of Activity in Noradrenergic Neurons of Locus Coeruleus during Slow Wave Sleep in the Rat: Brain Stem-Cortex Interplay for Memory Consolidation?* Cerebral Cortex, 2008. **18**(11): p. 2596-2603.
179. Kempadoo, K.A., et al., *Dopamine release from the locus coeruleus to the dorsal hippocampus promotes spatial learning and memory.* Proceedings of the National Academy of Sciences of the United States of America, 2016. **113**(51): p. 14835-14840.
180. Wagatsuma, A., et al., *Locus coeruleus input to hippocampal CA3 drives single-trial learning of a novel context.* Proceedings of the National Academy of Sciences of the United States of America, 2018. **115**(2): p. E310-E316.
181. Takeuchi, T., et al., *Locus coeruleus and dopaminergic consolidation of everyday memory.* Nature, 2016. **537**(7620): p. 357-+.
182. Ray, J.P. and J.L. Price, *The Organization of the Thalamocortical Connections of the Mediodorsal Thalamic Nucleus in the Rat, Related to the Ventral Forebrain Prefrontal Cortex Topography.* Journal of Comparative Neurology, 1992. **323**(2): p. 167-197.
183. Mitchell, A.S. and S. Chakraborty, *What does the mediodorsal thalamus do?* Front Syst Neurosci, 2013. **7**: p. 37.
184. Groenewegen, H.J., *Organization of the Afferent Connections of the Mediodorsal Thalamic Nucleus in the Rat, Related to the Mediodorsal Prefrontal Topography.* Neuroscience, 1988. **24**(2): p. 379-431.
185. Burwell, R.D., *The parahippocampal region: Corticocortical connectivity.* Parahippocampal Region, 2000. **911**: p. 25-42.
186. Zikopoulos, B. and H. Barbas, *Prefrontal projections to the thalamic reticular nucleus form a unique circuit for attentional mechanisms.* Journal of Neuroscience, 2006. **26**(28): p. 7348-7361.
187. Aggleton, J.P. and M. Mishkin, *Projections of the Amygdala to the Thalamus in the Cynomolgus Monkey.* Journal of Comparative Neurology, 1984. **222**(1): p. 56-68.
188. Ray, J.P., et al., *Sources of Presumptive Glutamatergic Aspartatergic Afferents to the Mediodorsal Nucleus of the Thalamus in the Rat.* Journal of Comparative Neurology, 1992. **320**(4): p. 435-456.
189. Haber, S.N. and R. Calzavara, *The cortico-basal ganglia integrative network: The role of the thalamus.* Brain Research Bulletin, 2009. **78**(2-3): p. 69-74.
190. Mitchell, A.S., *The mediodorsal thalamus as a higher order thalamic relay nucleus important for learning and decision-making.* Neuroscience and Biobehavioral Reviews, 2015. **54**: p. 76-88.
191. Watanabe, Y. and S. Funahashi, *Thalamic mediodorsal nucleus and working memory.* Neuroscience and Biobehavioral Reviews, 2012. **36**(1): p. 134-142.
192. Ferguson, B. and K. Delevich, *Mediodorsal Thalamus and Prefrontal Cortex: Specialized Partners in Cognitive Control.* Journal of Neuroscience, 2020. **40**(29): p. 5515-5517.
193. Parnaudeau, S., S.S. Bolkan, and C. Kellendonk, *The Mediodorsal Thalamus: An Essential Partner of the Prefrontal Cortex for Cognition.* Biol Psychiatry, 2018. **83**(8): p. 648-656.
194. Fuster, J.M. and G.E. Alexander, *Firing changes in cells of the nucleus medialis dorsalis associated with delayed response behavior.* Brain Res, 1973. **61**: p. 79-91.

195. Neave, N., A. Sahgal, and J.P. Aggleton, *Lack of Effect of Dorsomedial Thalamic Lesions on Automated Tests of Spatial Memory in the Rat.* Behavioural Brain Research, 1993. **55**(1): p. 39-49.
196. Hunt, P.R. and J.P. Aggleton, *Medial Dorsal Thalamic Lesions and Working Memory in the Rat.* Behavioral and Neural Biology, 1991. **55**(2): p. 227-246.
197. Beracochea, D.J., R. Jaffard, and L.E. Jarrard, *Effects of Anterior or Dorsomedial Thalamic Ibotenic Lesions on Learning and Memory in Rats.* Behavioral and Neural Biology, 1989. **51**(3): p. 364-376.
198. Bailey, K.R. and R.G. Mair, *Lesions of specific and nonspecific thalamic nuclei affect prefrontal cortex-dependent aspects of spatial working memory.* Behavioral Neuroscience, 2005. **119**(2): p. 410-419.
199. Floresco, S.B., D.N. Braaksma, and A.G. Phillips, *Thalamic-cortical-striatal circuitry subserves working memory during delayed responding on a radial arm maze.* Journal of Neuroscience, 1999. **19**(24): p. 11061-11071.
200. Parnaudeau, S., et al., *Inhibition of Mediodorsal Thalamus Disrupts Thalamofrontal Connectivity and Cognition.* Neuron, 2013. **77**(6): p. 1151-1162.
201. Bolkan, S.S., et al., *Thalamic projections sustain prefrontal activity during working memory maintenance (vol 20, pg 987, 2017).* Nature Neuroscience, 2018. **21**(8): p. 1138-1138.
202. Schmitt, L.I., et al., *Thalamic amplification of cortical connectivity sustains attentional control.* Nature, 2017. **545**(7653): p. 219-+.
203. Markowitsch, H.J., *Diencephalic amnesia: a reorientation towards tracts?* Brain Res, 1988. **472**(4): p. 351-70.
204. Mair, R.G., *On the role of thalamic pathology in diencephalic amnesia.* Rev Neurosci, 1994. **5**(2): p. 105-40.
205. Tanaka, Y., et al., *Amnesia following damage to the mammillary bodies.* Neurology, 1997. **48**(1): p. 160-5.
206. Victor, M., R.D. Adams, and G.H. Collins, *The Wernicke-Korsakoff syndrome. A clinical and pathological study of 245 patients, 82 with post-mortem examinations.* Contemp Neurol Ser, 1971. **7**: p. 1-206.
207. Harding, A., et al., *Degeneration of anterior thalamic nuclei differentiates alcoholics with amnesia.* Brain, 2000. **123**: p. 141-154.
208. Baxter, M.G., *Mediodorsal thalamus and cognition in non-human primates.* Front Syst Neurosci, 2013. **7**: p. 38.
209. Stokes, K.A. and P.J. Best, *Mediodorsal thalamic lesions impair "reference" and "working" memory in rats.* Physiol Behav, 1990. **47**(3): p. 471-6.
210. Wolff, M., et al., *Functional heterogeneity of the limbic thalamus: From hippocampal to cortical functions.* Neurosci Biobehav Rev, 2015. **54**: p. 120-30.
211. Pergola, G., et al., *The Regulatory Role of the Human Mediodorsal Thalamus.* Trends in Cognitive Sciences, 2018. **22**(11): p. 1011-1025.
212. Gaffan, D. and S. Watkins, *Mediodorsal Thalamic Lesions Impair Long-Term Visual Associative Memory in Macaques.* European Journal of Neuroscience, 1991. **3**(7): p. 615-620.
213. Varela, C., et al., *Anatomical substrates for direct interactions between hippocampus, medial prefrontal cortex, and the thalamic nucleus reuniens.* Brain Structure & Function, 2014. **219**(3): p. 911-929.
214. Krettek, J.E. and J.L. Price, *The cortical projections of the mediodorsal nucleus and adjacent thalamic nuclei in the rat.* J Comp Neurol, 1977. **171**(2): p. 157-91.
215. Georgescu, I.A., D. Popa, and L. Zagrean, *The Anatomical and Functional Heterogeneity of the Mediodorsal Thalamus.* Brain Sci, 2020. **10**(9).

216. Floresco, S.B. and A.A. Grace, *Gating of hippocampal-evoked activity in prefrontal cortical neurons by inputs from the mediodorsal thalamus and ventral tegmental area.* Journal of Neuroscience, 2003. **23**(9): p. 3930-3943.
217. Koch, M., *The neurobiology of startle.* Prog Neurobiol, 1999. **59**(2): p. 107-28.
218. Kohl, S., et al., *Prepulse inhibition in psychiatric disorders - Apart from schizophrenia.* Journal of Psychiatric Research, 2013. **47**(4): p. 445-452.
219. Swerdlow, N.R. and M.A. Geyer, *Using an animal model of deficient sensorimotor gating to study the pathophysiology and new treatments of schizophrenia.* Schizophrenia Bulletin, 1998. **24**(2): p. 285-301.
220. Lee, Y.L., et al., *A primary acoustic startle pathway: Obligatory role of cochlear root neurons and the nucleus reticularis pontis caudalis.* Journal of Neuroscience, 1996. **16**(11): p. 3775-3789.
221. Yeomans, J.S. and P.W. Frankland, *The acoustic startle reflex: Neurons and connections.* Brain Research Reviews, 1995. **21**(3): p. 301-314.
222. Davis, M., et al., *A Primary Acoustic Startle Circuit - Lesion and Stimulation Studies.* Journal of Neuroscience, 1982. **2**(6): p. 791-805.
223. Swerdlow, N.R., M.A. Geyer, and D.L. Braff, *Neural circuit regulation of prepulse inhibition of startle in the rat: current knowledge and future challenges.* Psychopharmacology, 2001. **156**(2-3): p. 194-215.
224. Fendt, M., L. Li, and J.S. Yeomans, *Brain stem circuits mediating prepulse inhibition of the startle reflex.* Psychopharmacology, 2001. **156**(2-3): p. 216-224.
225. Azzopardi, E., et al., *The Role of Cholinergic Midbrain Neurons in Startle and Prepulse Inhibition.* Journal of Neuroscience, 2018. **38**(41): p. 8798-8808.
226. Schmid, S., et al., *VAChT knock-down mice show normal prepulse inhibition but disrupted long-term habituation.* Genes Brain and Behavior, 2011. **10**(4): p. 457-464.
227. MacLaren, D.A.A., T. Markovic, and S.D. Clark, *Assessment of sensorimotor gating following selective lesions of cholinergic pedunculopontine neurons.* European Journal of Neuroscience, 2014. **40**(10): p. 3526-3537.
228. Sara, S.J. and S. Bouret, *Orienting and Reorienting: The Locus Coeruleus Mediates Cognition through Arousal.* Neuron, 2012. **76**(1): p. 130-141.
229. Astonjones, G. and F.E. Bloom, *Norepinephrine-Containing Locus Coeruleus Neurons in Behaving Rats Exhibit Pronounced Responses to Non-Noxious Environmental Stimuli.* Journal of Neuroscience, 1981. **1**(8): p. 887-900.
230. McBurney-Lin, J., et al., *Locus coeruleus-norepinephrine modulation of sensory processing and perception: A focused review.* Neuroscience and Biobehavioral Reviews, 2019. **105**: p. 190-199.
231. Hurley, L.M., D.M. Devilbiss, and B.D. Waterhouse, *A matter of focus: monoaminergic modulation of stimulus coding in mammalian sensory networks.* Current Opinion in Neurobiology, 2004. **14**(4): p. 488-495.
232. Logothetis, N.K., et al., *Hippocampal-cortical interaction during periods of subcortical silence.* Nature, 2012. **491**(7425): p. 547-553.
233. Hansen, N. and D. Manahan-Vaughan, *Locus Coeruleus Stimulation Facilitates Long-Term Depression in the Dentate Gyrus That Requires Activation of beta-Adrenergic Receptors.* Cerebral Cortex, 2015. **25**(7): p. 1889-1896.
234. Hansen, N. and D. Manahan-Vaughan, *Hippocampal long-term potentiation that is elicited by perforant path stimulation or that occurs in conjunction with spatial learning is tightly controlled by beta-adrenoreceptors and the locus coeruleus.* Hippocampus, 2015. **25**(11): p. 1285-1298.
235. Chrobak, J.J. and G. Buzsaki, *High-frequency oscillations in the output networks of the hippocampal-entorhinal axis of the freely behaving rat.* Journal of Neuroscience, 1996. **16**(9): p. 3056-3066.

236. Skelin, I., S. Kilianski, and B.L. McNaughton, *Hippocampal coupling with cortical and subcortical structures in the context of memory consolidation.* Neurobiology of Learning and Memory, 2019. **160**: p. 21-31.
237. Wang, S.H. and R.G. Morris, *Hippocampal-neocortical interactions in memory formation, consolidation, and reconsolidation.* Annu Rev Psychol, 2010. **61**: p. 49-79, C1-4.
238. Jay, T.M., et al., *Excitatory Amino Acid Pathway from the Hippocampus to the Prefrontal Cortex. Contribution of AMPA Receptors in Hippocampo-prefrontal Cortex Transmission.* Eur J Neurosci, 1992. **4**(12): p. 1285-1295.
239. Van der Werf, Y.D., et al., *Contributions of thalamic nuclei to declarative memory functioning.* Cortex, 2003. **39**(4-5): p. 1047-62.
240. Markowitsch, H.J., *Thalamic mediodorsal nucleus and memory: a critical evaluation of studies in animals and man.* Neurosci Biobehav Rev, 1982. **6**(3): p. 351-80.
241. Ketz, N.A., O. Jensen, and R.C. O'Reilly, *Thalamic pathways underlying prefrontal cortex-medial temporal lobe oscillatory interactions.* Trends Neurosci, 2015. **38**(1): p. 3-12.
242. Wu, M.F., B.N. Mallick, and J.M. Siegel, *Lateral geniculate spikes, muscle atonia and startle response elicited by auditory stimuli as a function of stimulus parameters and arousal state.* Brain Res, 1989. **499**(1): p. 7-17.
243. Kaufman, L.S., *PGO waves in rats in the non-paradoxical sleep states.* Brain Res, 1983. **276**(1): p. 73-80.
244. Steriade, M. and I. Timofeev, *Neuronal plasticity in thalamocortical networks during sleep and waking oscillations.* Neuron, 2003. **37**(4): p. 563-76.
245. Yeomans, J.S., et al., *Midbrain pathways for prepulse inhibition and startle activation in rat.* Neuroscience, 2006. **142**(4): p. 921-9.
246. Samuels, E.R., et al., *Modulation of the acoustic startle response by the level of arousal: Comparison of clonidine and modafinil in healthy volunteers.* Neuropsychopharmacology, 2007. **32**(11): p. 2405-2421.
247. Roumis, D.K. and L.M. Frank, *Hippocampal sharp-wave ripples in waking and sleeping states.* Current Opinion in Neurobiology, 2015. **35**: p. 6-12.
248. Tang, W.B., et al., *Hippocampal-Prefrontal Reactivation during Learning Is Stronger in Awake Compared with Sleep States.* Journal of Neuroscience, 2017. **37**(49): p. 11789-11805.
249. Timofeev, I. and S. Chauvette, *Sleep slow oscillation and plasticity.* Current Opinion in Neurobiology, 2017. **44**: p. 116-126.
250. Ramirez-Villegas, J.F., N.K. Logothetis, and M. Besserve, *Diversity of sharp-wave-ripple LFP signatures reveals differentiated brain-wide dynamical events.* Proceedings of the National Academy of Sciences of the United States of America, 2015. **112**(46): p. E6379-E6387.

2.5 List of manuscripts/papers and statement of contributions

M1:

Yang, M., Logothetis, N. K., & Eschenko, O. (2021). Phasic activation of the locus coeruleus attenuates the acoustic startle response via increasing cortical arousal. Scientific Reports, 11(1), 1-14.

Conception and design: MY and OE; data acquisition and analysis: MY; figures: MY; data interpretation: MY, NKL and OE; first draft: MY; substantial revision: OE.

M2:

Yang, M., Sara, S. J., Logothetis, N. K., & Eschenko, O. (2020). The locus coeruleus activity during hippocampal-cortical communication. In preparation**.**

Conception and design: MY and OE; data acquisition: MY and OE; data analysis: MY; figures: MY; data interpretation: MY, NKL, SJS and OE; first draft: MY; substantial revision: OE.

M3:

Yang, M., Logothetis, N. K., & Eschenko, O. (2019). Occurrence of hippocampal ripples is associated with activity suppression in the mediodorsal thalamic nucleus. Journal of Neuroscience, 39(3), 434-444.

Conception and design: MY and OE; data acquisition and analysis: MY; figures: MY; data interpretation: MY, NKL and OE; first draft: MY; substantial revision: OE.

scientific reports

OPEN

Phasic activation of the locus coeruleus attenuates the acoustic startle response by increasing cortical arousal

Mingyu Yang[1], Nikos K. Logothetis[1,2] & Oxana Eschenko[1]✉

An alerting sound elicits the Acoustic Startle Response (ASR) that is dependent on the sound volume and organisms' state, which is regulated by neuromodulatory centers. The locus coeruleus (LC) neurons respond to salient stimuli and noradrenaline release affects sensory processing, including auditory. The LC hyperactivity is detrimental for sensorimotor gating. We report here that priming microstimulation of the LC (100-ms at 20, 50, and 100 Hz) attenuated the ASR in rats. The ASR reduction scaled with frequency and 100 Hz-stimulation mimicked pre-exposure to a non-startling tone (prepulse). A rapid (~40 ms) EEG desynchronization following the LC stimulation suggested that the ASR reduction was due to elevated cortical arousal. The effects of LC stimulation on the ASR and EEG were consistent with systematic relationships between the ASR, awake/sleep state, and the cortical arousal level; for that matter, a lower ASR amplitude corresponded to a higher arousal level. Thus, the LC appears to modulate the ASR circuit via its diffuse ascending projections to the forebrain saliency network. The LC modulation directly in the brainstem and/or spinal cord may also play a role. Our findings suggest the LC as a part of the brain circuitry regulating the ASR, while underlying neurophysiological mechanisms require further investigation.

An alerting stimulus can induce an eye blink, contraction of the facial, neck, and skeletal muscles as well as various visceral reactions. These innate startle reflexes, which are triggered by abrupt environmental changes, initiate more complex forms of adaptive response from orienting and exploration[1] to defensive behaviors[2]. The startle reflex can be elicited through different sensory modalities, including visual, tactile, vestibular, or acoustic. The Acoustic Startle Response is known to depend on the sound volume, but also the arousal level or emotional state[3]. The ASR is attenuated by pre-exposure to a non-startling stimulus (prepulse). The ASR and prepulse inhibition (PPI) are commonly used for testing sensorimotor integration in animals and humans and as diagnostic tools for mental fatigue and various neuropsychiatric conditions with disrupted sensorimotor processing, such as schizophrenia, attention disorder, or autism[4,5]. The primary mammalian ASR circuit consists of a short pathway linking the auditory nerve and cochlear root neurons (CRN) with spinal motor neurons through the caudal pontine reticular nucleus (PnC)[6–8]. The PPI circuit is more complex and the mechanisms mediating PPI are not yet fully understood[9,10]. It is commonly accepted that the auditory prepulse is relayed through the CRN, the inferior (IC) and superior (SC) colliculi, and activates the pedunculopontine tegmental nucleus (PPTg), which sends inhibitory projections on the PnC giant neurons resulting in the ASR attenuation[3,9,10]. Despite the existence of multiple top-down and neuromodulatory inputs converging on the PnC[11], the predominant role for inhibiting the ASR circuit has been long assigned to the cholinergic projection from the PPTg to PnC[3]. However, new evidence challenged this long-standing view[12–14] encouraging reconsidering the functional connectivity of the ASR/PPI circuit.

The brainstem noradrenergic nucleus locus coeruleus is a part of the ascending arousal system[15]. The role of LC phasic response in mediating the orienting response and attention is well known[16]. Salient stimuli elicit phasic discharge of LC neurons[17,18] and associated noradrenaline (NA) release in the LC forebrain targets affects sensory processing[19,20], including auditory[21–23]. The results of pharmacological and lesion studies suggested that the LC-NA system exerts an excitatory effect on the ASR circuit[24–27]. The LC hyperactivity and enhanced NA transmission within distinct thalamocortical and ventral forebrain networks lead to the PPI deficiency[28,29]. In

[1]Department of Physiology of Cognitive Processes, Max Planck Institute for Biological Cybernetics, Tübingen, Germany. [2]Division of Imaging Science and Biomedical Engineering, University of Manchester, Manchester M13 9PT, UK. ✉email: oxana.eschenko@tuebingen.mpg.de

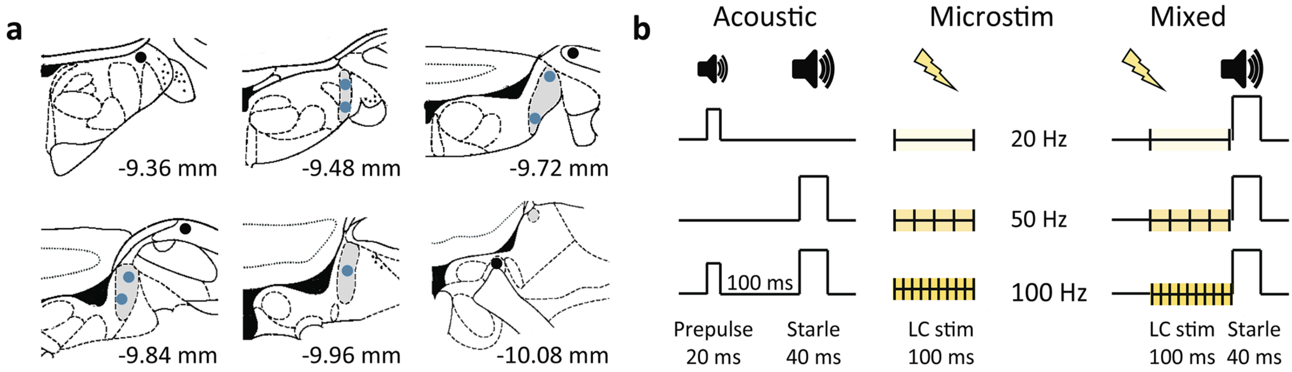

Figure 1. Experimental design. (**a**) Placement reconstruction of the stimulation electrode. The LC core is shown in grey; filled circles show the electrode tips. Different anterior–posterior planes are shown; numbers indicate the distance from bregma according to the rat brain atlas[84]. (**b**) Schematic representation of the experimental design. Each session included acoustic, microstimulation, and mixed (microstimulation preceded by startle) trials resulting in 9 trial types. The acoustic trials included prepulse, startle alone or preceded by prepulse. The microstimulation trials included delivery of a mild (0.05 mA) electric current at different pulse frequencies (20, 50, and 100 Hz) for 100 ms. During mixed trials, microstimulation preceded the startling sound. Forty repetitions of each trial type were randomly presented with a 10–20-s ITI.

contrast, the LC phasic response promotes cortical encoding of salient stimuli[30]. It has been long established that elevated tonic firing of the LC-NA neurons makes the LC sensory-evoked response less pronounced[31]; the latter possibly results in less efficient sensorimotor integration. To our knowledge, LC neural activity has not been characterized using the ASR/PPI paradigm, leaving the role of the LC auditory-evoked response in the sensorimotor gating underlying ASR and PPI unknown. In the present study, we mimicked the LC phasic response by applying a mild electric current to the LC cell bodies[32] and paired the LC stimulation with the startling sound. In the past, microstimulation proved to be a valuable tool for dissecting the ASR/PPI circuit. Earlier studies applied electrical stimulation to the PPTg, IC, SC, or the ventral pallidum to simulate prepulse[33]. In Parkinson's disease patients, microstimulation of the subthalamic nucleus reduced the ASR[34]. Here we report that phasic LC activation paired with a startle-eliciting sound attenuated the ASR to the same extent as the auditory prepulse.

Results

In total, 21 adult male rats were used in this study. Each rat was first habituated to the test chamber where rats were exposed to sounds and the electroencephalography (EEG) recording and microstimulation took place. The rat motor activity level was assessed by measuring the deflection amplitude of a movement-sensitive floor. Before the main experiment, each rat was subjected to preliminary tests aiming at adjusting the acoustic and microstimulation parameters. In all rats, the intensity of prepulse sound was adjusted not to elicit any above-threshold movement, whereas the startling sound was set to reliably evoke the ASR. In the first cohort of rats ($n = 14$), two skull screws were used for EEG monitoring and a stimulating electrode was implanted in the LC area. After post-surgical recovery rats were exposed to acoustic stimuli (prepulse: 10 kHz pure tone, 20 ms, 70 dB; startle: broadband noise, 40 ms, 100 dB) presented separately or sequentially (prepulse followed by startle) with a 100-ms interval in random order with a 10–20 s inter-trial interval (ITI). In the vast majority of the prepulse trials (range: 90–100%), the floor deflection amplitude remained within the 95% confidence interval (CI) calculated during episodes when no auditory stimuli were presented. The startling sound elicited above-threshold movement in 100% of trials in all rats. In the paired trials, when the startling sound was preceded by the prepulse, the ASR amplitude was consistently attenuated (Kolmogorov–Smirnov test, $p < 0.05$ for all rats). This phenomenon is commonly referred to as PPI. The average ASR reduction was $73.1 \pm 2.4\%$.

We next evaluated the effectiveness of microstimulation by the presence of a transient change in the EEG spectrogram. We have previously shown that the LC microstimulation in naturally sleeping rats caused an EEG power decrease in the delta (1–4 Hz) and sigma (12–16 Hz) bands and a power increase of frequencies above 30 Hz[35]. One rat had an invalid EEG signal and was excluded from the study. The 'effective' stimulation was observed in 7 out of 13 rats. Histological examination confirmed the electrode placement in the LC (Fig. 1a). The parameters for the LC stimulation have been further adjusted such that the strongest stimulation did not cause a motor response, awakening from sleep, or any aversive behaviors. The stimulation parameters were comparable to the ones used in our previous study[35]. In 6 rats, the application of electric current was 'ineffective' at any stimulation intensity. In 4 out of 6 rats, the electrode was located outside the LC (Fig. 1a); these rats made up a control (outside LC stimulation) group. In 2 rats, the electrode was in the LC (not shown); however, microstimulation was unreliable, likely due to the electrode damage or high impedance. Therefore, these 2 rats were excluded from the study.

The second cohort of rats ($n = 7$) was used for the assessment of sensorimotor gating as a function of arousal. The EEG was monitored, but no microstimulation was applied in this group. Preliminary testing using the same sound parameters as specified above showed that the ASR amplitude was mildly or not affected by preceding prepulse (Kolmogorov–Smirnov test, $p > 0.05$ for each rat). The average of ASR reduction was $21.6 \pm 2.0\%$ ($n = 7$

Experiment	Stimulation	Measurements	N rats (N sessions)	Sound level, dB prepulse/startle	PPI (%)*
Effect of LC phasic response on ASR	In LC	EEG, movement	7 (14)	70/100	70.8 ± 3.2
	Outside LC	EEG, movement	4 (14)		
Effect of arousal on ASR, PPI, and AEP	–	EEG, movement	3 (8)	75/100	74.4 ± 3.6
			4 (12)	70/105	78.5 ± 3.2

Table 1. Experimental groups and sound parameters. *Mean ± s.e.m are shown; %PPI did not differ between groups (one-way ANOVA, $F_{2,47} = 1.1$, $p = 0.3$).

rats). To obtain a reliable PPI, we adjusted the sound parameters after a series of calibration trials. In 3 rats, the combination of 75 dB-prepulse and 100 dB-startle was optimal, whereas in other 4 rats a combination of 70 dB-prepulse and 105 dB-startle produced the most consistent PPI. Using the adjusted sound parameters, the startling sound elicited the ASR in the vast majority of trials (94.8 ± 1.6%; n = 7 rats), whereas prepulse did not induce any above-threshold movement in 94.3 ± 1.7% of trials. The ASR amplitude was consistently attenuated by the prepulse (Kolmogorov–Smirnov test, $p < 0.05$ for each rat). Despite a slight difference in the auditory parameters, %PPI was comparable across experimental conditions (Table 1).

The data obtained from 18 rats were further analyzed (Table 1). Figure 1b illustrates the experimental design for the first cohort (n = 11). Each session included acoustic, microstimulation, and mixed (microstimulation preceded by startle) trials resulting in 9 trial types. The acoustic trials included prepulse, startle alone or preceded by prepulse. The microstimulation trials included delivery of a mild (0.05 mA) electric current at different pulse frequencies (20, 50, and 100 Hz) for 100 ms. During mixed trials, microstimulation preceded the startling sound. The second cohort (n = 7) was exposed to the acoustic trials only. In each session, 40 to 80 repetitions of each trial type were presented in random order with a 10–20 s ITI. The frontal EEG and rat's motor activity were continuously monitored.

Effect of priming LC stimulation on the acoustic startle response. To examine the role of LC phasic activation for the ASR, we applied a brief, 100-ms train of electric pulses in the direct proximity to the cell bodies of LC neurons 100 ms before presentation of a startling auditory tone (see "Materials and methods"). The ASR was measured by the deflection of a motion-sensitive floor. The effect of LC stimulation was validated in 14 sessions (n = 7 rats, 1–3 sessions per rat); stimulation outside the LC was assessed in 14 sessions (n = 4 rats, 1–5 sessions per rat). The ASR amplitude was substantially reduced when the startling sound was preceded by the LC stimulation. Figure 2a illustrates the data from a representative session. The ASR reduction was consistent across sessions (Wilcoxon signed-rank test, Z = 3.3, p = 0.001, r = 0.9). The repeated-measures analysis of variance (ANOVA) revealed the main effect of the stimulation frequency (20, 50, and 100 Hz) on the ASR amplitude ($F_{1.1,14.8} = 24.5$, $p = 0.00012$, $eta^2 = 0.7$; Greenhouse–Geisser corrected). Paired comparisons showed that LC stimulation at 50 and 100 Hz, but not at 20 Hz, significantly reduced the ASR (Fig. 2b). Furthermore, the effect scaled with the stimulation frequency such as the LC stimulation at 100 Hz caused the same degree of the ASR attenuation as the one produced by a prepulse sound (Wilcoxon signed-rank test, Z = 1.4, p = 0.16, r = 0.4; Fig. 2c). Importantly, the LC stimulation alone did not elicit a detectable motor response at any stimulation frequency as reflected by the floor deflections remaining within the 95% CIs for all trials. Stimulation outside the LC paired with the startle sound did not reduce the ASR (Wilcoxon signed-rank test, Z = 1.0, p = 0.3, r = 0.3).

The LC phasic activation may have transiently affected the functional connectivity within the ASR circuit and resulted in a stronger inhibition of the PnC giant neurons; the latter could occur due to non-specific activation of the ascending arousal system. We have previously reported that LC phasic activation is followed by a cortical state change[32,35,36]. To gain insights on the mechanism underlying the ASR attenuation by LC phasic activation, we performed a spectral analysis of the frontal EEG. Consistent with previous studies, the LC stimulation resulted in a rapid (~ 40 ms) change in the EEG spectral composition. Specifically, delta (1–4 Hz) power transiently decreased, while the power of higher frequencies, including the high-gamma (60–90 Hz) range, increased (Fig. 3a). We used the high-gamma range to avoid the EEG artifacts caused by the electric pulses at 50 Hz. The pattern of the EEG modulation was indicative of cortical arousal. To quantify the EEG modulation, we extracted the band-limited power in the delta and gamma ranges and z-score normalized to a 1-s window preceding the LC stimulation onset. The change of both delta and gamma power exceeded the threshold (± 1.96 z-score) for all sessions. We then compared the degree of power change as a function of stimulation strength. The repeated-measures ANOVA revealed the main effect of the stimulation frequency for both delta ($F_{2,26} = 17.3$, $p < 0.0001$, $eta^2 = 0.6$) and gamma ($F_{2,26} = 8.8$, $p = 0.001$, $eta^2 = 0.4$) bands with the maximal EEG modulation produced by the LC stimulation at 100 Hz (Fig. 3b). Interestingly, LC stimulation at 20 Hz was inefficient for both EEG and ASR modulation.

As described above, the LC phasic activation was accompanied by a transient change in the ongoing cortical state, which was reminiscent of microarousal. The LC stimulation repeated multiple times during the ~ 90-min session and thus may have also caused a shift in the rat behavioral state. We classified rat behavior into active awake, quiet awake, or non-rapid eye movement (NREM) sleep (see "Materials and methods") and compared across the LC-stimulated and control rats (outside-LC stimulation). Table 2 shows the percentage of time spent in each behavioral state. There was a significant effect of the behavioral state ($F_{2,52} = 4.1$, $p = 0.02$, $eta^2 = 0.1$), but no significant state × group interaction ($F_{2,52} = 1.2$, $p = 0.3$, $eta^2 = 0.05$). Thus, rats spent slightly less time in the active awake state; however, the LC stimulation did not affect rats' behavioral pattern.

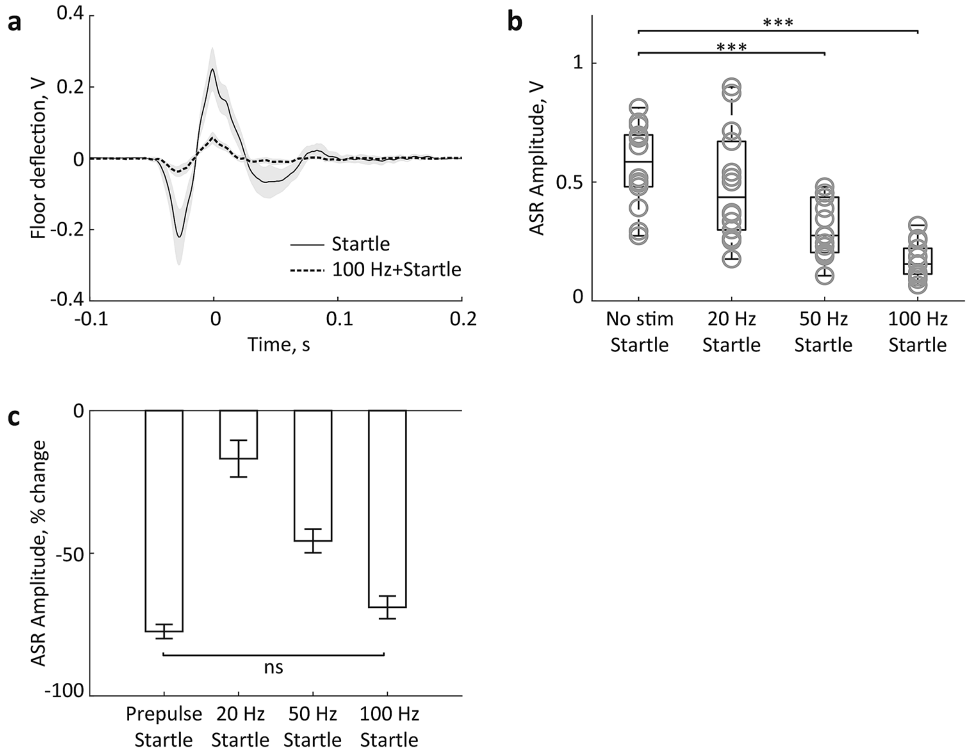

Figure 2. Priming LC stimulation attenuates the acoustic startle response. (**a**) The deflection shape of a movement-sensitive floor. Data from a representative session are shown. Traces are aligned to the maximal amplitude (t = 0) and averaged over the startle only trials (n = 40 trials) and the startle preceded by LC stimulation (n = 40 trials, 0.05 mA, 100 ms at 100 Hz); shadows show s.e.m. (**b**) The ASR amplitude elicited by the startle alone and the startle followed by LC stimulation at different frequencies. Box-whisker plots show the median, the first and third quartiles, min/max. Circles represent session averages. (**c**) The ASR amplitude change for different trial types. Note, the LC stimulation at 100 Hz mimicked the auditory prepulse. ***$p < 0.001$ (post hoc comparisons, Bonferroni corrected).

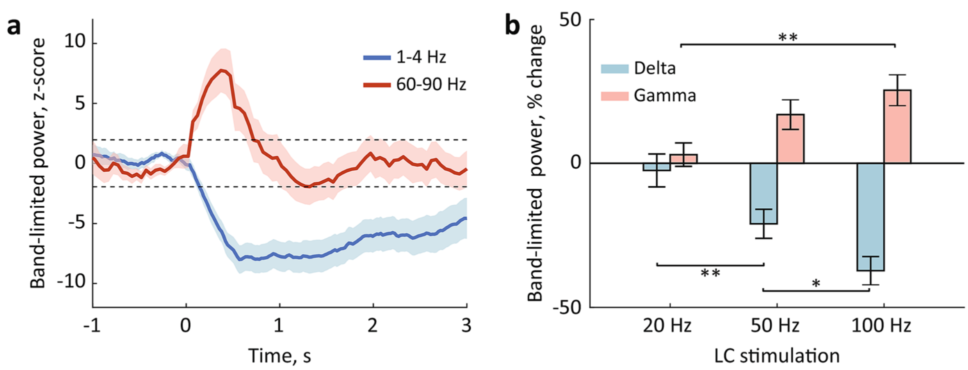

Figure 3. The EEG modulation by LC stimulation. (**a**) The EEG delta (1–4 Hz) and gamma (60–90 Hz) power around LC stimulation. Averages over 14 sessions (n = 7 rats) are plotted for LC stimulation at 100 Hz; shadows show s.e.m. (**b**) The delta and gamma power change produced by LC stimulation. *$p < 0.05$, **$p < 0.01$ (post hoc comparisons, Bonferroni corrected).

To summarize, the LC phasic activation shortly preceding the presentation of a salient sound resulted in the attenuated behavioral response. The EEG modulation induced by the LC stimulation was indicative of a transient increase of cortical arousal level, which could account for the ASR reduction. In contrast to tonic LC stimulation, a brief LC activation did not cause the behavioral state change. Our results point to the LC as a part of the ASR controlling network. The LC may directly modulate the ASR brainstem circuit via its descending projections and indirectly via its diffuse ascending projections to the brain regions comprising a saliency network.

	N rats (N sessions)	Active awake	Quiet awake	NREM sleep
In-LC stimulation	7 (14)	24.0 ± 3.4	44.6 ± 3.7	31.0 ± 4.0
Outside-LC stimulation	4 (14)	32.3 ± 4.2	37.7 ± 3.0	30.0 ± 5.2
Combined	11 (28)	28.1 ± 2.7*	41.2 ± 2.9	30.5 ± 3.3

Table 2. The awake/sleep states during testing. Percent session time is shown. *$p < 0.05$ for between-state comparison (Bonferroni corrected).

Effect of arousal on the acoustic startle response and prepulse inhibition. To directly examine the dependency of the ASR and PPI on the arousal level, we tested additional 7 rats on the acoustic trials while simultaneously monitored the frontal EEG; no microstimulation was applied in this group (Table 1). The prepulse, startle, and prepulse paired with startle were randomly presented to the spontaneously behaving rats. Each session contained 40 to 80 repetitions of each trial type. The data were collected from 20 sessions (2–4 sessions per rat). The ASR amplitude and % PPI substantially varied across trials (Fig. 4a). As we described above, the LC phasic activation reduced the ASR and increased the cortical arousal level. We assumed that a moment-to-moment fluctuation of the arousal level could be a variability source for the startle reactivity.

To characterize the cortical arousal level, we calculated the EEG synchronization index (SI). The EEG spectral analysis is broadly used for classifying the patterns of cortical activity associated with different levels of vigilance or different sleep stages[37]. The EEG-based methods have been validated by intracellular recordings[38]. It has been documented that during NREM sleep, the membrane potentials of cortical neurons fluctuate synchronously, which produces high-amplitude slow EEG rhythms; during awake, the membrane potential of cortical neurons is maintained at a depolarized level permitting non-synchronized neuronal firing, which in turn produces low-amplitude fast EEG oscillations[39]. The cortical arousal level is commonly assessed by the degree of synchronization of the cortical population. For example, Curto and colleagues[40] used a power ratio between 0–5 Hz and 0–50 Hz bands. In our previous work, we used a Down-State-Ratio or a band-limited power ratio for characterizing the ongoing cortical or behavioral state[35,36]. To calculate the SI, we extracted a delta (1–4 Hz)/gamma (30–90 Hz) power ratio over a 2-s time window before the stimulus onset. The SI-values varied from 0.1 to 28.2 and reflected moment-to-moment fluctuations of the cortical state (Fig. 4b,c). The distribution of SI-values for different behavioral states showed that $SI < 2.6$ indicated a high arousal state (active and quiet awake), while $SI > 2.6$ was indicative for NREM sleep (Fig. 4b). The SI did not discriminate the awake state with and without locomotion. Notably, a small proportion of NREM-episodes had low SI values, possibly indicating microarousal episodes. We split the low- and high-arousal trials according to the SI values and compared the behavioral variables. The ASR amplitude strongly depended on the arousal level (Wilcoxon signed-rank test, $Z = 3.6$, $p = 0.0003$, $r = 0.8$; Fig. 4d). At the same time, prepulse effectively attenuated the ASR regardless of the arousal level (Table 3). There was no difference in the efficiency of sensorimotor gating, as indicated by %PPI (Wilcoxon signed-rank test, $Z = 0.1$, $p = 0.9$, $r = 0.02$; Fig. 4e).

We next examined whether the effect of LC stimulation depended on the ongoing cortical state. We first quantified the EEG modulation induced by LC stimulation. We extracted the EEG delta and gamma power change (post- vs. pre-stimulation, see "Materials and methods" for details). The two-way ANOVA with the stimulation frequency (20, 50, 100 Hz) and arousal level (low vs. high) as repeated factors revealed that the EEG change depended on the stimulation frequency (delta: $F_{2, 26} = 19.8$, $p < 0.0001$, $eta^2 = 0.6$; gamma: $F_{2.26} = 10.1$, $p = 0.001$, $eta^2 = 0.4$) and the arousal level (delta: $F_{1,13} = 17.9$, $p = 0.001$, $eta^2 = 0.6$; gamma: $F_{1,13} = 10.3$, $p = 0.007$, $eta^2 = 0.4$). There was no significant frequency × arousal interaction for either delta ($F_{2,26} = 0.3$, $p = 0.7$, $eta^2 = 0.03$) or gamma ($F_{2,26} = 0.9$, $p = 0.4$, $eta^2 = 0.07$) power change. Thus, the EEG modulation in both delta and gamma ranges scaled with the stimulation frequency and was stronger during low arousal trials (Fig. 5a,b). Figure 5c shows the ASR amplitude for different stimulation frequencies and arousal levels. The repeated-measures ANOVA revealed the main effect of the stimulation frequency ($F_{1.1,14.1} = 20.0$, $p = 0.0004$, $eta^2 = 0.6$), but not the arousal level ($F_{1,13} = 1.7$, $p = 0.2$, $eta^2 = 0.1$). There was no significant frequency x arousal interaction ($F_{1.1, 14.6} = 1.5$, $p = 0.2$, $eta^2 = 0.1$). We also compared the magnitude of the ASR reduction calculated as a percentage change from the ASR amplitude elicited by startle only across stimulation frequencies and arousal levels (Fig. 5d). This analysis confirmed the effect of the stimulation frequency ($F_{1.3,16.6} = 26.5$, $p < 0.0001$, $eta^2 = 0.7$), but no effect of the arousal level ($F_{1,13} = 2.1$, $p = 0.2$, $eta^2 = 0.14$). There was no significant frequency x arousal interaction ($F_{1.4,18.2} = 0.8$, $p = 0.4$, $eta^2 = 0.06$).

Thus, both the EEG modulation and ASR attenuation produced by LC stimulation were proportional to the stimulation frequency. The neural response, as reflected by the EEG change, was also dependent on the ongoing cortical state. In contrast, both sensory gating (%PPI) and the effect of LC phasic activation on the ASR did not depend on the cortical arousal level.

Effect of arousal on the auditory evoked potential. We sought to examine if an Auditory Evoked Potential (AEP) varies with arousal. The AEPs were readily detected in the frontal EEG. Figure 6a shows a typical AEP shape with the characteristic N1 and P2 peaks. The maximal N1 and P2 amplitude were extracted, sorted according to the trial type (prepulse, startle, startle coupled with prepulse) and arousal level (low vs high). The N1- and P2-amplitudes were submitted to a two-way repeated-measures ANOVA with 3 trial types (prepulse, startle, startle coupled with prepulse) and two arousal levels as repeated factors. The ANOVA revealed a significant effect of the trial type for both N1 ($F_{1.5, 27.8} = 50.2$, $p < 0.0001$, $eta^2 = 0.7$) and P2 ($F_{2,38} = 15.1$, $p < 0.0001$,

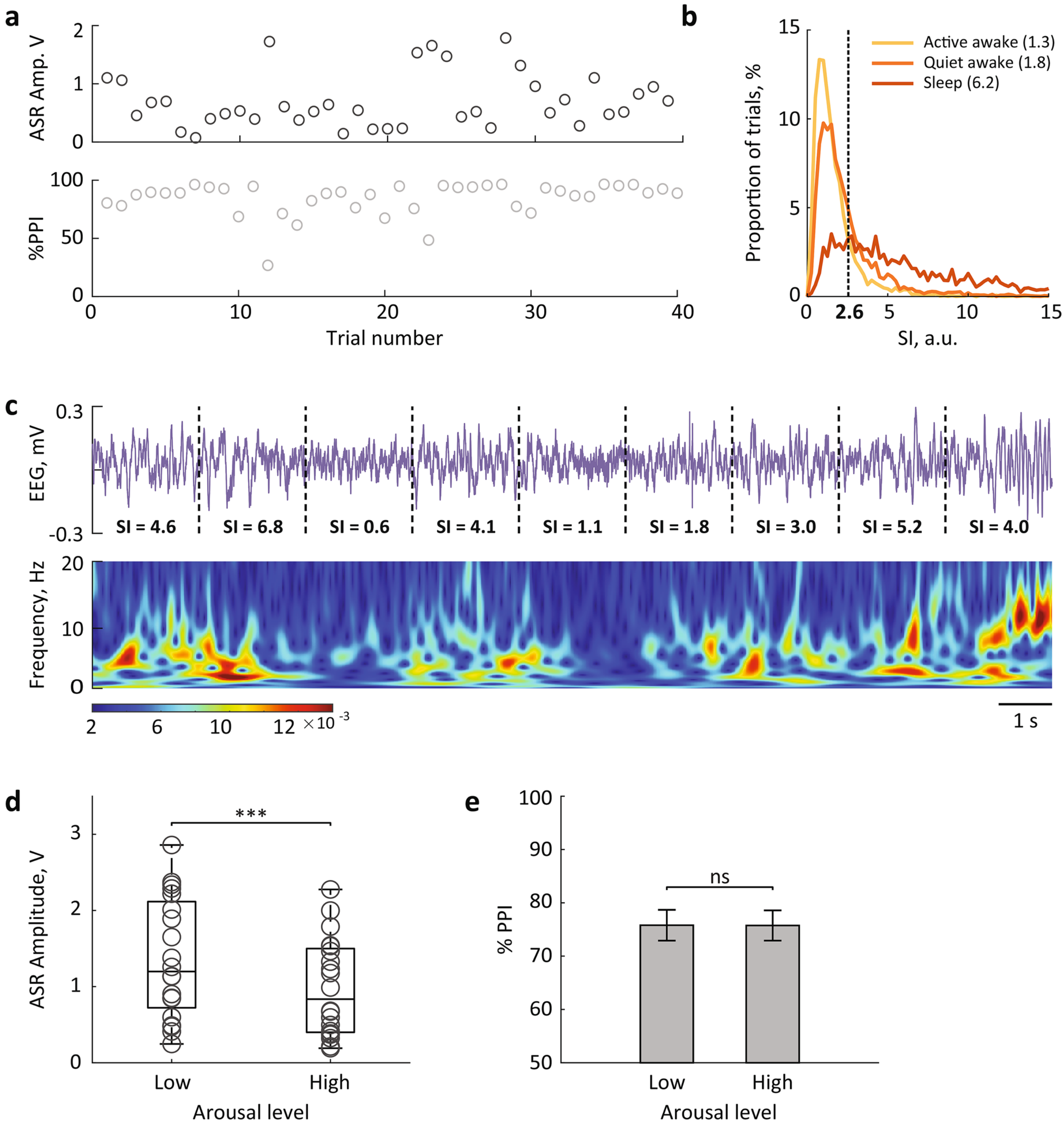

Figure 4. The ASR amplitude varies with arousal. (**a**) Trial-to-trial variability of the ASR amplitude (top) and %PPI (bottom) from a representative session. (**b**) Distribution and medians of SI-values during active awake, quiet awake and sleep states. The threshold for sorting the low and high arousal trials was chosen as the intersection between the SI distributions. (**c**) A representative EEG trace (top) and corresponding spectrogram (bottom) show the moment-to-moment fluctuation of the cortical arousal level; SI-value is indicated for each 2-s interval. (**d**,**e**) The ASR amplitude (**d**), but not %PPI (**e**) varied with arousal level. ***p < 0.001 (Wilcoxon signed-rank test).

Max floor deflection, volts	SI-high	SI-low
Startle trials	0.8 ± 0.2	1.2 ± 0.2
Prepulse + startle trials	0.1 ± 0.04***	0.2 ± 0.06***

Table 3. The prepulse sound attenuated the ASR at both low and high arousal levels. ***p < 0.001 for comparisons between different trial types (Wilcoxon signed-rank test).

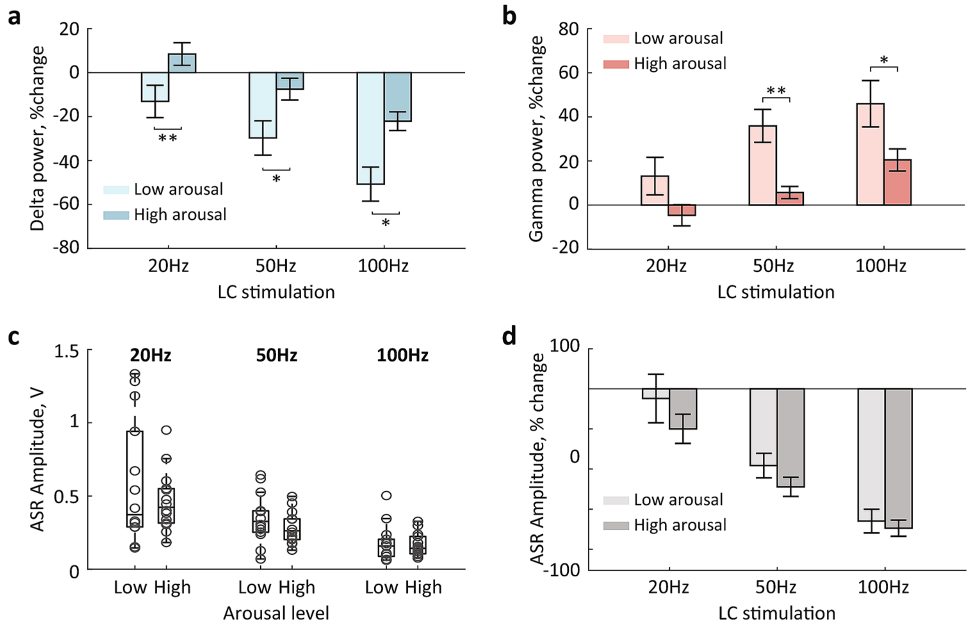

Figure 5. The effects of LC stimulation on the EEG and ASR. (**a**,**b**) The EEG delta (**a**) and gamma (**b**) power change produced by LC stimulation differed across arousal levels. (**c**,**d**) The ASR amplitude (**c**) and degree of ASR suppression (**d**) by preceding LC stimulation did not differ across arousal levels. *p < 0.05 and **p < 0.01 (Wilcoxon signed-rank test).

$eta^2 = 0.4$) amplitude, but no significant effect of arousal (N1: $F_{1,19} = 0.02$, $p = 0.9$, $eta^2 = 0.001$; P2: $F_{1,19} = 0.001$, $p = 0.97$, $eta^2 < 0.0001$). There was a significant trial type × arousal interaction for the N1-amplitude ($F_{1.5, 28.1} = 4.1$, $p = 0.04$, $eta^2 = 0.2$), but not the P2-amplitude ($F_{1.4, 27.3} = 2.2$, $p = 0.1$, $eta^2 = 0.1$). As expected, both N1- and P2-amplitude increased with higher sound intensity (Fig. 6b). Moreover, the N1-amplitude was lower when the startling sound was preceded by prepulse, just as the behavioral response (Fig. 2b). We observed no arousal-dependent effects on N1- and P2-amplitude (Fig. 6c,d). There was a tendency of a lower N1-amplitude for high arousal trials, but only for the trials with paired tones (Wilcoxon signed-rank test, $Z = 1.8$, $p = 0.07$, $r = 0.4$).

Finally, we assessed the relationships between the behavioral (ASR) and neuronal (AEP) response to acoustic stimulation by correlating the ASR and N1/P2 amplitudes. Since the prepulse tone did not elicit any reliable ASR, we included the startle trials and trials with paired tones in this analysis. We found systematic relationships between the ASR and N1, but not P2 (startle tone: $r = 0.3$, $p = 0.2$; paired tones: $r = 0.4$, $p = 0.1$). The ASR/N1 correlation was highly significant for each trial type (startle: $r = 0.8$, $p < 0.0001$; paired: $r = 0.6$, $p = 0.01$), but the correlation strength did not differ across arousal levels (Steiger's Z: startle: $Z = -1.2$, $p = 0.1$; paired: $Z = 0.9$, $p = 0.2$; Fig. 6e,f). Neither N1, nor P2 correlated with %PPI (N1: $r = 0.3$, $p = 0.2$; P2: $r = 0.1$, $p = 0.6$; not shown). Thus, both N1- and P2-amplitude reflected the auditory stimulus intensity, but only N1-amplitude was indicative of the behavioral responsivity to the auditory stimulation. The N1/ASR relationships, however, were not arousal-dependent.

Overall, our results are consistent with a view that activation of the arousal network underlies the ASR attenuation. We provided here several lines of evidence supporting this view. First, we have demonstrated that phasic LC activation reduced the ASR. Second, the LC stimulation rapidly elicited transient cortical arousal (as reflected by EEG delta and gamma power change). Third, we showed that a state of higher cortical arousal was associated with a weaker behavioral response. Our finding that the LC activation effectively modulated the ASR during states of high and low cortical arousal suggests that the LC may present a critical brainstem component regulating the ASR circuit.

Discussion

Our present study demonstrated that a brief phasic LC activation shortly preceding a startle-eliciting sound reduced the magnitude of the ASR in spontaneously behaving rats. The behavioral effect scaled with the frequency of LC stimulation and at 100 Hz mimicked the acoustic prepulse. The ASR attenuation by preceding LC activation was accompanied by a change of the EEG spectral components that were indicative of higher cortical arousal. In the microstimulation-free condition, the ASR amplitude was the lowest during the high arousal state. Thus, the effect of LC stimulation on the ASR may be mediated by activation of the arousal network; however, multiple alternative mechanisms including the LC directly affecting the brainstem ASR circuit, auditory input, or motor output cannot be ruled out.

A long-standing view attributed the ASR attenuation by prepulse to inhibition of the acoustically responsive PnC neurons by cholinergic input from the PPTg and the laterodorsal tegmentum (LDTg)[3]. Indeed, a priming stimulation of the PPTg or LDTg reduced the ASR[41]. However, the evidence is accumulating that the mechanism

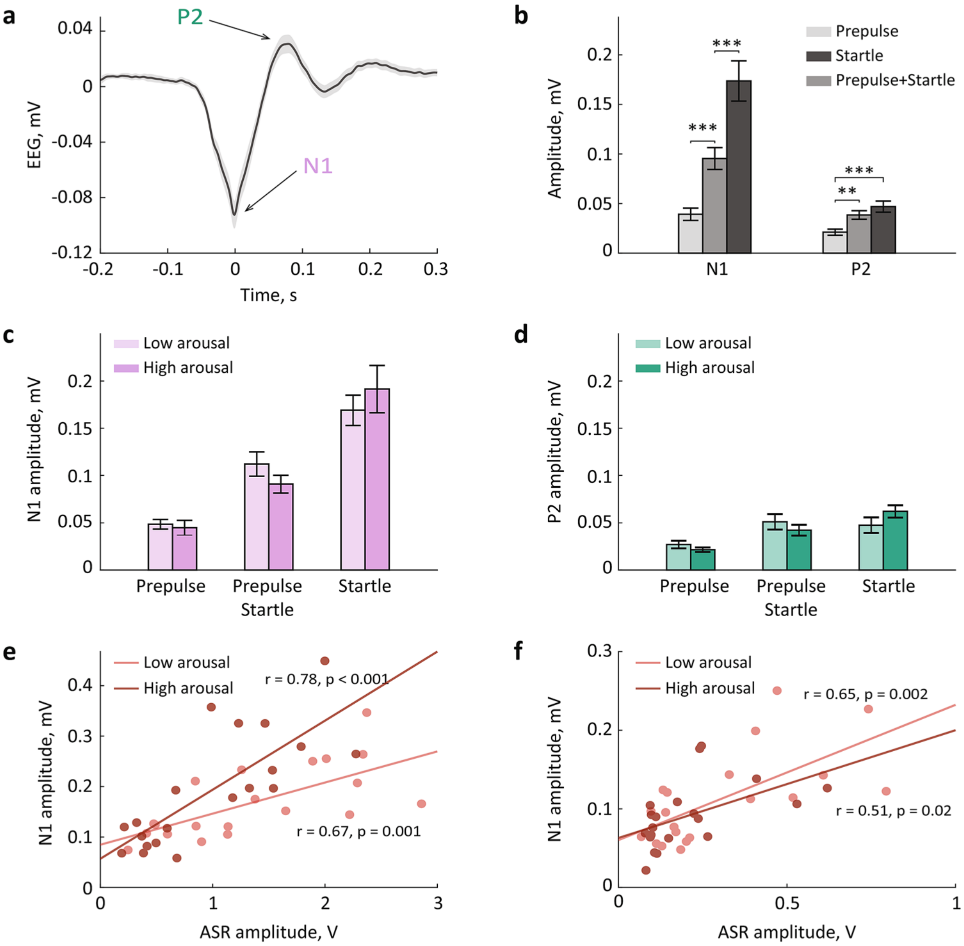

Figure 6. The auditory evoked potential varied across trial types, but not arousal levels. (**a**) A representative AEP trace. The peri-stimulus EEG was averaged over all startle only trials (n = 20 sessions, n = 7 rats); shadow shows s.e.m. Arrows point to the N1 and P2 peaks. (**b**) The N1- and P2-amplitude for different trial types. (**c**,**d**) The startle-elicited N1 (**c**) and P2 (**d**) amplitudes for low and high arousal trials. (**e**,**f**) The N1/ASR correlation for startle alone trials (**e**) and the trials with paired tones (**f**). **p < 0.01 and ***p < 0.001 (post hoc comparisons, Bonferroni corrected).

regulating the ASR/PPI circuit is more complex than previously thought. For example, it has been reported that knockout mice with reduced cholinergic tone had normal ASR and PPI[13]. Another study has shown that selective cholinergic lesions in the PPTg reduced the ASR without affecting the PPI[12]. Most recently, it has been documented that optogenetic activation of the PPTg cholinergic neurons enhanced the ASR[14]. Thus, GABAergic and/or glutamatergic PPTg neurons appear to be involved in the regulation of excitability within the ASR/PPI circuit[9]. Besides, it has been previously suggested that the role of cholinergic inputs to the ASR/PPI circuit may be restricted to the modulation of arousal[9]. Arousal mediating mechanism may underlie the effects of LC activation on the ASR.

The LC-NA neurons project diffusely throughout the forebrain and may affect sensorimotor processing via modulation of arousal[15]. Previous studies in rats and humans have demonstrated that pharmacological suppression of NA neurotransmission lowered arousal level and reduced the ASR amplitude[24,42,43], while enhanced NA neurotransmission disrupted the PPI, possibly due to hyperarousal[29]. A combination of the elevated tonic firing of LC-NA neurons with a reduced sensory-evoked LC phasic response that is associated with the states of high arousal[31,44] may result in less efficient sensorimotor integration. Here, we reported that during spontaneous behavior, pairing the LC stimulation with a startle-eliciting sound reduced the ASR. The ASR reduction after phasic LC activation was accompanied by a rapid (~ 40 ms) EEG desynchronization, as was reflected by a power decrease in lower (delta) and increase in higher (gamma) frequencies. The ASR reduction and EEG power change were state-dependent and proportional to the LC stimulation frequency. Thus, a transient increase of cortical arousal may underlie the ASR reduction. This view is consistent with the dependence of the ASR on the cortical arousal level. We consistently observed a higher proportion of low amplitude ASRs during active awake. The same observation was reported in an earlier study in cats[45], yet no difference across the awake/sleep cycle was found in rats[46]. In humans, the ASR amplitude is typically reduced by sedative drugs, including the ones acting on the cholinergic and noradrenergic receptors[42,43,47]. Thus, as was postulated for a higher-order cognition[48], the sensorimotor gating appears to benefit from the optimal level of the NA neurotransmission that is largely provided by a balanced tonic/phasic firing of the LC-NA neurons.

If the LC stimulation in our experiments mimicked the acoustic prepulse, regardless of the exact modulation target, LC neurons are expected to respond to acoustic stimuli of prepulse intensity. The LC auditory response is known to be highly dependent on sound parameters and behavioral context. Earlier studies reported that sounds of moderate volume (70 dB, 32 ms) did not elicit any LC response[49], while sounds eliciting an orienting response (> 96 dB) were effective[17,18,49,50]. In monkeys, LC response to a 70 ms burst of white noise at 75 dB was stronger during drowsiness than during cognitive task performance[31]. A recent study in rats demonstrated a robust LC response to 1 s tones at 76 dB[51], but LC response to shorter (0.25 s) sounds at 74 dB appears less reliable, as only 14% of neurons were responsive[52]. Although LC responses to short (20–40-ms) sounds, like the ones used in the ASR/PPI, remain to be characterized, existing evidence indicates that the LC may respond to prepulse. The latency of LC auditory response of 20–24 ms[18,53] is in good agreement with a delay of 20–500 ms between the prepulse and startle stimuli used in the PPI paradigm. It has been also reported that low-intensity sounds (~ 70 dB) reliably elicit a large-amplitude deflection of the extracellular potential in the LC with no accompanying motor response[53]. This sound-evoked potential resembles a ponto-geniculo-occipital (PGO) wave, a hallmark of REM sleep. The PGO-like waves occur outside REM sleep and indicate activation of the reticular alerting network[54,55]. Our observation that outside-LC stimulation failed to induce the EEG desynchronization was consistent with the absence of PGO-like waves in the pontine regions adjacent to the LC[53]. Thus, non-startling prepulse-like sounds induce enhanced peri-synaptic activity in the LC, while startling sounds evoke the LC phasic response and drive selection of adaptive behavior. The LC phasic photoactivation produced attentional signals, such as the P300 event-related potential, within the sensory processing network, including "false salience" in the absence of intense stimulus[30].

In our experiments, to elicit a synchronous discharge of LC neurons, we applied a mild electric current (0.05 mA) in direct proximity to the LC cell bodies. In our earlier study, we used similar stimulation parameters and demonstrated that unilateral current application elicits a robust discharge of LC neurons bilaterally; we also showed that stimulation-induced biphasic response profile (excitation followed by inhibition) resembled a naturalistic LC response to salient stimuli (e.g. foot shock)[32]. Moreover, the current intensity of 0.05 mA did not cause any neuronal damage around the electrode tip and the current spread did not exceed the size of the LC core[32]. Most importantly, in behaving rats, identical LC stimulation produced a transient change in the forebrain activity without causing awakening from natural sleep[35]. Although individual LC neurons typically fire at rates below 5 Hz, brief trains of pulses at 20–100 Hz possibly mimicked a synchronous discharge of the LC neuronal population; a burst-like discharge, as well as phasic stimulation, is more efficient for NA release[56,57]. Leaving aside a debatable cell-type selectivity of microstimulation, phasic LC activation was sufficient for increasing EEG arousal without causing awakening or any abrupt change of ongoing behavior. The LC stimulation at 20 Hz was not sufficient for the significant ASR reduction and caused no (or weak) EEG desynchronization. In contrast, the high-frequency (100 Hz) LC stimulation caused a pronounced change in the EEG and the magnitude of the ASR attenuation was comparable with the one produced by the auditory prepulse. Notably, the modulation of sensorimotor gating by LC phasic activation did not depend on the arousal level. We believe that in parallel to the effects in the forebrain, the LC stimulation caused a generalized reticular activation leading to a reduced ASR. The reticular formation being a site of NA action may explain a similar degree of the ASR modulation across different arousal levels.

Apart from activating the arousal network, the LC can affect the ASR/PPI circuit through modulating sensory input or auditory perception. The LC directly projects to the CRN[58] and other subcortical and cortical structures within the primary auditory pathway[59]. Pairing auditory stimulation with NA release leads to increased neuronal excitability and responsiveness in the auditory thalamus and cortex[22,23]. The LC projects to the IC, which is activated by the acoustic prepulse and exerts an inhibitory influence on the primary ASR pathway[41]. The IC receives up to 97% of its noradrenergic innervation from the LC[59,60] and NA release associated with LC activation may enhance the IC neuron excitability. The direct electrical stimulation of the IC attenuated the ASR[33]. Moreover, NA-mediated cortical arousal may engage cholinergic input to the IC via auditory cortex projections to the PPTg and LDTg[61]. Altogether, NA release within the auditory network may lead to a change in the auditory signal processing and perception. In our study, priming LC stimulation may have weakened the perception of the sound volume. In parallel, the LC may modulate the ASR/PPI circuit through its forebrain projections to the hippocampus, amygdala, or prefrontal cortex[62]. A long-standing view on the mechanism underlying the inhibitory effect of prepulse on the ASR considers the attentional shift towards a sudden sensory input[63]. Such an attentional shift may trigger reorienting and change of ongoing behavior[1]. The LC role in promoting attentional shift and reorienting is well known[16]. The orienting response toward a new stimulus may also inhibit the startle reflex[41]. Lastly, the LC can modulate motor outflow through its direct projections to the spinal motor neurons[64]. To the best of our knowledge, the role of the coeruleospinal pathway for modulation of the ASR/PPI circuit remains unclear. An earlier study showed that intrathecal administration of clonidine suppressed the ASR[25]. Phasic LC activation could reduce the excitability of spinal motor neurons and therefore the ASR magnitude via presynaptic inhibition[65]. The potentiation by NA of glycine-mediated inhibition in the spinal dorsal horn neurons has been also described[66].

In the present study, we also examined the effect of arousal on the AEPs recorded in the frontal EEG. The AEPs are recorded in many subcortical and cortical structures. The N1 and P2 peaks, two early AEP components, are commonly considered to reflect the sound intensity[67–69]. The AEP amplitude, like other sensory responses, is attenuated during low arousal states[70–72]. The state-dependency of AEPs greatly depends on their origin. The AEPs recorded from the rat primary auditory cortex were not modulated by vigilance state[73]. The EEG study in rats showed that the AEP amplitude in the frontal and parietal, but not in the occipital areas varied with arousal[70]. The AEPs originating from the reticular ascending inputs are typically state-dependent and rapidly habituate[74]. In the rat frontal EEG, we observed sound- but not arousal-modulated AEP. Differential AEP modulation was also observed in humans. In the frontal and central EEG, the N1 amplitude elicited by a low volume sound (~ 30 dB) decreased in lower arousal state[71], but N1 elicited by louder tones (~ 75 dB) was higher[75]. The inconsistent evidence for arousal-modulated AEP further illustrates that the state-dependency of the auditory processing depends on the engaged network and the features of sensory input. This notion is in agreement with previous reports that drugs disrupting the PPI may not affect the AEPs[47,76]. Finally, we revealed that the ASR and N1 amplitudes were correlated; thus, the N1 component of AEP may reflect both sensory input and motor output. Since the ASR/PPI tests are used for diagnostics, the event-related EEG oscillations, including the AEP, could provide a complementary tool to study psychopathology in clinical practice.

All in all, clearly there are multiple neural pathways, which underlie a rather complex regulation of a seemingly simple acoustic startle reflex. Different aspects of sensorimotor processing are reflected by various neural representations. The behavioral and neural correlates of sensorimotor processing may not share the same mechanism. Overall, our findings are consistent with a view that the startle reflex depends on the state of the organism. Our results suggest the involvement of the LC-NA system in the modulation of the ASR/PPI circuit, possibly via affecting the arousal network. The LC connectivity in the brainstem also supports the LC direct influencing the primary ASR/PPI circuit. The exact mechanisms underlying the effects of LC phasic activation on sensorimotor gating described here could and should be established in future studies.

Materials and methods

Animals. Twenty-one adult male Sprague–Dawley rats (Charles River Laboratory, Germany) weighing 300–450 g were used. After surgery rats were single-housed and had access to food and water ad libitum. Animals were tested between 10 a.m. and 6 p.m. during the dark phase of a 12 h light/dark cycle (8 a.m. lights off). All experiments were conducted following the German Animal Welfare Act (TierSchG) and Animal Welfare Laboratory Animal Ordinance (TierSchVersV). This is in full compliance with the guidelines of the EU Directive on the protection of animals used for scientific purposes (2010/63/EU). The study was reviewed by the ethics commission (§15 TierSchG) and approved by the state authority (Regierungspräsidium, Tübingen, Baden-Württemberg, Germany).

Surgery and electrode placement. Animals were anesthetized with isoflurane (initiation 4%, maintenance 1.5–2.0%). The depth of anesthesia was controlled by ensuring a lack of responses to mildly noxious stimuli (a hind paw pinch). Heart rate and blood oxygenation were monitored using a pulse oximeter (Nonin 8600V, Nonin Medical, Inc., Plymouth, MN); supplementary oxygen was provided to maintain the blood oxygenation level above 90%. Body temperature was maintained at ~ 37 °C throughout the entire anesthesia period. A fully anesthetized rat was fixed in a stereotaxic frame; the skull surface was adjusted horizontally. The skull was exposed and local anesthetic (Lidocard 2%, B. Braun, Germany) was applied on the skin edges to additionally numb the skin. Burr holes were made for electrodes and anchor screws. For EEG recording, a stainless steel screw (0.86 mm diameter, FST, Germany) was placed above the frontal cortex and the ground screw was placed above the cerebellum. Four anchor screws (1.19 mm diameter, FST, Germany) were placed on the skull side edges. Screws were fixed in the skull and additionally secured with tissue adhesive. The stimulation electrode (single platinum-iridium electrode, FHC, Bowdoin, ME) was placed in the LC using a high-precision stereotaxic micromanipulator (David Kopf Instruments, Tujunga, CA). The monopolar stimulation electrode was implanted at 15° angle 4.0–4.2 mm posterior to lambda, 1.0–1.2 mm lateral, and 5.5–6.2 mm deep. The accuracy of LC targeting was verified by online monitoring of neural activity. The LC neurons were identified by broad spike widths (~ 0.6 ms), regular low firing rate (1–2 spikes/s), and biphasic (excitation followed by inhibition) response to paw pinch. Once the electrode depth was optimized, the entire implant was secured on the skull with dental cement (Paladur, Heraeus Kulzer GmbH, Germany). The injection of analgesic (2.5 mg/kg, s.c; Finadyne, Essex) and antibiotic (5.0 mg/kg, s.c.; Baytril, Bayer) was given before rat awakening from anesthesia and repeated at 24 h intervals for 4 days. Animals were allowed 1 week of post-surgery recovery.

Electrophysiological recording and electrical stimulation. We used the same data acquisition setup as described elsewhere[35]. The EEG and ground electrodes were connected to the multichannel amplifier (MPC Plus, Alpha Omega Engineering, Israel) through an analog headstage (Plexon Inc, Dallas, USA), a flexible cable (Plexon Inc, Dallas, USA), and an in-house built preamplifier. The EEG signal was filtered (0.1–300 Hz), amplified (× 1k), and digitized using Power1401mkll (CED, UK). The stimulation and ground electrodes were connected to an in-house built current source via self-made cable via a 6-channel electrode pedestal (P1 Technologies, Roanoke, USA). The Spike2 software (CED, UK) and a digital-to-analog converter (Power 1401mkII, CED, UK) were used for controlling the current parameters. The voltage passed through the electrode tip was monitored via a custom-designed voltage output unit. The 100-ms trains of biphasic (cathodal leading) square pulses (0.4 ms, 0.05 mA) were delivered unilaterally at 20, 50, and 100 Hz. The stimulation parameters were selected based on our previous studies that characterized in detail the local and distal effects of the LC electrical stimulation[32,35]. Briefly, it has been shown that the current intensity of 0.05 mA does not cause neuronal damage around the electrode tip and the spread of depolarizing current does not exceed the size of the LC core. The unilateral current application elicited a robust discharge of LC neurons bilaterally and stimulation-induced discharge resembled a naturalistic LC response to salient stimuli. The LC stimulation at frequencies above 50 Hz induced a transient change in the forebrain activity without causing awakening from natural sleep. Before the main experiment, each rat was submitted to test stimulation when the stimulation effectiveness and the stimulation parameters were calibrated. The parameters of LC stimulation were selected such that the strongest stimulation induced a transient change in the EEG power spectrum without causing awakening from sleep or any adverse behaviors.

Behavioral testing. Rats were first habituated to a sound-attenuated chamber (60 cm × 40 cm × 40 cm) and the cable plugging procedure. After habituation, rats were tested on acoustic, microstimulation, and mixed (microstimulation/acoustic) trials as shown in Fig. 1b. The acoustic trials included startle (broadband noise, 40 ms, 100/105 dB), prepulse (10 kHz, 20 ms, 70/75 dB), or prepulse followed by startle with a 100-ms delay. The microstimulation trials included 100-ms trains of pulses at 20, 50, and 100 Hz. Mixed trials included microstimulation immediately followed by startle. Each trial type was randomly presented and repeated 40–80 times. The ITI varied between 10 and 20 s to avoid animal habituation to sounds. The trial presentation was controlled using the Spike2 software (CED, UK). Each session started with a 5-min habituation period, during which a continuous white background noise (50/55 dB) was presented. Each rat was tested in 1 to 5 sessions. The movement of the animal was measured via four floor-mounted vibration sensors; the floor deflection amplitude was converted to voltage and synchronized with EEG recording. The maximal movement amplitude was extracted from the 500-ms window after stimulus presentation. Baseline movement activity was calculated as maximal amplitude in a 1-s time window before the sound onset. The PPI was quantified as following: $\%PPI = (1 - ASR_{prepulse + startle}/ASR_{startle}) * 100\%$.

EEG spectral analysis. The effectiveness of LC stimulation was measured as a change in the EEG delta (1–4 Hz) and gamma (60–90 Hz) power. We used a high-gamma range to avoid EEG contamination with the artifacts produced by electric pulses at 50 Hz. The EEG delta oscillations are predominant during a low arousal state, such as NREM sleep and delta power fluctuates with arousal[77]. The EEG gamma activity is commonly interpreted as a signature of cortical and/or behavioral arousal[78,79]. Modulation of gamma oscillations has been implicated in saliency processing[80–82]. Based on extensive evidence, we used the EEG delta and gamma power change as a signature of cortical arousal. To quantify the EEG change, we extracted the band-limited power—1-s to 3-s around the stimulation onset using a multi-taper method (http://chronux.org/)[83]. The power was z-score normalized to a 1-s window before the stimulation onset and averaged across trials (20, 50, and 100 Hz). The power change above 1.96 z-score was considered as significant. To characterize the magnitude of the band-limited power change, we computed the power spectrum around LC stimulation; the 100-ms stimulation interval was excluded due to artifacts. The time window of ± 1 s and ± 0.2 s was used for the delta and gamma band, respectively. We then calculated the power change as a percentage of the pre-stimulation level.

To classify the behavioral state, each 2.5-s recording epoch was assigned to active awake, quiet awake, or NREM sleep using EEG and the movement detector. The epochs of active awake were identified by the presence of active locomotion; the epochs of quiet awake were identified by the absence of motor activity and above threshold theta (6–10 Hz)/delta (1–4 Hz) ratio; the epochs of NREM sleep were identified by the absence of motor activity and below threshold theta/delta ratio. The minimal duration of the same behavioral state was set to 20 s. The epochs in which the behavioral state could not be classified were excluded from the analysis (3.16 ± 0.25% of total recording time).

To quantify the cortical arousal level immediately preceding the stimulus presentation, we used a Synchronization Index (SI). The SI was calculated over a 2-s time window before the stimulus onset as a power ratio between delta (1–4 Hz) and gamma (30–90 Hz) bands. The SI distributions were calculated for each behavioral state and the SI-value at the intersection between distributions was used as a threshold for sorting the low and high arousal trials (Fig. 4b).

Statistical analysis. The ASR amplitude distributions from different trial types were compared using the Kolmogorov–Smirnov test. The non-parametric Wilcoxon signed-rank test was used for paired-comparisons of the population mean rank. The effect size of the Wilcoxon signed-rank test was calculated as $= \frac{Z}{\sqrt{Npair}}$. Different designs of analysis of variance (ANOVA) were used for comparing experimental conditions; the Greenhouse–Geisser correction was applied when the sphericity assumption was violated. The Bonferroni test was used for post-hoc comparisons. Pearson's linear correlation was used for correlation analysis. Steiger's Z test was used to compare the correlation strength. The statistical significance (α-value) was set at $p = 0.05$. The IBM SPSS Statistics (v.22) and Matlab (MathWorks) software packages were used for statistical analysis.

Perfusion and histology. After the final recording session, rats were euthanized (100 mg/kg, i.p., Narcoren, Merial) and perfused. Brains were removed and stored in paraformaldehyde until used. Before sectioning, brains were impregnated with sucrose until they sank. Serial 60-µm-thick coronal sections were cut on a horizontal freezing microtome (Microm HM 440E, Walldorf, Germany) and then directly Nissl stained or stored at − 20 °C in a cryoprotectant solution until further processing. All sections were examined using an AxioPhot or AxioImager microscope (Carl Zeiss, Goettingen, Germany). The electrode tracks were localized visually and digitized; the placement of the electrode tip was reconstructed.

Received: 29 May 2020; Accepted: 23 December 2020
Published online: 14 January 2021

References

1. Sokolov, E. N. Higher nervous functions; the orienting reflex. *Annu. Rev. Physiol.* **25**, 545–580. https://doi.org/10.1146/annurev.ph.25.030163.002553 (1963).

2. Grillon, C. Models and mechanisms of anxiety: Evidence from startle studies. *Psychopharmacology* **199**, 421–437. https://doi.org/10.1007/s00213-007-1019-1 (2008).
3. Koch, M. The neurobiology of startle. *Prog. Neurobiol.* **59**, 107–128 (1999).
4. Swerdlow, N. R. & Geyer, M. A. Using an animal model of deficient sensorimotor gating to study the pathophysiology and new treatments of schizophrenia. *Schizophr. Bull.* **24**, 285–301 (1998).
5. Kohl, S., Heekeren, K., Klosterkotter, J. & Kuhn, J. Prepulse inhibition in psychiatric disorders–apart from schizophrenia. *J. Psychiatr. Res.* **47**, 445–452. https://doi.org/10.1016/j.jpsychires.2012.11.018 (2013).
6. Davis, M., Gendelman, D. S., Tischler, M. D. & Gendelman, P. M. A primary acoustic startle circuit: Lesion and stimulation studies. *J. Neurosci.* **2**, 791–805 (1982).
7. Yeomans, J. S. & Frankland, P. W. The acoustic startle reflex: Neurons and connections. *Brain Res. Brain. Res. Rev.* **21**, 301–314. https://doi.org/10.1016/0165-0173(96)00004-5 (1995).
8. Lee, Y., López, D. E., Meloni, E. G. & Davis, M. A primary acoustic startle pathway: Obligatory role of cochlear root neurons and the nucleus reticularis pontis caudalis. *J. Neurosci.* **16**, 3775–3789. https://doi.org/10.1523/jneurosci.16-11-03775.1996 (1996).
9. Fendt, M., Li, L. & Yeomans, J. S. Brain stem circuits mediating prepulse inhibition of the startle reflex. *Psychopharmacology* **156**, 216–224. https://doi.org/10.1007/s002130100794 (2001).
10. Swerdlow, N. R., Geyer, M. A. & Braff, D. L. Neural circuit regulation of prepulse inhibition of startle in the rat: Current knowledge and future challenges. *Psychopharmacology* **156**, 194–215. https://doi.org/10.1007/s002130100799 (2001).
11. Li, L., Du, Y., Li, N., Wu, X. & Wu, Y. Top-down modulation of prepulse inhibition of the startle reflex in humans and rats. *Neurosci. Biobehav. Rev.* **33**, 1157–1167. https://doi.org/10.1016/j.neubiorev.2009.02.001 (2009).
12. MacLaren, D. A., Markovic, T. & Clark, S. D. Assessment of sensorimotor gating following selective lesions of cholinergic pedunculopontine neurons. *Eur. J. Neurosci.* **40**, 3526–3537. https://doi.org/10.1111/ejn.12716 (2014).
13. Schmid, S., Azzopardi, E., De Jaeger, X., Prado, M. A. M. & Prado, V. F. VAChT knock-down mice show normal prepulse inhibition but disrupted long-term habituation. *Genes Brain Behav.* **10**, 457–464. https://doi.org/10.1111/j.1601-183X.2011.00686.x (2011).
14. Azzopardi, E., Louttit, A. G., DeOliveira, C., Laviolette, S. R. & Schmid, S. The role of cholinergic midbrain neurons in startle and prepulse inhibition. *J. Neurosci.* **38**, 8798–8808. https://doi.org/10.1523/jneurosci.0984-18.2018 (2018).
15. Berridge, C. W. Noradrenergic modulation of arousal. *Brain Res. Rev.* **58**, 1–17. https://doi.org/10.1016/j.brainresrev.2007.10.013 (2008).
16. Sara, S. J. & Bouret, S. Orienting and reorienting: The locus coeruleus mediates cognition through arousal. *Neuron* **76**, 130–141. https://doi.org/10.1016/j.neuron.2012.09.011 (2012).
17. Foote, S. L., Aston-Jones, G. & Bloom, F. E. Impulse activity of locus coeruleus neurons in awake rats and monkeys is a function of sensory stimulation and arousal. *Proc. Natl. Acad. Sci. USA*. **77**, 3033–3037 (1980).
18. Aston-Jones, G. & Bloom, F. E. Norepinephrine-containing locus coeruleus neurons in behaving rats exhibit pronounced responses to non-noxious environmental stimuli. *J. Neurosci.* **1**, 887–900 (1981).
19. Hurley, L. M., Devilbiss, D. M. & Waterhouse, B. D. A matter of focus: Monoaminergic modulation of stimulus coding in mammalian sensory networks. *Curr. Opin. Neurobiol.* **14**, 488–495. https://doi.org/10.1016/j.conb.2004.06.007 (2004).
20. McBurney-Lin, J., Lu, J., Zuo, Y. & Yang, H. Locus coeruleus-norepinephrine modulation of sensory processing and perception: A focused review. *Neurosci. Biobehav. Rev.* **105**, 190–199. https://doi.org/10.1016/j.neubiorev.2019.06.009 (2019).
21. Glennon, E. *et al.* Locus coeruleus activation accelerates perceptual learning. *Brain Res.* **1709**, 39–49. https://doi.org/10.1016/j.brainres.2018.05.048 (2019).
22. Martins, A. R. O. & Froemke, R. C. Coordinated forms of noradrenergic plasticity in the locus coeruleus and primary auditory cortex. *Nat. Neurosci.* **18**, 1483–1492. https://doi.org/10.1038/nn.4090 (2015).
23. Edeline, J. M., Manunta, Y. & Hennevin, E. Induction of selective plasticity in the frequency tuning of auditory cortex and auditory thalamus neurons by locus coeruleus stimulation. *Heart Res.* **274**, 75–84. https://doi.org/10.1016/j.heares.2010.08.005 (2011).
24. Davis, M., Cedarbaum, J. M., Aghajanian, G. K. & Gendelman, D. S. Effects of clonidine on habituation and sensitization of acoustic startle in normal, decerebrate and locus coeruleus lesioned rats. *Psychopharmacology* **51**, 243–253. https://doi.org/10.1007/BF00431631 (1977).
25. Davis, M. & Astrachan, D. I. Spinal modulation of acoustic startle: Opposite effects of clonidine and d-amphetamine. *Psychopharmacology.* **75**, 219–225 (1981).
26. Adams, L. M. & Geyer, M. A. Effects of 6-hydroxydopamine lesions of locus coeruleus on startle in rats. *Psychopharmacology* **73**, 394–398 (1981).
27. von Coelln, R. *et al.* Loss of locus coeruleus neurons and reduced startle in parkin null mice. Report No. 0401297101, (2004).
28. Alsene, K. M., Rajbhandari, A. K., Ramaker, M. J. & Bakshi, V. P. Discrete forebrain neuronal networks supporting noradrenergic regulation of sensorimotor gating. *Neuropsychopharmacology* **36**, 1003–1014 (2011).
29. Alsene, K. M. & Bakshi, V. P. Pharmacological stimulation of locus coeruleus reveals a new antipsychotic-responsive pathway for deficient sensorimotor gating. *Neuropsychopharmacology* **36**, 1656–1667 (2011).
30. Vazey, E. M., Moorman, D. E. & Aston-Jones, G. Phasic locus coeruleus activity regulates cortical encoding of salience information. *Proc. Natl. Acad. Sci.* **115**, E9439–E9448. https://doi.org/10.1073/pnas.1803716115 (2018).
31. Rajkowski, J., Kubiak, P. & Aston-Jones, G. Locus coeruleus activity in monkey: Phasic and tonic changes are associated with altered vigilance. *Brain Res. Bull.* **35**, 607–616 (1994).
32. Marzo, A., Totah, N. K., Neves, R. M., Logothetis, N. K. & Eschenko, O. Unilateral electrical stimulation of rat locus coeruleus elicits bilateral response of norepinephrine neurons and sustained activation of medial prefrontal cortex. *J. Neurophysiol.* **111**, 2570–2588. https://doi.org/10.1152/jn.00920.2013 (2014).
33. Li, L. & Yeomans, J. S. Using intracranial electrical stimulation to study the timing of prepulse inhibition of the startle reflex. *Brain Res. Protoc.* **5**, 67–74. https://doi.org/10.1016/S1385-299X(99)00056-2 (2000).
34. Costa, J., Valls-Solé, J., Valldeoriola, F., Pech, C. & Rumià, J. Single subthalamic nucleus deep brain stimuli inhibit the blink reflex in Parkinson's disease patients. *Brain* **129**, 1758–1767. https://doi.org/10.1093/brain/awl143 (2006).
35. Novitskaya, Y., Sara, S. J., Logothetis, N. K. & Eschenko, O. Ripple-triggered stimulation of the locus coeruleus during post-learning sleep disrupts ripple/spindle coupling and impairs memory consolidation. *Learn. Mem.* **23**, 238–248. https://doi.org/10.1101/lm.040923.115 (2016).
36. Neves, R. M., Keulen, S. V., Yang, M., Logothetis, N. K. & Eschenko, O. Locus coeruleus phasic discharge is essential for stimulus-induced gamma oscillations in the prefrontal cortex. *J. Neurophysiol.* **119**, 904–920. https://doi.org/10.1152/jn.00552.2017 (2018).
37. McCormick, D. A., McGinley, M. J. & Salkoff, D. B. Brain state dependent activity in the cortex and thalamus. *Curr. Opin. Neurobiol.* **31**, 133–140. https://doi.org/10.1016/j.conb.2014.10.003 (2015).
38. Poulet, J. F. & Petersen, C. C. Internal brain state regulates membrane potential synchrony in barrel cortex of behaving mice. *Nature* **454**, 881–885. https://doi.org/10.1038/nature07150 (2008).
39. Steriade, M. Synchronized activities of coupled oscillators in the cerebral cortex and thalamus at different levels of vigilance. *Cereb. Cortex* **7**, 583–604 (1997).
40. Curto, C., Sakata, S., Marguet, S., Itskov, V. & Harris, K. D. A simple model of cortical dynamics explains variability and state dependence of sensory responses in urethane-anesthetized auditory cortex. *J. Neurosci.* **29**, 10600–10612. https://doi.org/10.1523/JNEUROSCI.2053-09.2009 (2009).

41. Yeomans, J. S., Lee, J., Yeomans, M. H., Steidl, S. & Li, L. Midbrain pathways for prepulse inhibition and startle activation in rat. *Neuroscience* **142**, 921–929. https://doi.org/10.1016/j.neuroscience.2006.06.025 (2006).
42. Kumari, V. *et al.* Effects of procyclidine on prepulse inhibition of the acoustic startle response in healthy human volunteers. *Psychopharmacology* **154**, 221–229. https://doi.org/10.1007/s002130000656 (2001).
43. Samuels, E. R., Hou, R. H., Langley, R. W., Szabadi, E. & Bradshaw, C. M. Modulation of the acoustic startle response by the level of arousal: Comparison of clonidine and modafinil in healthy volunteers. *Neuropsychopharmacology* **32**, 2405–2421. https://doi.org/10.1038/sj.npp.1301363 (2007).
44. Berridge, C. W., Schmeichel, B. E. & Espana, R. A. Noradrenergic modulation of wakefulness/arousal. *Sleep Med. Rev.* **16**, 187–197. https://doi.org/10.1016/j.smrv.2011.12.003 (2012).
45. Wu, M. F., Mallick, B. N. & Siegel, J. M. Lateral geniculate spikes, muscle atonia and startle response elicited by auditory stimuli as a function of stimulus parameters and arousal state. *Brain Res.* **499**, 7–17. https://doi.org/10.1016/0006-8993(89)91130-x (1989).
46. Kaufman, L. S. PGO waves in rats in the non-paradoxical sleep states. *Brain Res.* **276**, 73–80. https://doi.org/10.1016/0006-8993(83)90549-8 (1983).
47. Abduljawad, K. A., Langley, R. W., Bradshaw, C. M. & Szabadi, E. Effects of clonidine and diazepam on prepulse inhibition of the acoustic startle response and the N1/P2 auditory evoked potential in man. *J. Psychopharmacol.* **15**, 237–242. https://doi.org/10.1177/026988110101500402 (2001).
48. Aston-Jones, G. & Cohen, J. D. An integrative theory of locus coeruleus-norepinephrine function: Adaptive gain and optimal performance. *Annu. Rev. Neurosci.* **28**, 403–450 (2005).
49. Grant, S. J., Aston-Jones, G. & Redmond, D. E. Responses of primate locus coeruleus neurons to simple and complex sensory stimuli. *Brain Res. Bull.* **21**, 401–410. https://doi.org/10.1016/0361-9230(88)90152-9 (1988).
50. Rasmussen, K., Morilak, D. A. & Jacobs, B. L. Single unit activity of locus coeruleus neurons in the freely moving cat: I. During naturalistic behaviors and in response to simple and complex stimuli. *Brain Res.* **371**, 324–334. https://doi.org/10.1016/0006-8993(86)90370-7 (1986).
51. Hayat, H. *et al.* Locus coeruleus norepinephrine activity mediates sensory-evoked awakenings from sleep. *Sci. Adv.* **6**, eaaz4232. https://doi.org/10.1126/sciadv.aaz4232 (2020).
52. Uematsu, A. *et al.* Modular organization of the brainstem noradrenaline system coordinates opposing learning states. *Nat. Neurosci.* **20**, 1602. https://doi.org/10.1038/nn.4642 (2017).
53. Kaufman, L. S. & Morrison, A. R. Spontaneous and elicited PGO spikes in rats. *Brain Res.* **214**, 61–72 (1981).
54. Morrison, A. R. Relationships between phenomena of paradoxical sleep and their counterparts in wakefulness. *Acta Neurobiol. Exp.* **39**, 567–583 (1979).
55. Wu, M.-F. & Siegel, J. M. Facilitation of the acoustic startle reflex by ponto-geniculo-occipital waves: Effects of PCPA. *Brain Res.* **532**, 237–241. https://doi.org/10.1016/0006-8993(90)91765-9 (1990).
56. Berridge, C. W. & Abercrombie, E. D. Relationship between locus coeruleus discharge rates and rates of norepinephrine release within neocortex as assessed by in vivo microdialysis. *Neuroscience* **93**, 1263–1270 (1999).
57. Florin-Lechner, S. M., Druhan, J. P., Aston-Jones, G. & Valentino, R. J. Enhanced norepinephrine release in prefrontal cortex with burst stimulation of the locus coeruleus. *Brain Res.* **742**, 89–97 (1996).
58. Hormigo, S. *et al.* The noradrenergic projection from the locus coeruleus to the cochlear root neurons in rats. *Brain Struct. Funct.* **220**, 1477–1496. https://doi.org/10.1007/s00429-014-0739-3 (2015).
59. Klepper, A. & Herbert, H. Distribution and origin of noradrenergic and serotonergic fibers in the cochlear nucleus and inferior colliculus of the rat. *Brain Res.* **557**, 190–201. https://doi.org/10.1016/0006-8993(91)90134-H (1991).
60. Hormigo, S., Gomez-Nieto, R. & Lopez, D. E. The selective neurotoxin DSP-4 impairs the noradrenergic projections from the locus coeruleus to the inferior colliculus in rats. *Front. Neural Circuits* **6**, 41. https://doi.org/10.3389/fncir.2012.00041 (2012).
61. Schofield, B. R. Projections from auditory cortex to midbrain cholinergic neurons that project to the inferior colliculus. *Neuroscience* **166**, 231–240. https://doi.org/10.1016/j.neuroscience.2009.12.008 (2010).
62. Loughlin, S. E., Foote, S. L. & Bloom, F. E. Efferent projections of nucleus locus coeruleus: Topographic organization of cells of origin demonstrated by three-dimensional reconstruction. *Neuroscience* **18**, 291–306 (1986).
63. Lang, P. J., Bradley, M. M. & Cuthbert, B. N. Emotion, attention, and the startle reflex. *Psychol. Rev.* **97**, 377–395 (1990).
64. Heckman, C. J., Mottram, C., Quinlan, K., Theiss, R. & Schuster, J. Motoneuron excitability: The importance of neuromodulatory inputs. *Clin. Neurophysiol.* **120**, 2040–2054. https://doi.org/10.1016/j.clinph.2009.08.009 (2009).
65. Garraway, S. M. & Hochman, S. Modulatory actions of serotonin, norepinephrine, dopamine, and acetylcholine in spinal cord deep dorsal horn neurons. *J. Neurophysiol.* **86**, 2183–2194. https://doi.org/10.1152/jn.2001.86.5.2183 (2001).
66. Lang, B., Li, H., Kang, J. F. & Li, Y. Q. Alpha-2 adrenoceptor mediating the facilitatory effect of norepinephrine on the glycine response in the spinal dorsal horn neuron of the rat. *Life Sci.* **73**, 893–905. https://doi.org/10.1016/s0024-3205(03)00352-7 (2003).
67. Beagley, H. A. & Knight, J. J. Changes in auditory evoked response with intensity. *J. Laryngol. Otol.* **81**, 861–873. https://doi.org/10.1017/s0022215100067815 (1967).
68. Crowley, K. E. & Colrain, I. M. A review of the evidence for P2 being an independent component process: Age, sleep and modality. *Clin. Neurophysiol.* **115**, 732–744. https://doi.org/10.1016/j.clinph.2003.11.021 (2004).
69. Potter, T. *et al.* Characterization of volume-based changes in cortical auditory evoked potentials and prepulse inhibition. *Sci. Rep.* **7**, 11098. https://doi.org/10.1038/s41598-017-11191-3 (2017).
70. Qi, R., Li, M., Ma, Y. & Chen, N. State-dependent changes in auditory sensory gating in different cortical areas in rats. *PLoS ONE* https://doi.org/10.1371/journal.pone.0126684 (2015).
71. Ogilvie, R. D., Simons, I. A., Kuderian, R. H., MacDonald, T. & Rustenburg, J. Behavioral, event-related potential, and EEG/FFT changes at sleep onset. *Psychophysiology* **28**, 54–64. https://doi.org/10.1111/j.1469-8986.1991.tb03386.x (1991).
72. Miyazato, H., Skinner, R. D., Reese, N. B., Mukawa, J. & Garcia-Rill, E. Midlatency auditory evoked potentials and the startle response in the rat. *Neuroscience* **75**, 289–300. https://doi.org/10.1016/0306-4522(96)00176-5 (1996).
73. Nir, Y., Vyazovskiy, V. V., Cirelli, C., Banks, M. I. & Tononi, G. Auditory responses and stimulus-specific adaptation in rat auditory cortex are preserved across NREM and REM sleep. *Cereb. Cortex* **25**, 1362–1378. https://doi.org/10.1093/cercor/bht328 (2015).
74. Teneud, L., Miyazato, H., Skinner, R. D. & Garcia-Rill, E. Cholinergic modulation of the sleep state-dependent P13 midlatency auditory evoked potential in the rat. *Brain Res.* **884**, 196–200. https://doi.org/10.1016/S0006-8993(00)02983-8 (2000).
75. Nordby, H., Hugdahl, K., Stickgold, R., Bronnick, K. S. & Hobson, J. A. Event-related potentials (ERPs) to deviant auditory stimuli during sleep and waking. *NeuroReport* **7**, 1082–1086. https://doi.org/10.1097/00001756-199604100-00026 (1996).
76. Graham, S. J., Langley, R. W., Bradshaw, C. M. & Szabadi, E. Effects of haloperidol and clozapine on prepulse inhibition of the acoustic startle response and the N1/P2 auditory evoked potential in man. *J. Psychopharmacol.* **15**, 243–250. https://doi.org/10.1177/026988110101500411 (2001).
77. Lancel, M. Cortical and subcortical EEG in relation to sleep-wake behavior in mammalian species. *Neuropsychobiology* **28**, 154–159 (1993).
78. Maloney, K. J., Cape, E. G., Gotman, J. & Jones, B. E. High-frequency gamma electroencephalogram activity in association with sleep-wake states and spontaneous behaviors in the rat. *Neuroscience* **76**, 541–555. https://doi.org/10.1016/s0306-4522(96)00298-9 (1997).

79. Cape, E. G. & Jones, B. E. Differential modulation of high-frequency gamma-electroencephalogram activity and sleep-wake state by noradrenaline and serotonin microinjections into the region of cholinergic basalis neurons. *J. Neurosci.* **18**, 2653–2666. https://doi.org/10.1523/jneurosci.18-07-02653.1998 (1998).
80. De Pascalis, V., Cacace, I. & Massicolle, F. Perception and modulation of pain in waking and hypnosis: Functional significance of phase-ordered gamma oscillations. *Pain* **112**, 27–36. https://doi.org/10.1016/j.pain.2004.07.003 (2004).
81. Gross, J., Schnitzler, A., Timmermann, L. & Ploner, M. Gamma oscillations in human primary somatosensory cortex reflect pain perception. *PLoS Biol.* **5**, e133. https://doi.org/10.1371/journal.pbio.0050133 (2007).
82. Tiemann, L., Schulz, E., Gross, J. & Ploner, M. Gamma oscillations as a neuronal correlate of the attentional effects of pain. *Pain* **150**, 302–308. https://doi.org/10.1016/j.pain.2010.05.014 (2010).
83. Mitra, P. & Bokil, H. *Observed Brain Dynamics* (Oxford University Press, Oxford, 2008).
84. Paxinos, G. & Watson, C. *The Rat Brain in Stereotaxic Coordinates* 5th edn. (Elsevier Academic Press, Amsterdam, 2005).

Acknowledgements
We thank Silvia van Keulen and Julia Weinert for help with behavioral testing, Katalin Kalya for help with histology, Axel Oeltermann and Joachim Werner for technical support.

Author contributions
Conception and design: M.Y. and O.E.; data acquisition and analysis: M.Y.; new software: M.Y.; figures: M.Y.; data interpretation: M.Y., N.K.L. and O.E.; first draft: M.Y.; substantial revision: O.E.. All authors reviewed the manuscript and approved the submitted version.

Funding
Open Access funding enabled and organized by Projekt DEAL.

Competing interests
The authors declare no competing interests.

Additional information
Correspondence and requests for materials should be addressed to O.E.

Reprints and permissions information is available at www.nature.com/reprints.

Publisher's note Springer Nature remains neutral with regard to jurisdictional claims in published maps and institutional affiliations.

The locus coeruleus activity during hippocampal-cortical communication

Mingyu Yang[1], Susan J. Sara, Nikos K. Logothetis[1,2], Oxana Eschenko[1*]

[1] Department of Physiology of Cognitive Processes, Max Planck Institute for Biological Cybernetics, Tuebingen, Germany
[2] Division of Imaging Science and Biomedical Engineering, University of Manchester, M13 9PT Manchester, UK

*Corresponding author: Oxana Eschenko, Email: oxana.eschenko@tuebingen.mpg.de

Abstract: 340 words

Main text: 3,898 words

Number of figures: 4

Number of pages: 22

Key words: ripples, spindles, hippocampus, memory consolidation, arousal, locus coeruleus, noradrenaline, rat, sleep

Abstract (340 words)

The brainstem noradrenergic nucleus Locus Coeruleus (LC) is the primary source of norepinephrine (NE) in the forebrain. The LC-NE system plays a critical role in regulating arousal, it is involved in mediating many visceral responses and also a variety of cognitive functions including memory formation. Activating LC neurons during sleep is associated with a decrease in the occurrence of hippocampal ripples and sleep spindles; both oscillatory events have been suggested to mediate the hippocampal-cortical communication underlying system-level consolidation. Experimentally induced ripple-triggered phasic LC stimulation during post-learning sleep causes memory deficit, possibly due to interference with the cellular- and system-level memory consolidation mechanisms. Currently, the involvement of LC-NE system in the hippocampal-cortical information transfer remains largely unexplored. In the present study, we examined temporal coupling between the LC spiking activity, hippocampal ripples, and sleep spindles. In general, we observed a consistent suppression of LC population activity around hippocampal ripples. LC activity started decreasing several seconds earlier before ripple onsets. The early decrease of LC firing rate was most likely due to the transition of cortical activity to a more synchronized state allowing generation of ripples, as jittering ripples in a 5-sec time window did not change the temporal dynamics of LC MUA modulation. Interestingly, there also existed a brief suppression of LC neurons that was locked to ripple onsets and the degree of this ripple-associated LC MUA suppression greatly varied across the subsets of ripples, yet no systematic relations were found with the ripple properties such as amplitude or inter-ripple frequency. Notably, suppression of LC activity was much stronger around awake ripples compared to sleep ripples. Furthermore, during NREM sleep, LC activity showed earlier decreasing around spindle-coupled ripples than spindle-uncoupled ones. Overall, our present study characterized the precise temporal relationship between hippocampal ripples and LC activity during different brain states. It provides new evidence for the engagement of the LC in ripple-associated memory processing and raises further questions about the causal role of LC in

mediating ripple generation and synergistic interactions across multiple cortical and subcortical brain structures during hippocampal ripples.

Introduction

During states of awake immobility or non-rapid eye movement (NREM) sleep the hippocampal neural activity is characterized by an irregular transient synchronization that is reflected in the extracellular potential as a sharp-wave-ripple complex (SPW-R) [1, 2]. Hippocampal ripples, the high-frequency (120-250 Hz) oscillation in the SPW-R, can be detected in the CA1 pyramidal layer of the dorsal hippocampus, and have been suggested to mediate off-line memory processing [3, 4]. This original hypothesis receives continuous experimental support. Indeed, ripples occur more frequently after spatial experience [5, 6] and post-learning disruption of ripples is detrimental for spatial memory consolidation [7, 8]. Furthermore, ripple-associated reactivation of behaviorally relevant activity of neuronal assemblies in the hippocampus (and also other brain regions) is thought as a mechanism of system-level memory consolidation [9-14], as well as an indicator of memory retrieval [15-18] or a correlate of action planning [19-21]. In recent years, it became evident that ripples reflect not only synchronization within the hippocampus, but indicate a time window of cross-regional coordination within large-scale networks [22, 23]. The ripple-associated cross-regional communication may occur through coordinated up/down-regulation of neural activity across cortical and subcortical structures, including neuromodulation centers [21, 24]. Several electrophysiological studies have demonstrated temporally coordinated activity around ripples in multiple brain structures, including the amygdala [9], the ventral tegmental area (VTA) [25], the median raphe [26] and the thalamus [22, 27-29].

The Locus Coeruleus (LC), a small pontine noradrenergic nucleus, is critical for learning, synaptic plasticity and memory consolidation [30-33]. The noradrenergic neurotransmission has been long suggested to play a critical role during the late phase of memory consolidation [15, 34, 35], which may coincide with the protein-dependent phase of synaptic consolidation [36, 37]. Earlier, we reported a delayed increase of LC activity during post-learning NREM sleep [38]. Temporal relationship between LC activity and thalamo-cortical sleep spindles has been long known[39]. Recent study showed that during NREM sleep LC spiking is correlated with a decrease in spindle power [40]. We have previously demonstrated that the firing of LC neurons is phase-locked to cortical slow oscillations [41] that orchestrate spindle and ripple occurrence [42, 43]. However, the direct relationships between LC activity and hippocampal ripples have not yet been demonstrated, whereas indirect evidence is controversial. A study in murine slice showed that increasing NE concentration in the hippocampus resulted in increase of ripple incidence and their amplitudes [44]. The ripple-triggered LC activation by local microstimulation in behaving rat had no influence on ripple generation [40, 45]. In the present study, we sought to characterize the ripple-associated LC activity in spontaneously behaving rats. Our results provide evidence for a state-dependent engagement of LC in modulating the hippocampal-cortical communication.

Results

Results described below are based on 17 recording sessions collected from 4 rats (2 to 9 sessions per rat) and containing broadband (0.1 Hz- 8 kHz) extracellular potentials simultaneously recorded in the LC and dHPC. All recordings were made during rats' active (dark) phase of their circadian rhythm for 1.1- 3.8 hours while animals were allowed to behave spontaneously. Cortical state was monitored by the frontal EEG continuously.

Influence of cortical state on LC activity and hippocampal ripple rate

Since ripple rate and firing rate of LC neurons both depend on the ongoing behavioral/brain state, we first sought to characterize the modulation of LC population activity and hippocampal ripples by cortical arousal state. The moment-to-moment fluctuation of the cortical state was quantified by using a synchronization index (SI). The SI was calculated as a power ratio between low (1- 4Hz) and high (30- 90Hz) frequency band over a 2-sec time window. Ripple oscillations were identified by thresholding (5 SDs) of a z-score normalized ripple band power envelope (band-pass: 140 - 250 Hz, smoothing at 25Hz) extracted from the CA1 dHPC LFPs (Fig. 1A, middle traces). On average, 1030-3441 ripple events were detected per session, ripple rate was 19.9 ± 1.7 ripples per minute and the averaged ripple amplitude was 10.6 ± 0.6 SDs. The LC population activity was characterized by multiunit spike times (referred here as multiunit activity, MUA; Fig. 1A, bottom trace). Pair-wise correlation showed that SI was negatively correlated with the firing rate of LC neurons ($r = -0.28 \pm 0.05$, $p < 0.01$), while positively correlated with the ripple occurrence ($r = 0.16 \pm 0.04$, $p < 0.01$; Fig. 1B).

To disentangle the ripple-associated change of LC activity from the influence of cortical state, we created a sequence of 'surrogate' events to capture the cortical state change around ripples while not to associate with the increased hippocampal ripple power. To achieve this, for each given session, ten groups of 'surrogate' events were calculated by distributing the same number of ripples detected every 1-10 sec in a random order. Cortical delta power (1-4Hz) and hippocampal ripple power around each group of 'surrogate' events (Fig. 1C) were examined to determine the optimal time window for shuffling ripples. 'Surrogate' events computed with a 5-sec time window was associated with increased cortical power and unchanged hippocampal ripple power (power exceeding 95% CI of baseline activity; see Methods for more details), and thus were chosen for controlling the confounding effect from the transition of cortical states. Furthermore, consistent with the negative correlation between cortical synchronization level and LC firing rate, we observed a decrease of LC activity around 'surrogate' events in all sessions (Fig. 1D).

LC spiking is transiently suppressed around hippocampal ripples

To characterize the ripple-associated LC activity and minimize the influence of cortical states, the 'corrected' peri-ripple LC MUA firing rate was calculated by subtracting the LC activity around 'surrogate' events from the corresponding values of the time series around ripples (Fig. 2A). Consistent downregulation of LC neural activity around ripples was observed in all sessions. To characterize the ripple-associated LC MUA modulation with higher signal-to-noise ratio, we calculated the c-MIs (area above/below the PETH curve, see Methods for more details, figs. 2A&B) every 0.5 sec along each PETH and significant modulation was confirmed for all recording sessions (below lower bound of 95% confidence interval (CI) of baseline MIs). We next analyzed the temporal dynamics of ripple-associated LC MUA modulation in more details. Specifically, we first up-sampled the c-MIs to the time resolution 0.01 sec by interpolation and then extracted time windows when LC activity differed from 95% CI of baseline MIs. Specifically, LC MUA suppression started 1.63 ± 0.07 sec (range: 1.22 – 2.26 sec) before ripple onsets, reached peak modulation at 0.59 ± 0.08 sec (range: 0.5 – 1 sec) before ripples and lasted for 1.69 ± 0.09 sec (range: 1.26 – 2.39 sec).

LC activity modulation around different ripple subtypes

We assumed that the magnitude of LC MUA modulation varied across subsets of ripples. To quantify this prediction, for each dataset we first randomly selected 20% of total number of ripples detected in each session. We next characterized the modulation depth (MIs) by computing area above/below the averaged PETHs over the subset of ripples within a time window [-2, 0] before ripple onsets when LC activity became significantly suppressed. The same procedure was repeated 5000 times, and resulted in a distribution of subsampling-MIs (s-MIs) for each session (see Methods). The s-MIs indicated that the magnitude of LC MUA modulation, indeed, substantially varied across different ripple subsets (s-MI range: -12.2 to 3.6 a.u.; Fig. 3A). In total, ~95% of s-MIs were associated with significant suppression.

To identify the factors underlying the heterogeneous modulations of LC activity around ripples, we first examined whether degrees of LC suppression depended on the ripple intrinsic features. No systematic relationships were revealed between the MIs and corresponding values of the ripple amplitude or intra-ripple frequency (Repeated measures ANOVA, ns, for all sessions; Fig. 3B). The LC MUA modulation may depend on a temporal pattern of ripple occurrence. Therefore, we split all detected ripples into 'isolated' or 'clustered' ripples (see Methods, fig. 3C). This comparison revealed no MI-difference of LC suppression between the isolated (MI: -3.63 ± 0.31) and clustered (MI: -4.72 ± 0.27) ripples (Wilcoxon signed-rank test, $p = 0.37$). However, compared to the clustered ripples, LC MUA recovered to a significantly higher firing rate after isolated ripples (Wilcoxon signed-rank test, $p < 0.05$; Fig. 3D).

Finally, we compared MIs around ripples occurring during either awake or NREM sleep. Using the frontal EEG, we classified each 10-s segment into awake or non-REM (NREM) sleep episode (Details see methods). We then split all detected ripples into the ones occurring during awake or sleep (A-ripples and S-ripples, respectively). We plotted the LC MUA PETHs centered at either A-ripples or S-ripples and calculated the corresponding c-MIs. Consistent LC MUA suppression around A-ripples was observed across all sessions while 4 out of 17 sessions showed no modulation of LC activity around S-ripples. Regarding the temporal dynamics, suppression of LC activity lasted longer around A-ripples (1.83 ± 0.26 sec vs.1.32 ± 0.16 sec around A- and S- ripples; Wilcoxon signed-rank test, $p = 0.04$; fig. 4A). Overall, the LC MUA suppression was stronger around A-ripples (MI: -7.71 ± 0.75) vs S-ripples (MI: -3.13 ± 0.53, Wilcoxon signed-rank test, p = 0.0005). A-ripples and S-ripples differed in intra-ripple frequency (191.31 ± 1.53 Hz sec vs. 181.99 ± 2.07 Hz respectively, Wilcoxon signed-rank test, p = 0.002) but not in amplitude (11.05 ± 0.70 SDs vs.10.33 ± 0.56 SDs respectively, Wilcoxon signed-rank test, ns). However, as modulation depth was similar across ripples with different intra-ripple frequencies, it was more likely that the different degrees of LC suppression around A- and S- ripples was due to the behavioral states when ripples occurred.

As previously reported [29], a subset of S-ripples co-occurring with sleep spindles were associated with bi-directional modulations in the thalamus. The temporal correlation of ripple and spindle events was evident by a transient EEG power increase in the spindle band (12-16Hz) on a peri-ripple EEG spectrogram (Fig. 4B). Sleep spindles were then detected and the times of spindle on- and offsets were extracted (see Methods for details) and S-ripples were further subdivided into spindle-coupled and spindle-uncoupled ones (Fig. 4C). LC MUA was suppressed earlier around spindle-coupled ripples (1.68 ± 0.20 sec vs.1.05 ± 0.11 SDs before spindle-coupled and -uncoupled ripples, Wilcoxon signed-rank test, p = 0.02, Fig. 4D). However, the modulation depth of LC was not different between the spindle coupled and -uncouple ripples (MIs: -3.86 ± 0.68 SDs vs.-3.11 ± 0.35, respectively, Wilcoxon signed-rank test, ns).

Finally, the hippocampal-cortical coherence around spindle-coupled and spindle-uncoupled ripples exhibited strikingly different profiles at ~10Hz and ~20Hz (Fig 4E). This result further pointed to different type of cross-regional interaction during spindle-coupled and spindle-uncoupled ripples.

Discussion

In the present study, we reported a consistent suppression of LC population activity around hippocampal ripple occurrence. LC activity started decreasing several seconds earlier before ripple onsets but the early decreasing was most likely due to the ripple-related cortical state transition. Interestingly, LC exhibited brief suppression before ripple onsets and the degree of LC MUA suppression around ripples greatly varied across the subsets of ripples, yet no systematic relations were found with the ripple amplitude or inter-ripple frequency. Notably, ripples that occurred during distinct brain states correlated with different modulation of LC activity. Suppression of LC activity was much stronger around awake ripples compared to sleep ripples. Furthermore, during NREM sleep, LC activity showed earlier suppression around spindle-coupled ripples than spindle-uncoupled ones. Overall, our present study characterized the precise temporal relationship between hippocampal ripples and LC activity under different brain state. It provides new evidence for the engagement of the LC in ripple-associated memory processing and raised further questions about the causal role of LC in mediating ripple generation and synergistic interactions across multiple cortical and subcortical brain structures during ripples.

The consistent and long-lasted suppression of LC activity around ripple-containing episodes (~5 sec) was expected based on the function of the LC in modulating arousal state. Ripples mainly occur during low-arousal state such as awake immobility or NREM sleep [2], when LC firing rate is relatively low compared to active exploratory state [46]. Moreover, optogenetic activating the LC caused sleep-to-awake transition and inhibiting the LC reduced wakefulness, further revealing the causal role of LC in tuning arousal [47].

Interestingly, a brief suppression of LC activity occurred before ripple onsets and diminished when ripple times jittered within 5-sec time window, suggesting the suppression of LC activity was specific to hippocampal ripples. The magnitude of suppression varied across subsets of ripples, and ~5% of ripples were not associated with any modulation. Previous work has demonstrated that modulation of reward responsive neurons in the VTA was greater around ripples containing replay of previous task experience than ripples that did not [25]. Another recent study showed that stimulation of the LC at a low frequency during post-learning sleep did not change the ripple rate but decreased the stability of the place cell replay and further impaired the spatial memory consolidation [40]. Based on these findings, we speculated that different degrees of the preceding LC suppression might bias the content of memory reactivation during the following ripples. Brief silence of the LC activity might contribute to a higher fidelity of memory reactivation.

Ripples play a critical role in memory consolidation but further examination suggests that the mechanism underlying awake and sleep ripples and the exact mnemonic function they serve might be different [21, 48]. Compared to sleep ripples, awake ripples are associated with stronger and more structured reactivation and the reactivation is more correlated with the recent experience [49]. Moreover, the interaction between the hippocampus and other brain regions, such as ACC, VTA and thalamus is stronger around awake ripples [25, 29, 50]. In this study, we also observed a stronger suppression of the LC activity around awake ripples. On one hand, it could be due to the higher LC activity during awake state which requires to be lowered to a larger degree to achieve the optimal level for ripple generation. On the other hand, the stronger LC suppression might correlate with inhibiting irrelevant information for the reactivation of recently encoded memory trace to be better consolidated.

Different from awake ripples, sleep ripples are coordinated with cortical slow oscillations and spindles [24]. Previous studies demonstrated that cortical and thalamic neurons exhibit different firing patterns around the spindle-coupled and -uncoupled ripples [27, 29, 51]. Furthermore, the precise temporal correlation between the hippocampal and cortical oscillations has been causally linked to memory consolidation involving transferring newly encoded information from the hippocampus to the cortex for long-term storage [52, 53]. Here we observed that LC activity differed for these two types of ripples, with an earlier suppression around spindle-coupled ripples, which could facilitate the transfer of memory trace replayed during spindle-coupled ripples to the cortex.

Ripples can trigger hippocampal LTP and LTD [54, 55]. The ripple-associated LC suppression seems to be inconsistent with the role of LC in facilitating LTD and LTP by co-releasing NA and DA through its terminals in the hippocampus [36, 37, 56-58]. It is notable that all the previous studies have been conducted either in vitro or in awake animals. However, the LC has been shown to exert distinct influence on different stages (e.g. encoding, retrieval) of hippocampal-dependent memory processing, and LC-associated modulation also depends on the ongoing behavioral states. For examples, stimulation of the LC in awake animals facilitated memory encoding [59], while ripple-triggered LC stimulation during post-learning sleep impaired memory consolidation [45]. To conclude, LC is a critical node in the ripple-associated large neuronal network. Suppression of the LC activity is necessary for ripple-dependent memory consolidation by creating an optimal brain state and possibly by inhibiting consolidating irrelevant information. Further experiments are needed to explore the role of LC in hippocampal-dependent synaptic plasticity and memory consolidation.

Materials & Methods

Animals

Six adult male Sprague-Dawley rats were used. Data from four rats were collected for a previous study [41] and reanalyzed. Additional two rats (Charles River Laboratory, Germany) were kept on a 12h light-dark cycle (8:00 am lights on) and single-housed after surgery. Recordings were performed during the dark cycle. Similar surgery and recording procedures were used as reported in detail elsewhere [29, 41]. The study was performed in accordance with the German Animal Welfare Act (TierSchG) and Animal Welfare Laboratory Animal Ordinance (TierSchVersV). This is in full compliance with the guidelines of the EU Directive on the protection of animals used for scientific purposes (2010/63/EU). The study was reviewed by the ethics commission (§15 TierSchG) and approved by the state authority (Regierungspräsidium, Tübingen, Baden-Württemberg, Germany).

Surgery and electrode placement

Procedures for stereotaxic surgery under isoflurane anesthesia have been described in detail elsewhere [29]. Briefly, anesthesia was initiated with 4% and maintained with 1.5-2.0% isoflurane. Body temperature, heart rate and blood oxygenation were monitored throughout the entire anesthesia period. The depth of anesthesia was controlled by a lack of pain and sensory response (hind paw pinch). A fully anesthetized rat was fixed in a stereotaxic frame with the head angle at zero degree. The skull was exposed and local anesthetic (Lidocard 2%, B. Braun, Melsungen, Germany) was applied on the skin edges. Craniotomies were performed on the right hemisphere above target regions. Additional burr holes were made for EEG, grown and anchor screws (stainless steel, 0.86-1.19 mm diameter, Fine Science Tools, Heidelberg, Germany). Dura mater was removed. For extracellular recording, single platinum-iridium electrodes (FHC, Bowdoin, ME) were placed in the anterior cingulate cortex (ACC, AP/ML: 2.8 mm/0.8mm from Bregma and DV: ~1.8 mm from from the dura surface). For recording of the hippocampal ripples, the electrode was mounted on a self-made movable microdrive and inserted above the CA1 pyramidal layer of the dorsal hippocampus (dHPC, -3mm/2mm/~2mm). For LC recording, microwire brush arrays (MicroProbes, MD) and silicon probe (Cambridge Neurotech, Cambridge, UK) mounted on a microdrive (Cambridge Neurotech, Cambridge, UK) were implanted above LC (~4.2 mm/~1.2 mm from Lamda; DV: ~5.5-6.2 mm) with a 15-degree angle. The accuracy of LC targeting was verified by online monitoring of neural activity. The LC neurons were identified by broad spike widths (~0.6 msec), regular low firing rate (1 –2 spikes/s) and biphasic (excitation followed by inhibition) response to paw pinch. For EEG recording, a screw was placed above the frontal cortex. The ground screw was placed above the cerebellum. Screws were fixed in the skull and additionally secured with tissue adhesive. The entire implant was secured on the skull with dental cement (RelyX™ Unicem 2 Automix, 3M, MN). A copper mesh was mounted around the implant for shielding and protection of exposed connection wires. During post-surgery recovery period, analgesic (Carprofen 5.0 mg/kg, s.c.; Rimadyl) and antibiotic (10.0 mg/kg, s.c.; Baytril, Bayer) were given for 3 and 5 days, respectively. Electrode placements was histologically verified.

Electrophysiological recording and data analysis

Rats were first habituated to the sleeping box and cable plugging procedure. The electrodes were connected to the Neuralynx Digital Lynx acquisition system via two 32-channel head stage (Neuralynx, Bozeman, MT). The electrode placement in the LC was optimized by lowering the electrodes with a maximal 0.05 mm step and monitoring spiking activity on the high-passed (300 Hz – 8kHz) extracellular signal. The depth of dHPC electrodes was adjusted by gradually lowering the electrode (maximum 0.05 mm per day) until reliable ripple activity was observed. Once the electrode position was optimized, the broadband (0.1Hz - 8kHz) extracellular signals were acquired and digitized at 32kHz and referenced to the ground screw. The animals' movement was monitored by video tracking (25 frames per sec) with the aid of LEDs attached to the head stage. All recordings were performed between 10 a.m. and 7 p.m.

Classification of behavioral states

We classified the rat spontaneous behavior into awake and NREM sleep using frontal EEG or cortical LFPs by applying a standard sleep scoring algorithm described in detail elsewhere [45]. Briefly, animal movement speed was extracted from the video recording synchronized with neural signal. The theta/delta (θ/δ) ratio was calculated from the artifact-free EEG in 2.5-sec epochs. The epochs of awake state were identified by the presence of active locomotion and above threshold θ/δ ratio; the epochs of NREM sleep were identified by the absence of motor activity and below threshold θ/δ ratio. The minimal duration of the same behavioral state was set to 10 sec; data segments with less steady behavioral states were excluded from further analysis.

Event detection

For detection of the hippocampal ripples, a broadband (0.1Hz - 8kHz) extracellular signal recorded from the dHPC (pyramidal layer, CA1 subfield) was band-pass (140 – 250 Hz) filtered, rectified and low-pass filtered (25Hz). The resulting signal was z-score normalized and ripple oscillations were detected by signal thresholding at 5 standard deviations (SDs). A 70-ms refractory window was applied. Ascending and descending crossings at 1 SD defined the ripple on- and off-set, respectively. Clustered and isolated ripples were classified based on the inter-ripple interval (IRI) as described in detail elsewhere [60]. Briefly, IRIs were extracted and log(IRI) distribution was analyzed. Bimodal log(IRI) distribution indicated ripple occurrence with shorter and longer IRIs. A crossing point of two distributions was used for classifying the ripple type. Ripples with short IRI (< 0.33 sec) were classified as 'clustered' and treated as a single ripple event; the onset time was defined by the first ripple in a cluster. Ripples with IRI > 0.33 sec were classified as 'isolated'.

For detection of sleep spindles, EEG signal was band-pass (12 - 16 Hz) filtered, down-sampled (200 Hz) and the root mean square (0.2 s smoothing) was calculated. Spindle detection threshold was defined at 3 SDs of the signal amplitude during NREM sleep episodes. Ascending and descending signal crossings at 1SD defined spindle on- and off-set, respectively. The minimal sleep spindle duration was set to 0.5 sec.

Analysis of peri-event neural activity

For analysis of peri-ripple modulation of LC activity, we used a method described in details elsewhere [29]. First, the spike times of LC multiunit activity (MUA) were extracted by high-pass (600Hz) filtering of the broadband extracellular signal recorded from LC and thresholding at -0.05 mV. The LC MUA was triggered by ripple onset and the averaged peri-event spike histogram (PETH) was generated ± 5 sec around all detected ripples (5-ms bins, Gaussian smoothed with a 10 ms-window). A grand average of PSTHs was built across all events for each recording session. To compensate for possible state-dependent fluctuations of LC MUA, a 'surrogate' event sequence was generated by distributing randomly the same number of time points within a certain time window; the jittering procedure was repeated 100 times. The averaged PETH was generated ± 5 sec around surrogate events. Time series of LC MUA around the surrogate events were subtracted from the corresponding values around ripples and the resulting ('corrected') PETHs were z-score normalized to the baseline LC firing rate. To quantify peri-ripple dynamics of LC MUA, a continuous modulation index (c-MI) was calculated by extracting the area above/below the curve of each PETH for each 1-s epoch along the ± 5s peri-ripple window. To determine the significance of modulation, we built PETHs around 'shuffled' ripple times generated by permutation of the IRIs and calculated the MIs for each of the 5000 shuffled PETHs; 95% confidence interval (CI) served as significance threshold. To quantify the LC MUA modulation around subsets of ripples, s-MI was computed for a subset of ripples (20% of all detected ripples in each session) and the same procedure was repeated 5000 times. The s-MI distribution was analyzed.

Spectral analysis

For LFP analysis, we applied the Morlet-wavelet time-frequency analysis to estimate spectral power and computed coherence with the MATLAB toolbox Chronux (http://www.chronux.org) [61].

References

1. Buzsaki, G., *Hippocampal Sharp Wave-Ripple: A Cognitive Biomarker for Episodic Memory and Planning.* Hippocampus, 2015. **25**(10): p. 1073-1188.
2. Ylinen, A., et al., *Sharp Wave-Associated High-Frequency Oscillation (200-Hz) in the Intact Hippocampus - Network and Intracellular Mechanisms.* Journal of Neuroscience, 1995. **15**(1): p. 30-46.
3. Buzsáki, G., *Rhythms of the brain*. 2006, Oxford ; New York: Oxford University Press. xiv, 448 p.
4. Buzsaki, G., *Neural Syntax: Cell Assemblies, Synapsembles, and Readers.* Neuron, 2010. **68**(3): p. 362-385.
5. Eschenko, O., et al., *Sustained increase in hippocampal sharp-wave ripple activity during slow-wave sleep after learning.* Learning & Memory, 2008. **15**(4): p. 222-228.
6. Ramadan, W., O. Eschenko, and S.J. Sara, *Hippocampal Sharp Wave/Ripples during Sleep for Consolidation of Associative Memory.* Plos One, 2009. **4**(8).
7. Ego-Stengel, V. and M.A. Wilson, *Disruption of Ripple-Associated Hippocampal Activity During Rest Impairs Spatial Learning in the Rat.* Hippocampus, 2010. **20**(1): p. 1-10.
8. Girardeau, G., et al., *Selective suppression of hippocampal ripples impairs spatial memory.* Nature Neuroscience, 2009. **12**(10): p. 1222-1223.
9. Girardeau, G., I. Inema, and G. Buzsaki, *Reactivations of emotional memory in the hippocampus-amygdala system during sleep.* Nature Neuroscience, 2017. **20**(11): p. 1634-+.
10. Ji, D.Y. and M.A. Wilson, *Coordinated memory replay in the visual cortex and hippocampus during sleep.* Nature Neuroscience, 2007. **10**(1): p. 100-107.
11. Lansink, C.S., et al., *Hippocampus Leads Ventral Striatum in Replay of Place-Reward Information.* Plos Biology, 2009. **7**(8).
12. Lee, A.K. and M.A. Wilson, *Memory of sequential experience in the hippocampus during slow wave sleep.* Neuron, 2002. **36**(6): p. 1183-1194.
13. Nadasdy, Z., et al., *Replay and time compression of recurring spike sequences in the hippocampus.* Journal of Neuroscience, 1999. **19**(21): p. 9497-9507.
14. Peyrache, A., et al., *Replay of rule-learning related neural patterns in the prefrontal cortex during sleep.* Nature Neuroscience, 2009. **12**(7): p. 919-U143.
15. Foster, D.J. and M.A. Wilson, *Reverse replay of behavioural sequences in hippocampal place cells during the awake state.* Nature, 2006. **440**(7084): p. 680-683.
16. Jadhav, S.P., et al., *Awake Hippocampal Sharp-Wave Ripples Support Spatial Memory.* Science, 2012. **336**(6087): p. 1454-1458.
17. Joo, H.R. and L.M. Frank, *The hippocampal sharp wave-ripple in memory retrieval for immediate use and consolidation.* Nature Reviews Neuroscience, 2018. **19**(12): p. 744-757.
18. Wu, C.T., et al., *Hippocampal awake replay in fear memory retrieval.* Nature Neuroscience, 2017. **20**(4): p. 571-+.

19. Diba, K. and G. Buzsaki, *Forward and reverse hippocampal place-cell sequences during ripples.* Nature Neuroscience, 2007. **10**(10): p. 1241-1242.

20. Skelin, I., S. Kilianski, and B.L. McNaughton, *Hippocampal coupling with cortical and subcortical structures in the context of memory consolidation.* Neurobiology of Learning and Memory, 2019. **160**: p. 21-31.

21. Tang, W.B. and S.P. Jadhav, *Sharp-wave ripples as a signature of hippocampal-prefrontal reactivation for memory during sleep and waking states.* Neurobiology of Learning and Memory, 2019. **160**: p. 11-20.

22. Logothetis, N.K., *Neural-Event-Triggered fMRI of large-scale neural networks.* Current Opinion in Neurobiology, 2015. **31**: p. 214-222.

23. Logothetis, N.K., et al., *Hippocampal-cortical interaction during periods of subcortical silence.* Nature, 2012. **491**(7425): p. 547-553.

24. Todorova, R. and M. Zugaro, *Hippocampal ripples as a mode of communication with cortical and subcortical areas.* Hippocampus, 2020. **30**(1): p. 39-49.

25. Gomperts, S.N., F. Kloosterman, and M.A. Wilson, *VTA neurons coordinate with the hippocampal reactivation of spatial experience.* Elife, 2015. **4**.

26. Wang, D.V., et al., *Mesopontine median raphe regulates hippocampal ripple oscillation and memory consolidation.* Nature Neuroscience, 2015. **18**(5): p. 728-+.

27. Varela, C. and M.A. Wilson, *mPFC spindle cycles organize sparse thalamic activation and recently active CA1 cells during non-REM sleep.* Elife, 2020. **9**.

28. Viejo, G. and A. Peyrache, *Precise coupling of the thalamic head-direction system to hippocampal ripples.* Nature Communications, 2020. **11**(1).

29. Yang, M.Y., N.K. Logothetis, and O. Eschenko, *Occurrence of Hippocampal Ripples is Associated with Activity Suppression in the Mediodorsal Thalamic Nucleus.* Journal of Neuroscience, 2019. **39**(3): p. 434-444.

30. Hansen, N., *The Longevity of Hippocampus-Dependent Memory Is Orchestrated by the Locus Coeruleus-Noradrenergic System.* Neural Plasticity, 2017. **2017**.

31. Poe, G.R., et al., *Locus coeruleus: a new look at the blue spot.* Nature Reviews Neuroscience, 2020.

32. Sara, S.J., *The locus coeruleus and noradrenergic modulation of cognition.* Nat Rev Neurosci, 2009. **10**(3): p. 211-223.

33. Sara, S.J., *Locus Coeruleus in time with the making of memories.* Current Opinion in Neurobiology, 2015. **35**: p. 87-94.

34. Roullet, P. and S. Sara, *Consolidation of memory after its reactivation: Involvement of beta noradrenergic receptors in the late phase.* Neural Plasticity, 1998. **6**(3): p. 63-68.

35. Tronel, S., M.G.P. Feenstra, and S.J. Sara, *Noradrenergic action in prefrontal cortex in the late stage of memory consolidation.* Learning & Memory, 2004. **11**(4): p. 453-458.

36. Hansen, N. and D. Manahan-Vaughan, *Hippocampal long-term potentiation that is elicited by perforant path stimulation or that occurs in conjunction with spatial learning is tightly controlled by beta-adrenoreceptors and the locus coeruleus.* Hippocampus, 2015. **25**(11): p. 1285-1298.

37. Hansen, N. and D. Manahan-Vaughan, *Locus Coeruleus Stimulation Facilitates Long-Term Depression in the Dentate Gyrus That Requires Activation of beta-Adrenergic Receptors.* Cerebral Cortex, 2015. **25**(7): p. 1889-1896.

38. Eschenko, O. and S.J. Sara, *Learning-Dependent, Transient Increase of Activity in Noradrenergic Neurons of Locus Coeruleus during Slow Wave Sleep in the Rat: Brain Stem-Cortex Interplay for Memory Consolidation?* Cerebral Cortex, 2008. **18**(11): p. 2596-2603.

39. Aston-Jones, G. and F.E. Bloom, *Activity of norepinephrine-containing locus coeruleus neurons in behaving rats anticipates fluctuations in the sleep-waking cycle.* J Neurosci, 1981. **1**(8): p. 876-886.

40. Swift, K.M., et al., *Abnormal Locus Coeruleus Sleep Activity Alters Sleep Signatures of Memory Consolidation and Impairs Place Cell Stability and Spatial Memory.* Current Biology, 2018. **28**(22): p. 3599-+.

41. Eschenko, O., et al., *Noradrenergic Neurons of the Locus Coeruleus Are Phase Locked to Cortical Up-Down States during Sleep.* Cerebral Cortex, 2012. **22**(2): p. 426-435.

42. Steriade, M., *The corticothalamic system in sleep.* Frontiers in Bioscience-Landmark, 2003. **8**: p. D878-D899.

43. Steriade, M., *Grouping of brain rhythms in corticothalamic systems.* Neuroscience, 2006. **137**(4): p. 1087-1106.

44. ul Haq, R., et al., *Pretreatment with -adrenergic receptor agonists facilitates induction of LTP and sharp wave ripple complexes in rodent hippocampus.* Hippocampus, 2016. **26**(12): p. 1486-1492.

45. Novitskaya, Y., et al., *Ripple-triggered stimulation of the locus coeruleus during post-learning sleep disrupts ripple/spindle coupling and impairs memory consolidation.* Learning & Memory, 2016. **23**(5): p. 238-248.

46. Astonjones, G. and F.E. Bloom, *Activity of Norepinephrine-Containing Locus Coeruleus Neurons in Behaving Rats Anticipates Fluctuations in the Sleep-Waking Cycle.* Journal of Neuroscience, 1981. **1**(8): p. 876-886.

47. Carter, M.E., et al., *Tuning arousal with optogenetic modulation of locus coeruleus neurons.* Nature Neuroscience, 2010. **13**(12): p. 1526-U117.

48. Roumis, D.K. and L.M. Frank, *Hippocampal sharp-wave ripples in waking and sleeping states.* Current Opinion in Neurobiology, 2015. **35**: p. 6-12.

49. Tang, W.B., et al., *Hippocampal-Prefrontal Reactivation during Learning Is Stronger in Awake Compared with Sleep States.* Journal of Neuroscience, 2017. **37**(49): p. 11789-11805.

50. Wang, D.V. and S. Ikemoto, *Coordinated Interaction between Hippocampal Sharp-Wave Ripples and Anterior Cingulate Unit Activity.* Journal of Neuroscience, 2016. **36**(41): p. 10663-10672.

51. Peyrache, A., F.P. Battaglia, and A. Destexhe, *Inhibition recruitment in prefrontal cortex during sleep spindles and gating of hippocampal inputs.* Proceedings of the National Academy of Sciences of the United States of America, 2011. **108**(41): p. 17207-17212.

52. Latchoumane, C.F.V., et al., *Thalamic Spindles Promote Memory Formation during Sleep through Triple Phase-Locking of Cortical, Thalamic, and Hippocampal Rhythms.* Neuron, 2017. **95**(2): p. 424-+.

53. Maingret, N., et al., *Hippocampo-cortical coupling mediates memory consolidation during sleep.* Nature Neuroscience, 2016. **19**(7): p. 959-964.

54. Sadowski, J.H.L.P., M.W. Jones, and J.R. Mellor, *Sharp-Wave Ripples Orchestrate the Induction of Synaptic Plasticity during Reactivation of Place Cell Firing Patterns in the Hippocampus.* Cell Reports, 2016. **14**(8): p. 1916-1929.

55. Norimoto, H., et al., *Hippocampal ripples down-regulate synapses.* Science, 2018. **359**(6383): p. 1524-+.

56. Kempadoo, K.A., et al., *Dopamine release from the locus coeruleus to the dorsal hippocampus promotes spatial learning and memory.* Proceedings of the National Academy of Sciences of the United States of America, 2016. **113**(51): p. 14835-14840.

57. Takeuchi, T., et al., *Locus coeruleus and dopaminergic consolidation of everyday memory.* Nature, 2016. **537**(7620): p. 357-+.

58. Wagatsuma, A., et al., *Locus coeruleus input to hippocampal CA3 drives single-trial learning of a novel context.* Proceedings of the National Academy of Sciences of the United States of America, 2018. **115**(2): p. E310-E316.

59. Lemon, N., et al., *Locus Coeruleus Activation Facilitates Memory Encoding and Induces Hippocampal LTD that Depends on beta-Adrenergic Receptor Activation.* Cerebral Cortex, 2009. **19**(12): p. 2827-2837.

60. Selinger, J.V., et al., *Methods for characterizing interspike intervals and identifying bursts in neuronal activity.* J Neurosci Methods, 2007. **162**(1-2): p. 64-71.

61. Mitra, P. and H. Bokil, *Observed brain dynamics*. 2008, Oxford ; New York: Oxford University Press. xxii, 381 p.

Figure Captions

Figure 1. Modulatory effect of cortical states on LC population activity and hippocampal ripples. A. Representative traces of simultaneously recorded CA1-LFP and LC MUA. Dashed line in the middle trace marks the ripple detection threshold; red dot marks ripple event. B. Fluctuation of firing rate of LC neurons and rate of ripple occurrence depended on the cortical state, which was indicated by the synchronization index (SI) as the ratio between low frequency (1-10Hz) and high frequency (30-90Hz) power. C. Averaged cortical delta power and hippocampal ripple power are shown around each group of ‘surrogate’ events created by varying time windows from 1 to 10 seconds. D. The averaged PETHs of LC MUA around ‘surrogate’ events computed with a 5-sec shuffling time window are shown for 17 LC MUA recordings obtained from 4 rats (bin size: 5ms, smoothed with a 10ms Gaussian window and z-score normalized).

Figure 2. The LC population activity is suppressed around hippocampal ripples. A. The averaged PETH of LC MUA across all sessions around ripples (blue) and around ‘surrogate’ events (black). C-MIs were computed as the area below/above the curve every 0.5 sec along the time axis of the PETH. B. Averaged c-MIs of LC MUA PETHs around onsets of all detected ripples are shown for each recording session.

Figure 3. Heterogeneous modulation of LC activity around subsets of hippocampal ripples. A. Distribution of s-MIs extracted for ripple-associated (red) and permuted-events-associated (blue) PETHs. The vertical dashed lines mark the upper and lower limits of 95% confidence intervals. B. MIs did not show difference across subsets of ripples with different levels of ripple amplitudes and intra-ripple frequencies. C. Representative traces for isolated (marked by red circles) and clustered (marked by blue circles) ripples. D. C-MIs of PETHs of LC MUAs around isolated (red) and clustered (blue) ripples. Horizontal black bar indicates significant difference between c-MIs around two types of ripples, $p < 0.05$ (Wilcoxon signed-rank test).

Figure 4. Ripple-associated LC suppression is state-dependent. A. C-MIs of PETHs of LC MUAs around awake (red) and sleep (blue) ripples. Horizontal bars indicate significant suppression of LC MUA; Comparison of MIs within time window [-2 0] sec before awake (red) and sleep (blue) ripples was shown in the inset. *** $p < 0.001$ (Wilcoxon signed-rank test). B. Peri-ripple spectrogram of the frontal EEG around ripples occurring during awake (A-ripples) and NREM sleep (S-ripples). C. Representative traces of the frontal EEG and CA1 LFP during NREM sleep episode. Blue dots mark spindle-coupled ripple, red dots mark spindle-uncoupled ripples. D. C-MIs of PETHs of LC MUAs around spindle-coupled (red) and uncoupled (blue) ripples. Horizontal bars indicate significant suppression of LC MUA; Comparison of MIs within time window [-2 0] sec around spindle-uncoupled (red) and coupled (blue) ripples was shown in the inset. E. Coherence between the hippocampus and cortex around spindle-coupled (S-coupled) and –uncoupled (S-uncoupled) ripples.

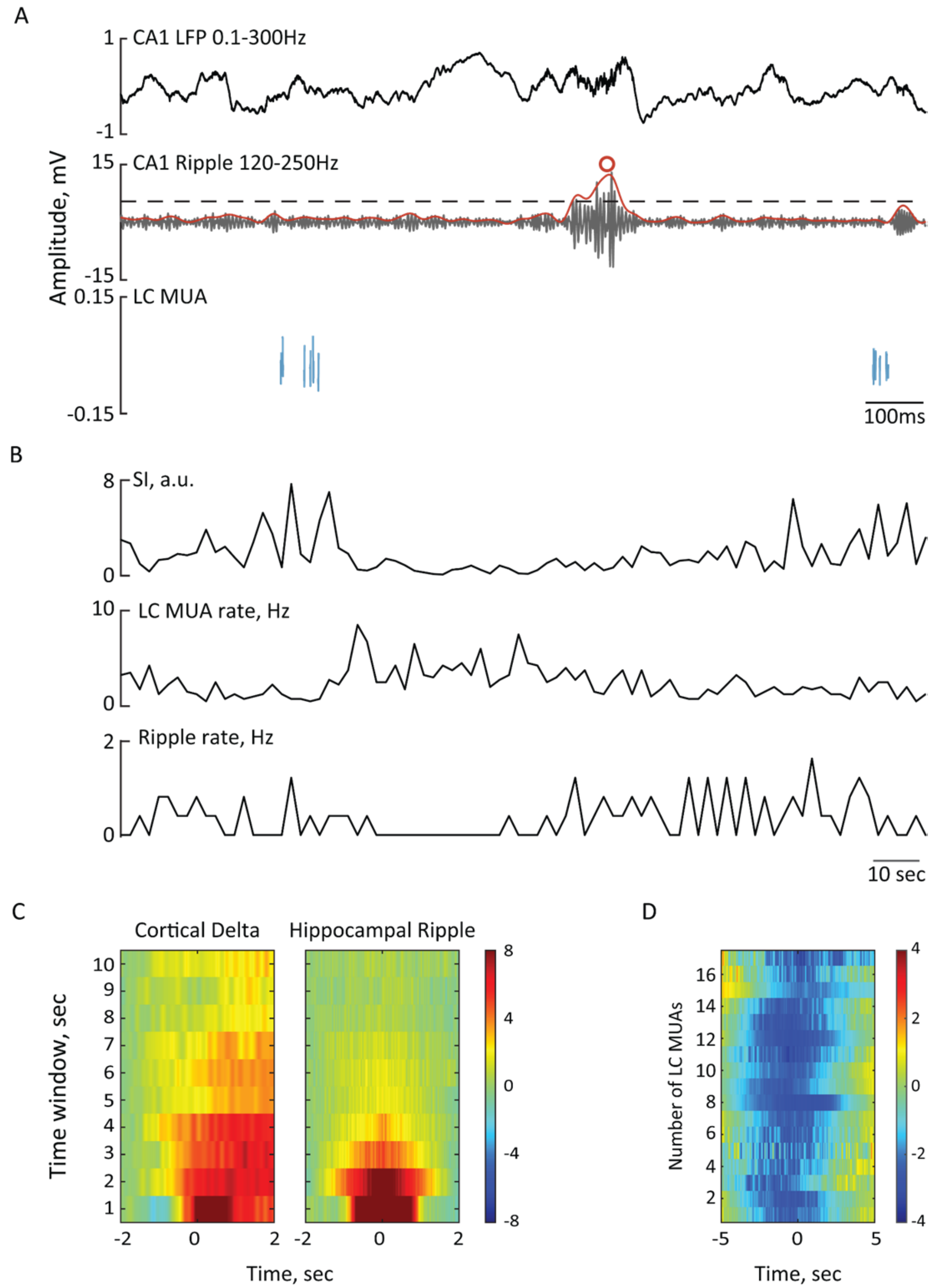

Figure 1. Modulatory effect of cortical states on LC population activity and hippocampal ripples.

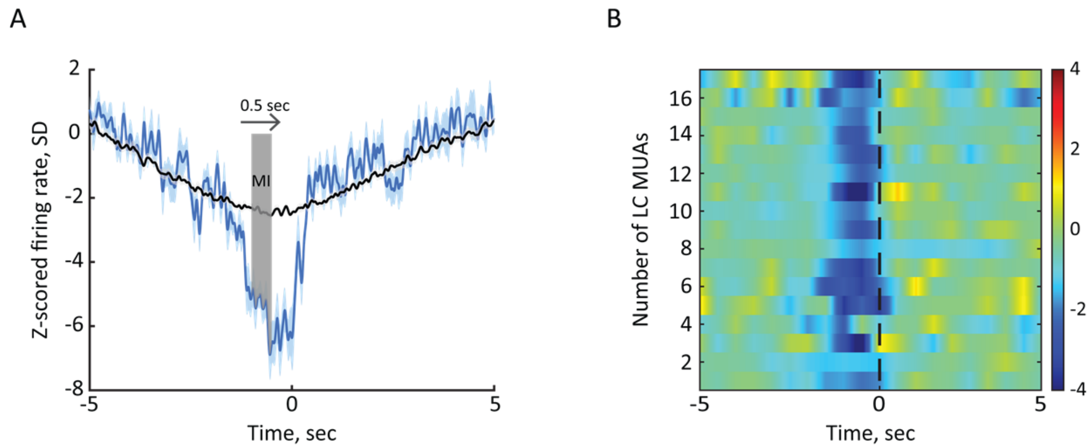

Figure 2. The LC population activity is suppressed around hippocampal ripples.

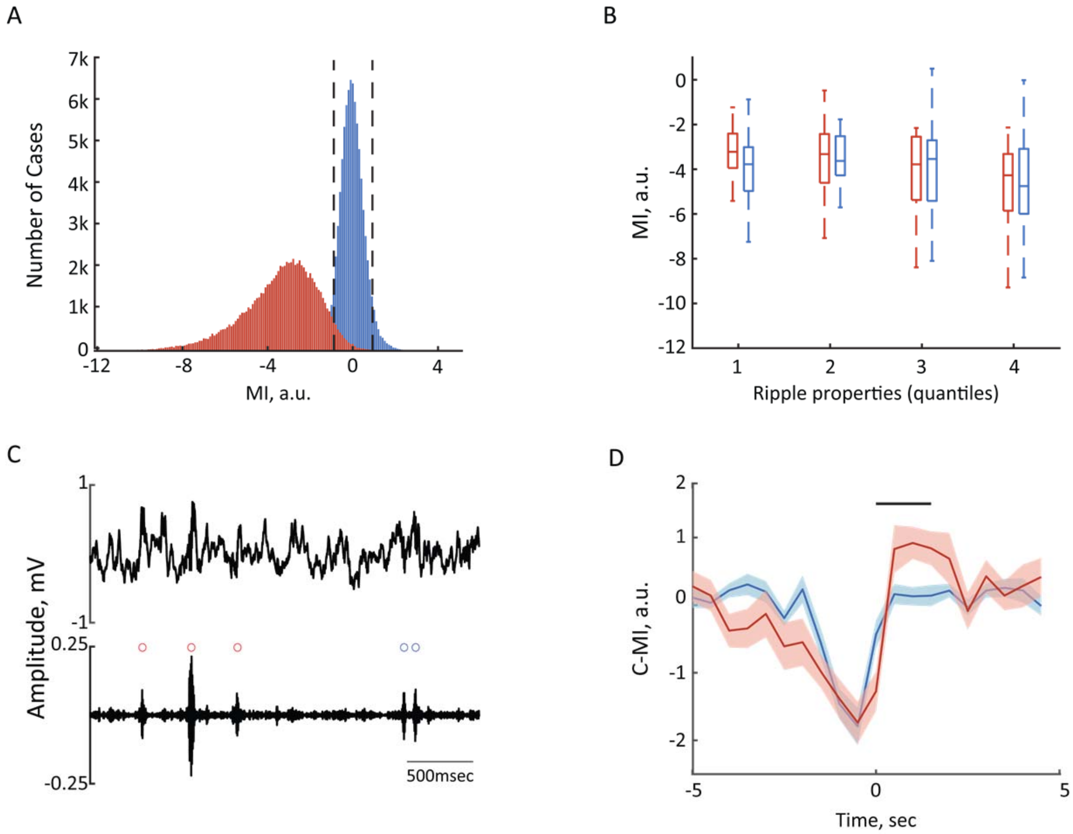

Figure 3. Heterogeneous modulation of LC activity around subsets of hippocampal ripples.

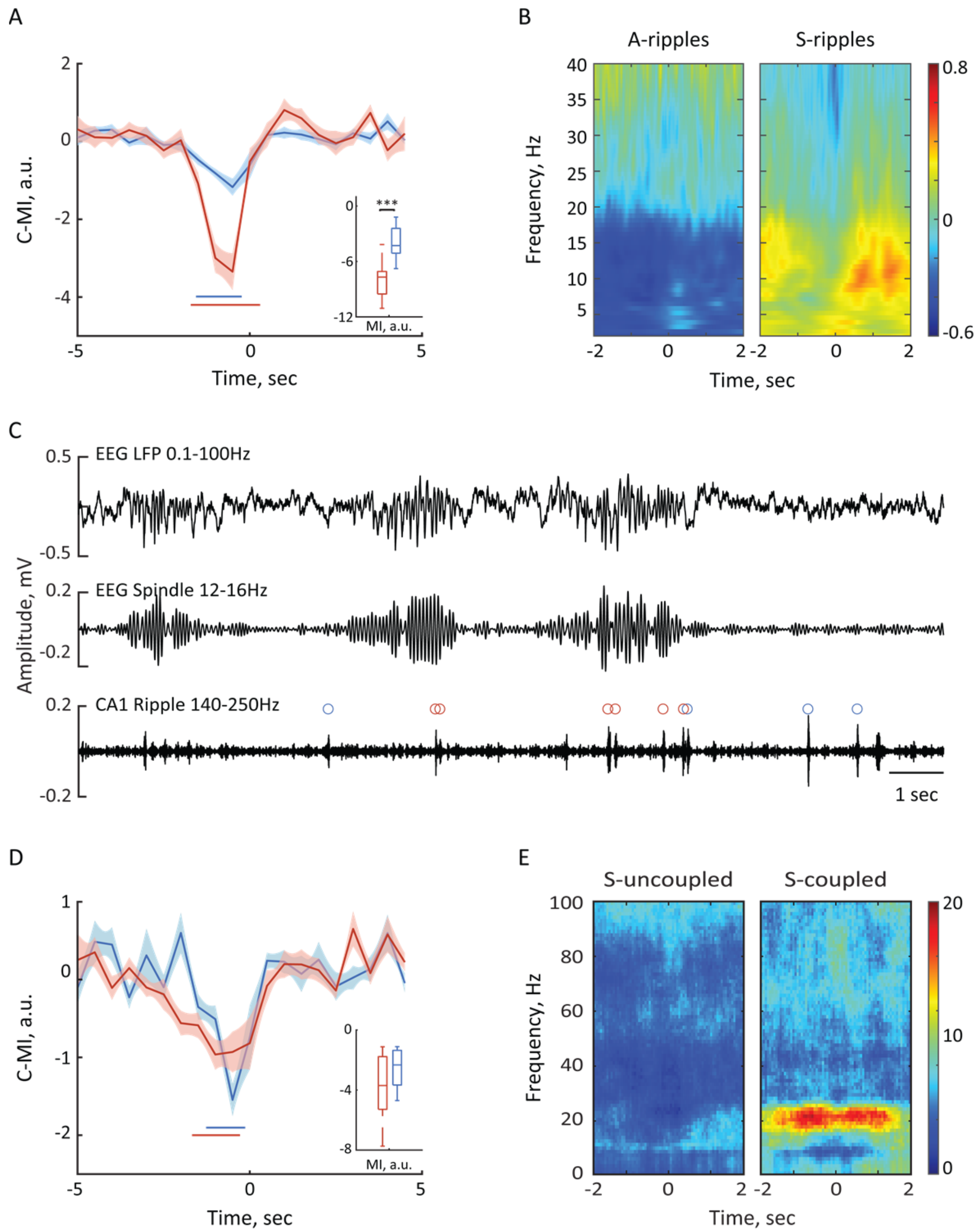

Figure 4. Ripple-associated LC suppression is state-dependent.

Systems/Circuits

Occurrence of Hippocampal Ripples is Associated with Activity Suppression in the Mediodorsal Thalamic Nucleus

Mingyu Yang,[1] **Nikos K. Logothetis,**[1,2] **and Oxana Eschenko**[1]
[1]Max Planck Institute for Biological Cybernetics, Tübingen D-72076, Germany, and [2]Centre for Imaging Sciences, Biomedical Imaging Institute, The University of Manchester, Manchester M13 9PT, United Kingdom

Forming reliable memories requires coordinated activity within distributed brain networks. At present, neural mechanisms underlying systems-level consolidation of declarative memory beyond the hippocampal–prefrontal interactions remain largely unexplored. The mediodorsal thalamic nucleus (MD) is reciprocally connected with the medial prefrontal cortex (mPFC) and also receives inputs from parahippocampal regions. The MD may thus modulate functional connectivity between the hippocampus and the mPFC at different stages of information processing. Here, we characterized, in freely behaving Sprague Dawley male rats, the MD neural activity around hippocampal ripples, indicators of memory replay and hippocampal–cortical information transfer. Overall, the MD firing rate was transiently (0.76 ± 0.06 s) decreased around ripples, with the MD activity suppression preceding the ripple onset for 0.41 ± 0.04 s (range, 0.01–0.95 s). The degree of MD modulation correlated with ripple amplitude, differed across behavioral states, and also depended on the dynamics of hippocampal–cortical population activity. The MD suppression was the strongest and the most consistent during awake ripples. During non–rapid eye movement sleep, MD firing rate decreased around spindle-uncoupled ripples, but increased around spindle-coupled ripples. Our results suggest a competitive interaction between the thalamocortical and hippocampal–cortical networks supporting "on-line" and "off-line" information processing, respectively. We hypothesize that thalamic activity suppression during spindle-uncoupled ripples is favorable for memory replay, as it reduces interference from sensory relay. In turn, the thalamic input during hippocampal–cortical communication, as indicated by spindle/ripple coupling, may contribute to selectivity and reliability of information transfer. Both predictions need to be tested in future experiments.

Key words: cortical state; hippocampus; mediodorsal thalamus; memory consolidation; sharp-wave ripples; sleep

Significance Statement

Systems mechanisms of declarative memory consolidation beyond the hippocampal–prefrontal interactions remain largely unexplored. The connectivity of the mediodorsal thalamic nucleus (MD) with extrahippocampal regions and with medial prefrontal cortex underlies its role in execution of diverse cognitive functions. However, little is known about the MD involvement in "off-line" consolidation. We found that MD neural activity was transiently suppressed around hippocampal ripples, except for ripples co-occurring with sleep spindles, when the MD activity was elevated. The thalamic activity suppression at times of spindle-uncoupled ripples may be favorable for memory replay, as it reduces interference with sensory relay. In turn, the thalamic input during hippocampal–cortical communication, as indicated by spindle/ripple coupling, may contribute to selectivity and reliability of information transfer.

Introduction

Higher-order brain functions rely on fine-tuned interactions within large-scale brain networks. The network-level information processing takes place during alert behaviors, but also during so-called "off-line" states when sensory input is absent. The hippocampal–cortical network is essential for the encoding, consolidation, and retrieval of declarative memory (Wang and Morris, 2010; Eichenbaum, 2017). The two-stage model of the hippocampal-dependent memory consolidation (Buzsáki, 1989) postulates that experience-induced changes of neural activity in the hippocampus (HPC) are mediated "on-line" by theta rhythm and "off-line" by high-frequency (~200 Hz) oscillations, or ripples, produced by synchronized discharge of CA1 neurons (Ylinen et al., 1995; Chrobak and Buzsáki, 1996). The hippocampal ripples preferentially occur

Received July 25, 2018; revised Oct. 1, 2018; accepted Oct. 20, 2018.

Author contributions: M.Y. wrote the first draft of the paper; N.K.L. and O.E. edited the paper; O.E. designed research; M.Y. performed research; N.K.L. contributed unpublished reagents/analytic tools; M.Y. analyzed data; O.E. wrote the paper.

We thank Michel Beserve and Masataka Watanabe for valuable comments on the manuscript; Katalin Kalya for help with histology; and Eduard Krampe, Axel Oeltermann, and Joachim Werner for technical support. This research was supported by the Max Planck Society.

The authors declare no competing financial interests.

Correspondence should be addressed to Dr. Oxana Eschenko, Max Planck Institute for Biological Cybernetics, Max-Planck-Ring 8, Tubingen D-72076, Germany. E-mail: oxana.eschenko@tuebingen.mpg.de.

https://doi.org/10.1523/JNEUROSCI.2107-18.2018

 0270-6474/19/390434-11$15.00/0

during periods of enhanced cortical excitability (Sirota et al., 2003; Battaglia et al., 2004; Mölle et al., 2006) and coincide with thalamocortical sleep spindles (Siapas and Wilson, 1998). The ripple-associated replay of experience-activated neurons is thought to reflect memory trace reactivation and promote selective synaptic plasticity (Skelin et al., 2018). The coordinated hippocampal and cortical population activity is thought to mediate information transfer from the HPC to cortex for long-term storage (Buzsáki, 1989; Wang and Morris, 2010; Skelin et al., 2018).

The hippocampal–prefrontal pathway is the most extensively studied circuit in the context of mechanisms of declarative memory. Clearly, memory supporting network is not limited to these two brain regions; yet, the neural interactions beyond the hippocampal–prefrontal pathway remain largely unexplored. Our fMRI-based mapping of the whole brain activity at times of ripples in macaques revealed a characteristic pattern of positive and negative BOLD responses (Logothetis et al., 2012). Specifically, many cortical and limbic regions were activated during ripples, while a subset of subcortical areas, including the thalamus, showed activity suppression (Logothetis et al., 2012). Subsequent electrophysiological examination confirmed the ripple-associated inhibition in the lateral geniculate nucleus (Logothetis, 2015). The results of our fMRI study are consistent with numerous reports about tight temporal coupling between the population bursts in the HPC and neuronal activity in associative (Peyrache et al., 2009; Wierzynski et al., 2009; Wang and Ikemoto, 2016; Wilber et al., 2017) and primary sensory (Sirota et al., 2003; Ji and Wilson, 2007; Rothschild et al., 2017) cortices. Enhanced activity around ripples has been also shown in the ventral striatum (Lansink et al., 2008). Furthermore, bidirectional modulation was reported for neurons in the ventral tegmental area (VTA; Gomperts et al., 2015) and basolateral amygdala (BLA; Girardeau et al., 2017), while activity suppression was found in the median raphe (Wang et al., 2015) and the midline thalamic nuclei (Lara-Vásquez et al., 2016).

In the present study, we sought to characterize the ripple-associated activity in the mediodorsal thalamic nucleus (MD). The MD integrates various types of information and mediates it to the medial prefrontal cortex (mPFC) for execution of diverse cognitive functions (Mitchell, 2015), including memory (Markowitsch, 1982; Van Der Werf et al., 2003). Although there are no known direct projections between the MD and HPC (Groenewegen, 1988; Varela et al., 2014), the MD contributes to declarative memory as a part of extrahippocampal circuit (Ketz et al., 2015). The MD receives afferents from the lateral entorhinal and perirhinal cortices, which provide parallel multisensory input to the MD and HPC (Groenewegen, 1988; Burwell, 2000). The MD is reciprocally connected with the mPFC, which in turn receives direct input from the HPC (Jay et al., 1992). The MD is thought to gate the hippocampal–cortical and cortical–cortical interactions that are relevant for declarative memory (Floresco and Grace, 2003; Ketz et al., 2015). However, the role of MD in off-line processing has not been explored. Here, we report that the MD activity is systematically suppressed around ripples. We also found that the ripple-associated MD modulation varied across awake and sleep states. The MD suppression was more consistent and robust during awake state, while synergistic activation of the MD–HPC–mPFC network occurred during non–rapid eye movement (NREM) sleep at times of ripple/spindle coupling. Collectively, our results suggest competitive interactions between large-scale brain networks mediating different stages of information processing.

Materials and Methods

Animals. Eight adult male Sprague Dawley rats (Charles River Laboratories) weighting 300–450 g were used. After surgery rats were single-housed and kept on a 12 h light/dark cycle (8:00 A.M. lights on). All the experiments were performed during dark cycle. The study was performed in accordance with the German Animal Welfare Act (TierSchG) and Animal Welfare Laboratory Animal Ordinance Tierschutz-Versuchstierverordnung (TierSchVersV), and was in full compliance with the guidelines of the EU Directive 2010/63/EU on the protection of animals used for scientific purposes. The study was reviewed by the ethics commission Tierschutzgesetz, (TierSchG, Section 15) and approved by the state authority (Regierungspräsidium, Tübingen, Baden-Württemberg, Germany).

Anesthesia. Implantation of electrodes was performed under isoflurane anesthesia (initiation 4%, maintenance 1.5–2.0%). The depth of anesthesia was controlled by ensuring a lack of responses to mildly noxious stimuli (pinch of hind paw). Heart rate and blood oxygenation were monitored using a pulse oximeter (Nonin 8600V, Nonin Medical); supplementary oxygen was provided to maintain the blood oxygenation level above 90%. Body temperature was maintained at 37°C throughout the entire anesthesia period.

Surgery and electrode placement. A fully anesthetized rat was fixed in a stereotaxic frame with the head angle at 0°. The skull was exposed, and a local anesthetic (Lidocard 2%, B. Braun) was applied on the skin edges to additionally numb the skin. Burr holes were made for electrodes and anchor screws. Dura mater was removed when necessary. For EEG recordings, a stainless-steel screw (0.86 mm diameter, Fine Science Tools) was placed above the frontal cortex, and the ground screw was placed above the cerebellum. Four anchor screws (1.19 mm diameter, Fine Science Tools) were placed on the skull side edges. Screws were fixed in the skull and additionally secured with tissue adhesive. For extracellular recording in the MD and HPC, twisted wires or tube tetrodes (Kapoor et al., 2013) were used. The tetrodes were made from insulated nichrome wire (12 μm diameter, Sandvik Wire and Heating Technology) and assembled into a microdrive (Versadrive; Neuralynx). A custom design of the microdrive allowed targeting the MD with up to six tetrodes and dorsal HPC (dHPC) with up to two tetrodes. Before implantation, tetrode impedance was adjusted to 150–500 kΩ by gold plating. The drive with electrodes was fixed in a stereotaxic micromanipulator (David Kopf Instruments) and slowly lowered until the electrode tips targeting the MD reached ~5.0 mm below the brain surface. The tips of dHPC electrodes were fixed ~3.0 mm higher and expected to reach ~2.0 mm depth. A single platinum-iridium electrode (FHC) was implanted in the mPFC. The final adjustment of the electrode position was guided by on-line monitoring of neural activity. The entire implant was secured on the skull with dental cement (Paladur, Heraeus Kulzer). A copper mesh was mounted around the implant to protect exposed wires and also to isolate recording electrodes from the electrical noise. The injection of analgesic (2.5 mg/kg, s.c.; Finadyne, Essex) and antibiotic (5.0 mg/kg, s.c.; Baytril, Bayer) was given before rat awakening from anesthesia and repeated at 24 h intervals during next 4 d. Animals were allowed 1 week of postsurgery recovery.

Electrophysiological recording. Rats were first habituated to the recording setup and cable plugging procedure. The head implant was connected to the Neuralynx Digital Lynx acquisition system via two 16-channel head stages with red/green tracking LEDs (Neuralynx). The electrode placement in the MD was optimized by lowering the electrodes in 0.05–0.1 mm steps and monitoring spiking activity on the high-passed (300 Hz to 8 kHz) extracellular signal. The depth of dHPC electrodes was adjusted by gradually lowering the tetrodes (maximum 0.05 mm per day) until reliable ripple activity was observed. Once the electrode position was optimized, the broad-band (0.1 Hz to 8 kHz) extracellular signals were acquired and digitized at 32 kHz. The brain activity was referenced to the ground electrode. The animals' movement was monitored by video tracking (25 frames per second) with the aid of LEDs attached to the head stage. All recordings were performed between 10:00 A.M. and 7:00 P.M. for up to 2 h.

Single-unit isolation. The MD single units were isolated using two or four tetrode channels. Extracellular signals were high-pass (600 Hz) filtered and the spike waveforms with negative peaks exceeding −0.05 mV were extracted. The template-matching algorithm based on the principal component analysis was used for clustering the spike waveforms of individual units (Spike2 software, Cambridge Electronic Design). Various specific measurements of the spike waveform were additionally used for cluster refinement. A unit cluster was classified as a single-unit activity (SUA) if the refractory period (time between two consecutive spikes) was at least 1 ms. When the recording quality and the spike sorting did not allow unambiguous single-unit isolation, the spike cluster was conservatively classified as multiunit activity (MUA).

Classification of behavioral states. We classified the rat spontaneous behavior into awake and NREM sleep using frontal EEG or PFC local field potentials (LFPs) by applying a standard sleep-scoring algorithm described in detail previously (Novitskaya et al., 2016). Briefly, animal movement speed was extracted from the video recording synchronized with neural signal. The θ/δ ratio was calculated from the artifact-free EEG in 2.5 s epochs. The epochs of awake state were identified by the presence of active locomotion and above threshold θ/δ ratio; the epochs of NREM sleep were identified by the absence of motor activity and below threshold θ/δ ratio. The minimal duration of the same behavioral state was set to 20 s; data segments with less steady behavioral states were excluded from further analysis.

Detection of cortical spindles. Sleep spindles were detected from the artifact-free EEG channel by bandpass (12–16 Hz) filtering, downsampling to 200 Hz, and thresholding of the spindle band power envelop (root mean square (RMS) with 0.2 s smoothing window; spindle RMS). The spindle detection threshold was calculated as 3 SDs of the spindle RMS during NREM sleep. The minimal length of sleep spindle was set to 0.5 s of continuous spindle RMS values above the threshold. The spindle onsets and offsets were defined at 1 SD threshold ascending and descending crossings, respectively.

Detection of hippocampal high-frequency oscillations. The transient high-frequency population bursts were detected from the LFPs recorded in the pyramidal layer of the dorsal CA1. The LFP signal was bandpass (gamma band, 70–120 Hz; ripple band, 120–250 Hz) filtered, rectified, and low-pass filtered at 25 Hz. The resulting signal was *z*-score normalized. The high-frequency events were identified by signal amplitude exceeding a threshold of 5 SDs for ripples and 4 SDs for gamma events. The event onsets and offsets were defined at the 1 SD threshold ascending and descending crossings, respectively. We used a 70 ms refractory window to prevent double detection of the same event. The Morlet-wavelet time-frequency analysis was used to classify the events into gamma, gamma/ripple, and ripple oscillations based on intraevent frequency. For exploring the temporal pattern of ripple occurrence, we used a method based on computing the logarithm of inter-ripple intervals (IRIs), described in detail previously (Selinger et al., 2007). Briefly, the bimodal log(IRI) distribution indicated two temporal patterns of ripple occurrence with shorter and longer IRIs. We identified the crossing time of two distributions and used it for classifying “clustered” and “isolated” ripples. Ripples with short IRIs (<0.33 s) were considered as a ripple cluster and treated as a single ripple event. The time of the first ripple in the cluster was considered the ripple onset time. Spindle-coupled ripples were defined as ripples occurring between onsets and offsets of spindles.

Analysis of perievent neural activity. To examine neural activity around transient oscillatory events (ripples, spindles, gammas), perievent spike histograms (PETHs) were generated ±2 s around the event onsets and smoothed with a Gaussian window (window size, 6 ms; bin size, 2 ms). To minimize the impact of slow fluctuations of the neuronal excitability that is synchronized throughout the entire forebrain, we applied an event permutation procedure. In specific, we created a “surrogate” event sequence by randomly distributing the same number of events detected every 4 s in a given session. The permutation procedure was repeated 100 times and the PETHs were generated ±2 s around the surrogate events. The time series (2 ms bins) of MD MUA/SUA around the surrogate events were subtracted from the corresponding values around “true” events, and the resulting (“corrected”) PETHs were *z*-score normalized to the MD MUA/SUA firing rate during the entire 4 s time window of the surrogate PETHs.

To quantify perievent changes of neural activity, a modulation index (MI) was calculated by extracting the area above/below the curve of each PETH ± 0.5 s around time 0. To determine the significance of modulation, we built PETHs around surrogate events generated by permutation of the interevent intervals and calculated the MIs for each of 5000 shuffled PETHs. The 95% confidence interval (CI) served as the significance threshold. The onset/offset and the duration of the firing rate change were defined by the ±1 SD threshold crossing of normalized perievent MD MUA. For examining MD modulation around subsets of ripples, for each data set, the ripple times were bootstrapped, and the bootstrapped MI (b-MI) was computed for 100 randomly selected ripples. Then the same procedure was repeated 5000 times, and the distribution of b-MIs was plotted, also for awake and NREM sleep ripples.

Experimental design and statistical analysis. The LFPs and MUA recordings from different placements in the MD were considered independent if a linear distance between the sites exceeded 140 μm (Buzsáki, 2004). A one-way ANOVA was used for independent measures. In the case of repeated observations, a repeated-measures ANOVA or paired *t* test was used when data met the criteria for normality; otherwise, a Wilcoxon signed-rank test was used. For ANOVAs, when the sphericity assumption was violated, the Greenhouse–Geisser correction method was applied. Bonferroni's test was used for *post hoc* comparisons. Pearson's linear correlations were used when appropriate. The statistical significance α value was set at $p = 0.05$. The IBM SPSS Statistics (version 22) and MATLAB (MathWorks) software packages were used for statistical analysis.

Perfusion and histology. After the last recording session, rats were killed with a lethal dose of pentobarbital sodium (100 mg/kg i.p.; Narcoren, Merial) and perfused transcardially with 0.9% saline followed by 4% paraformaldehyde in 0.1 M phosphate buffer (PB), pH 7.4. The brains were removed and stored in the same fixative. Before sectioning, whole brains were placed in 0.1 M PB buffer containing 30% sucrose until they sank. Serial 60-μm-thick coronal sections were then cut on a horizontal freezing microtome (Microm HM 440E; Thermo Fisher Scientific, Waltham, MA), collected in 0.1 M PB, and then directly stained or stored at −20°C in a cryoprotectant solution (30% ethylene glycol and 10% sucrose in 0.05 M PB) until further processing. Nissl staining was performed according to a standard procedure. Briefly, sections were mounted on gelatin-coated glass slides, defatted, stained with cresyl violet, rinsed with acetic acid, dehydrated, and coverslipped. All sections were examined using an AxioPhot or AxioImager microscope (Carl Zeiss). Positions of the electrode tips were assessed visually and digitized.

Results

We obtained 42 simultaneous recordings in the CA1 area of the dHPC, prelimbic area of the PFC, and MD in eight rats. Figure 1*A* illustrates the electrodes targeting the dHPC and MD. We sampled MD activity from different subregions of the MD using multiple tetrodes and by lowering tetrodes after each recording session (see Materials and Methods). Two to 17 different electrode placements per rat resulted in total of 49 MD recordings from the medial ($n = 19$), central ($n = 10$), and lateral ($n = 20$) sections of the MD. Figure 1*B* shows the reconstruction of the deepest recording sites in the MD. Preliminary analyses did not reveal any difference in neural activity across the MD sites; therefore, the results described below were obtained using combined data sets from different MD subregions, and, for simplicity, we will refer to all thalamic recordings as MD.

Neural activity in the MD is suppressed around hippocampal ripples

We first characterized the overall population activity in the MD around hippocampal ripples. Ripples were detected by thresholding at 5 SDs of the bandpass-filtered (120–250 Hz; smoothed at 25 Hz), rectified, and *z*-score-normalized CA1 LFP signal (Fig. 2,

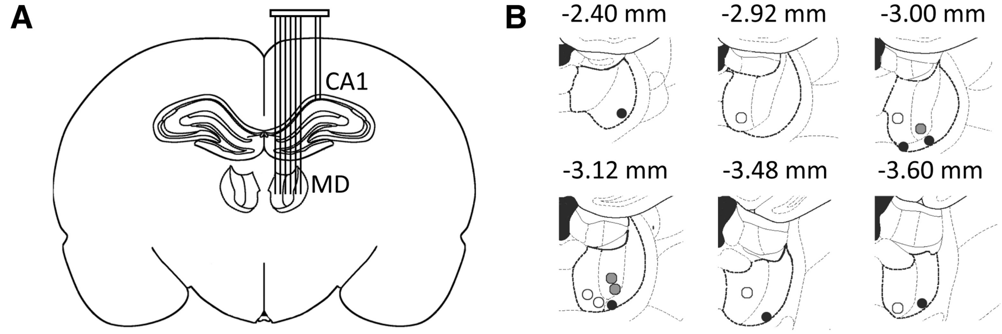

Figure 1. Simultaneous multisite electrophysiological recording in freely behaving rats. ***A***, Schematic illustration of the electrode placements in the dHPC and MD. Tetrodes (2 for dHPC and up to 6 for MD) were mounted on a movable microdrive allowing depth adjustment of each tetrode individually. ***B***, Reconstruction of the deepest recording sites within the MD is shown on different anterior–posterior planes. White circles, Medial MD; gray circles, central MD; black circles, lateral MD.

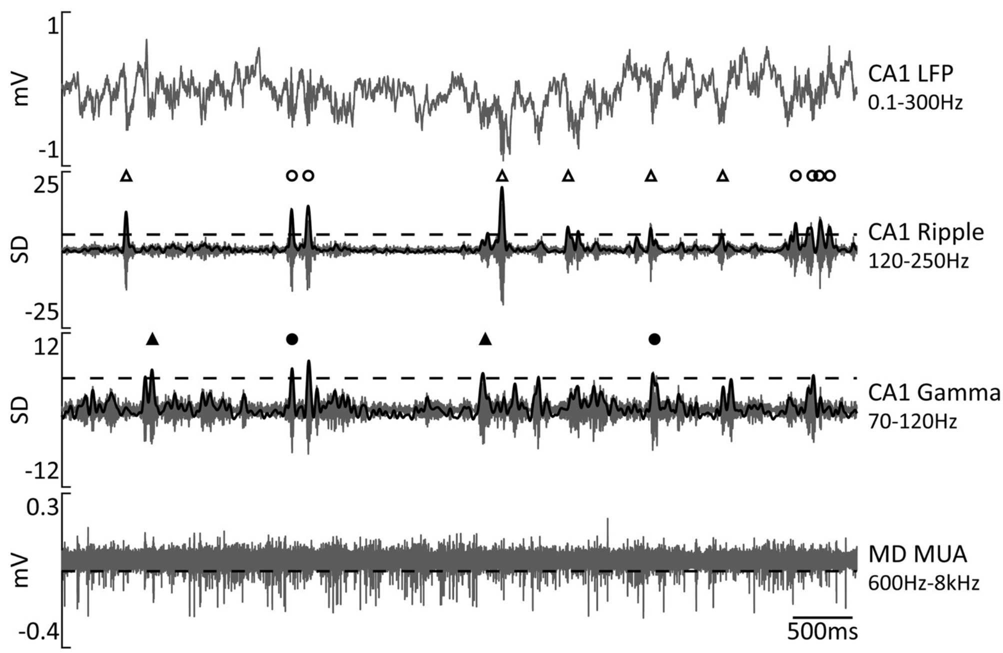

Figure 2. Detection of ripple and gamma oscillations. Representative traces of simultaneously recorded neural activity in the dHPC (top) and MD (bottom). The two middle traces show bandpass-filtered dHPC LFPs; black solid lines show rectified and smoothed signals. Horizontal dashed lines mark the detection threshold for ripples at 5 SDs, gamma events at 4 SDs, and spikes at −0.05 mV. Symbols above two middle traces mark transient oscillatory events. Open triangles mark isolated ripples, open circles mark clustered ripples, black triangles mark gamma events, and black circles mark gamma/ripple events.

middle). On average, 1013.4 ± 66.3 ripples were detected per each recording session. The multiunit spike times (referred to here as multiunit activity) were extracted from the wide-band (0.1 Hz–8 kHz) extracellular signal recorded in the MD by high-pass (600 Hz) filtering and thresholding at −0.05 mV (Fig. 2, bottom). For each recording session and each MD site, a PETH was generated at ±2 s around ripple onsets and subsequently corrected for spiking activity fluctuation around randomly distributed surrogate events (for details, see Materials and Methods). A significant transient suppression of the MD MUA around ripples was present in essentially all MD sites (Fig. 3*A*). We also calculated a modulation index (Fig. 3*C*) and tested each MD MUA case for significant modulation (see Materials and Methods). The periripple firing rate decrease was significant for all 49 MD MUA recordings (mean MI lower than the lower limit of 95% CIs). To characterize in more detail the dynamics of ripple-associated modulation of MD MUA, for each session-averaged PETH, we extracted the onset, peak time, and duration of the firing rate change, as illustrated in Figure 3*C*. Remarkably, in most cases, a decrease of the MD firing rate preceded the ripple onset, occurring, on average 0.41 ± 0.04 s (range, 0.01–0.95 s) before the ripple. The MD suppression lasted, on average, for 0.76 ± 0.06 s (range, 0.13–2.10 s) and peaked at 0.11 ± 0.01 s after ripple onset (range, 0.04–0.39 s). Figure 3*D* shows the distribution for the MD inhibition onset (red line), duration (blue), and times of the minimal firing rate (black). There was no difference in the onset, peak time, or duration of MD MUA suppression across different MD subregions (one-way ANOVA, onset, $F_{(2,37)} = 0.72$, $p = 0.50$; peak time, $F_{(2,37)} = 0.14$, $p = 0.87$; duration, $F_{(2,37)} = 0.36$, $p = 0.70$).

It is possible, however, that the multiunit population response does not capture the response profiles of the individual MD neurons. Therefore, we also characterized the ripple-associated firing rate modulation of the MD single units. The recording quality permitted reliable isolation of 40 single units ($n = 6$ rats). The ripple-associated suppression was present in all MD single units (Fig. 3*B*). We thus considered the MD neurons as responding homogeneously and used MD MUA for further analyses.

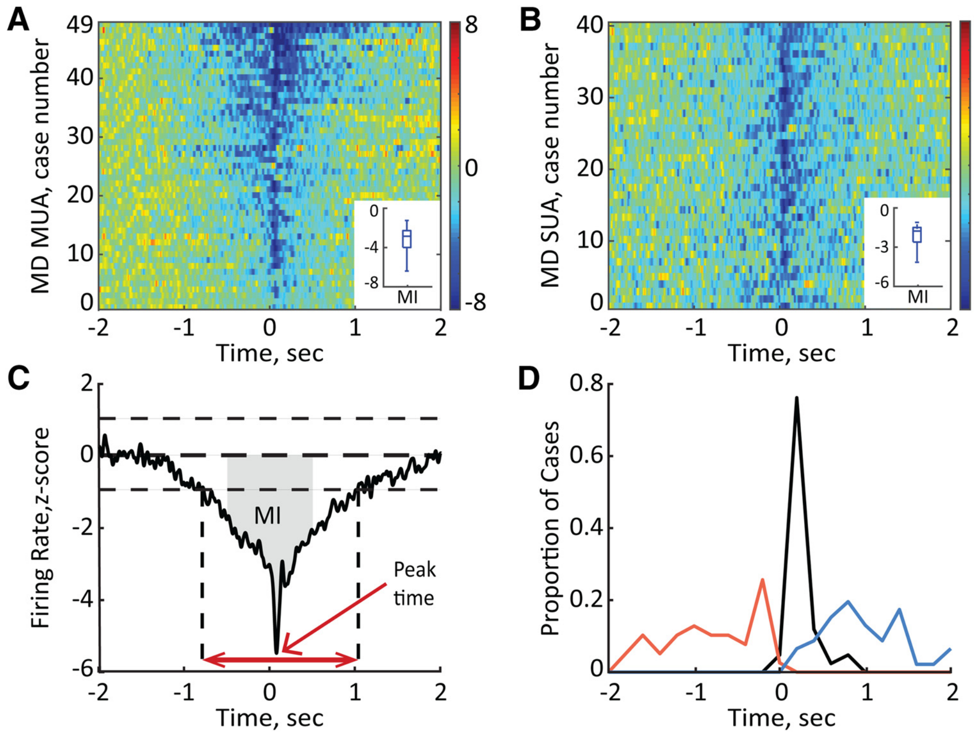

Figure 3. Ripple-associated suppression of the MD neural activity. ***A***, ***B***, Normalized firing rate is plotted for MD MUA (***A***) and MD single units (***B***). The averages around onsets of all detected ripples are shown for 49 MD MUA recordings obtained from different MD sites in eight rats and 40 single units ($n = 6$ rats). The cases are sorted according to the values of the MI. Color bars show *z* scores. Insets, Median and variability outside the upper and lower quartiles are indicated. ***C***, Quantitative characterization of the ripple-associated firing rate change. The MI was calculated as the area (gray) between the curve and $y = 0$ within ± 0.5 s around the ripple onset ($t = 0$). The onset and offset of modulation were detected by ± 1 SD threshold crossings (vertical dashed lines). The time between onset and offset was considered the duration of modulation (red double-headed arrow). The peak time was determined as the time with the minimum firing rate (red arrow) ***D***, The distribution of onsets (red), peak times (black), and offsets (blue) of the MD firing rate change relative to ripple onset ($t = 0$) for all MD MUA cases ($n = 49$) shown in ***A***.

The degree of MD suppression correlates with ripple features

We examined whether the degree of MD MUA modulation systematically varied with ripple intrinsic properties. To this end, we split all detected ripples according to their amplitude or intraripple frequency into quartiles and extracted for each ripple group the corresponding MI. A significant linear correlation was found between the MI and ripple amplitude ($r = -0.28$, $p < 0.0001$); a stronger MD MUA suppression was associated with ripples of higher amplitude (Fig. 4*A*). No such relationships were revealed between MI and intraripple frequency ($r = 0.096$, $p = 0.18$).

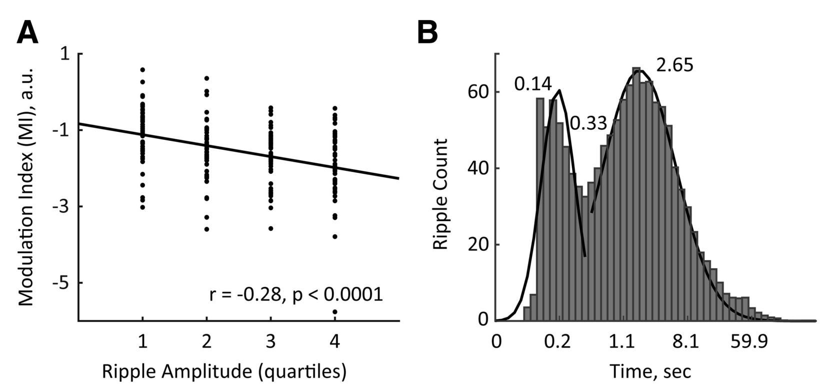

Figure 4. The degree of MD modulation correlated with ripple amplitude and the temporal pattern of ripple occurrence. ***A***, The MIs from all 49 MD MUA cases are plotted according to the quartiles of ripple amplitude. The black line shows the linear regression. Note that stronger MD suppression (lower MIs) corresponds to ripples of higher amplitude. ***B***, The log-scale distribution of inter-ripple intervals with Gaussian fittings (black lines). Numbers indicate the peak times and the crossing time of two Gaussians. Note that there is a bimodal distribution of inter-ripple intervals.

We also studied whether the MD modulation depended on the temporal pattern of ripple occurrence. The visual inspection of the bandpass-filtered (120–250 Hz) CA1 LFPs indicated that some ripples occur in close (<0.33 s) temporal proximity to each other, while other ripples are rather sparse (Figs. 2, middle, 4*B*). Thus, we classified the detected ripples as isolated or clustered (see Materials and Methods). Clusters typically consisted of two to seven ripples. We computed the PETHs of the MD MUA around isolated and clustered ripples (in the case of ripple clusters, the first ripple onset was used as $t = 0$) and observed a much stronger MD suppression around isolated ripples (-2.75 ± 0.19 vs -1.94 ± 0.11 for MIs of isolated vs clustered ripples, respectively; paired *t* test, $t_{(40)} = 4.12$, $p < 0.001$). Overall, the amplitude of isolated ripples was slightly lower than that of clustered ripples (8.86 ± 0.23 vs 9.71 ± 0.27 SDs, for isolated vs clustered ripples, respectively; paired *t* test, $t_{(40)} = 11.12$, $p < 0.0001$). The difference in the temporal pattern of ripple occurrence did not affect the strong negative correlation between the MI and ripple amplitude, as such relationships were present for both types of ripples (isolated, $r = -0.24$, $p < 0.001$; clustered, $r = -0.27$, $p < 0.0001$).

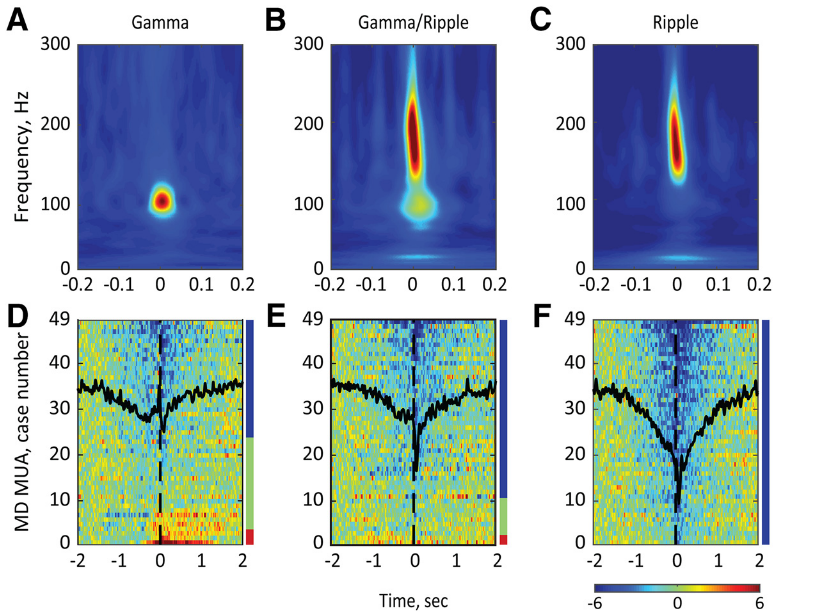

Figure 5. The MD activity modulation around different types of high-frequency population bursts in the dHPC. ***A–C***, Representative perievent spectrograms for gamma (left), gamma/ripple (middle), and ripple (right) events. ***D–F***, Normalized and color-coded MD firing rates are plotted for all MD MUA cases ($n = 49$) around the gamma (***D***), gamma/ripple (***E***), and ripple (***F***) events. The horizontal color bar shows *z* scores. Overlaid black lines show the averaged MD population dynamics around corresponding event types. The color bar on the right of each plot shows the proportion of MD MUA cases with ripple-associated suppression (blue), ripple-associated activation (red), and no modulation (green). Note the strongest MD suppression around ripples and bidirectional changes of the MD firing rate around gamma and gamma/ripple events.

Modulation of MD activity around gamma oscillations

We also characterized the dynamics of MD MUA around transients of high-gamma (70–120 Hz) oscillations (or gamma events), which is another prominent type of population activity in the HPC (Sullivan et al., 2011). We detected the gamma events by thresholding at 4 SDs of the bandpass-filtered (70–120 Hz; smoothed at 25Hz), rectified, and *z*-score-normalized CA1 LFP signal (Fig. 2, middle). Consistent with the existing literature (Ramirez-Villegas et al., 2015), a substantial fraction of gamma events (40.78 ± 1.92%) co-occurred with ripples. Based on the spectral composition of the detected transient high-frequency oscillations, we split them into "pure" gamma, "mixed" gamma/ripple, and "pure" ripple events (Fig. 5*A*–*C*). The MD MUA was significantly suppressed around pure ripples in all cases ($n = 49$), while around gamma/ripple and pure gamma events, the MD MUA decrease was detected in 79.6% ($n = 39$) and 53.1% ($n = 26$) of cases, respectively. Consequently, the mean MI was the lowest for pure ripples (−2.87 ± 0.15), indicating a more consistent decrease of the MD firing rate, compared to other event types (−1.81 ± 0.18 and −1.42 ± 0.13 for gamma/ripple and pure gamma events, respectively). Figure 5*D*–*F* shows the profiles of the MD firing rate for each event type. Finally, we compared the magnitude of MD suppression across event types by submitting only significantly modulated cases to repeated-measures ANOVA. There was a significant main effect of the event type ($F_{(2, 62)} = 31.99$, $p < 0.0001$). *Post hoc* tests showed that the MD MUA suppression was the strongest around pure ripples and the weakest around pure gamma events. Based on this result, for further analysis we considered only ripple oscillations without accompanying gamma power increase.

Ripple-associated modulation of MD activity depends on behavioral state

We further explored whether the ripple-associated modulation of MD MUA depended on the behavioral state. We classified the behavioral state as awake or NREM sleep using frontal EEG or PFC LFPs (see Materials and Methods), as also described in detail previously (Novitskaya et al., 2016). Briefly, animal movement speed was extracted from the video recording synchronized with the neural signal. The θ/δ ratio was calculated from the artifact-free EEG in 2.5 s epochs. The epochs of awake state were identified by the presence of active locomotion and an above-threshold θ/δ ratio; the epochs of NREM sleep were identified by the absence of motor activity and a below-threshold θ/δ ratio. Consistent with the existing literature (Llinás and Steriade, 2006), MD activity was higher during awake state than during NREM sleep (27.99 ± 1.78 Hz vs 10.21 ± 0.75 Hz for awake vs NREM sleep, respectively; Wilcoxon signed-rank test, $p < 0.0001$). Ripples occurred more frequently during NREM sleep than during awake epochs (7.84 ± 0.59 ripples/min vs 22.96 ± 1.28 ripples/min, respectively; Wilcoxon signed-rank test, $p < 0.0001$). We then repeated the analysis as described above for all ripples, but subdivided ripples according to the behavioral state. For each of 49 MD MUA cases, the averaged MI was calculated for awake and sleep ripples, and the significance of modulation was defined based on the averaged MI value. During awake state, a significant ripple-associated MD suppression was present in 43 of 49 MD MUA cases (87.8%), while fewer cases (35 of 49, or 71.4%, showed significant MD modulation during NREM sleep; $\chi^2_{(1)} = 4.91$, $p = 0.027$). Furthermore, the MD suppression during awake state was significantly stronger than during NREM sleep when only significantly modulated MD cases were considered (−2.49 ± 0.21 vs −1.60 ± 0.11 for MI of ripples during awake state vs NREM sleep, respectively; Wilcoxon signed-rank test, $p = 0.00057$).

Bidirectional modulation of MD activity during sleep ripples

We next examined how MD MUA varied across individual ripples. To this end, for each data set, the ripple times were bootstrapped and the b-MI was computed for 100 randomly selected ripples. Then, the same procedure was repeated 5000 times (for details, see Materials and Methods). This analysis confirmed that MD inhibition accompanied the majority of b-MIs (78.10 ± 0.28%); however, some b-MIs were associated with either enhanced or unchanged MD MUA (0.61 ± 0.02% and 21.29 ± 0.30%, respectively; Fig. 6*A*). Subdividing ripples according to the behavioral state (awake vs sleep) revealed that the b-MIs were mostly negative during awake state, while both positive and negative b-MIs were obtained during NREM sleep (Fig. 6*B*). Specifically, a significant MD suppression was present in 88.39 ± 4.27% of b-MIs during awake state versus 59.79 ± 4.34% of b-MIs during NREM sleep. The MD enhanced activity around ripples was observed in 0.35 ± 0.2% and 1.11 ± 0.7% of b-MIs during awake state and sleep, respectively. The difference in the distribution of

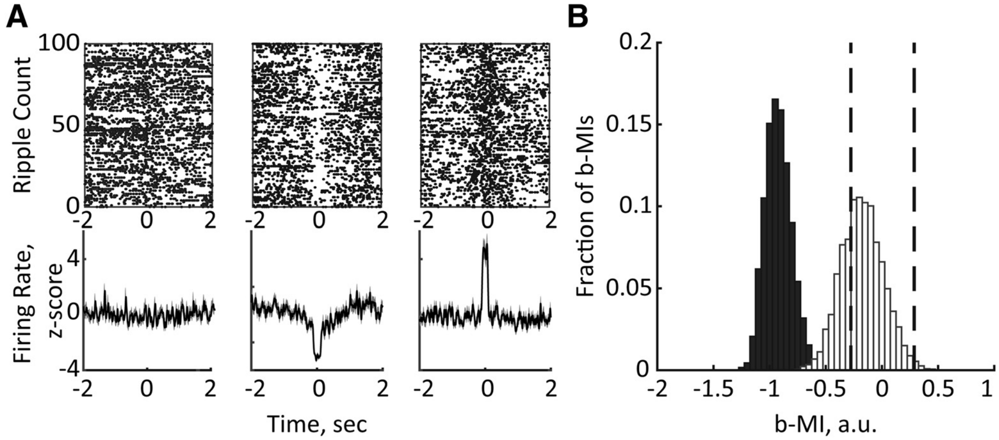

Figure 6. Ripple-associated MD modulation varies across behavioral states. ***A***, Bidirectional changes of MD MUA around ripples. Example raster plots (top) and corresponding averages of *z*-scored MD firing rates (bottom) are plotted around 100 randomly selected ripples. ***B***, Distribution of b-MIs generated by bootstrapping ripples during awake state (black) and NREM sleep (white). The vertical dashed lines mark the lower and upper limits of 95% confidence interval. Note that all b-MIs during awake state are negative, indicating consistent MD suppression, while both negative and positive b-MIs were obtained during NREM sleep.

b-MIs showing decreased, increased, or unmodulated MD MUA was statistically significant ($\chi^2_{(2)} = 1064.99$, $p < 0.0001$). This result is consistent with a stronger MD suppression around awake ripples as revealed by MI.

The MD activity is not suppressed around ripples co-occurring with sleep spindles

Besides fluctuations of neural activity in the HPC and MD thalamus across awake and sleep states, a temporal coupling exists between the hippocampal ripples and sleep spindles, which is thought to enable the hippocampal–cortical information transfer underlying memory consolidation (Siapas and Wilson, 1998; Maingret et al., 2016; Latchoumane et al., 2017). It is also well established that sleep spindles emerge as a result of synchronized interplay within the thalamocortical circuit (Contreras and Steriade, 1997; Llinás and Steriade, 2006). Sleep spindles were detected during NREM sleep episodes as described previously (Novitskaya et al., 2016), and the times of spindle onsets and offsets were extracted. We first split ripples occurring during awake state (34.3 ± 2.1%) from the remaining ripples occurring during NREM sleep, and the latter were further subdivided into spindle-uncoupled (51.8 ± 0.7%) and spindle-coupled (13.9 ± 0.6%) ripples. Figure 7*A–C* shows representative epochs depicting different patterns of ripple/spindle coupling. Ripples occurring during different behavioral/brain states differ by their intrinsic properties. We compared the intraripple frequency and the ripple amplitude among three patterns of event occurrence. The repeated-measures ANOVA revealed a significant effect of the condition for both the intraripple frequency ($F_{(2,\ 181.11)} = 4117.99$, $p < 0.0001$) and the ripple amplitude ($F_{(2,\ 164.57)} = 1119.10$, $p < 0.0001$). The subsequent *post hoc* comparisons (Bonferroni corrected) showed that awake ripples had the highest intraripple frequency and the highest amplitude, while the spindle-coupled ripples had the lowest intraripple frequency and amplitude (Fig. 8). Table 1 summarizes the correlation strength between the ripple amplitude and MI for different subtypes of ripples.

We thus studied whether the ripple-associated MD activity depended on ongoing hippocampal–cortical population dynamics. Remarkably, two distinct patterns of MD MUA were observed during NREM sleep around ripples that were coupled or uncoupled with sleep spindles (Fig. 7*E*,*F*). Specifically, around spindle-uncoupled ripples, the MD was primarily suppressed (85.71%, $n = 42$), whereas no change (24 of 49 cases, 48.98%) or a transient increase (20 of 49 cases, 40.82%) of the firing rate was present around spindle-coupled ripples (Fig. 6*F*). The profile of MD MUA was almost identical around ripple-coupled spindles and around all detected sleep spindles (Fig. 9). Since during NREM sleep the MD suppression was predominant during spindle-uncoupled ripples as it was during awake ripples, we compared the magnitude of MD suppression between these two subsets of ripples. The MD suppression was significantly stronger around awake ripples (mean MI, −2.46 ± 0.20 vs −1.97 ± 0.11 for awake vs spindle-uncoupled sleep ripples, respectively; Wilcoxon signed-rank test, $p = 0.02$).

Discussion

In the present study, we have characterized neural activity in the MD, an associative thalamic nucleus, during epochs of memory replay as indicated by hippocampal ripples (Skelin et al., 2018). Overall, the MD spiking was transiently suppressed around both awake and sleep ripples. Notably, a decrease of MD firing rate systematically preceded the ripple onset. A stronger MD suppression corresponded to the ripples with higher amplitude and ones occurring sparsely (not in clusters). Strikingly, periripple MD modulation was fine-tuned to the thalamocortical activity dynamics such that the MD suppression was observed around ripples occurring outside sleep spindles. In contrast, during spindle-coupled ripples, no MD suppression was present, and in about half of cases, the MD firing was increased. We also characterized the MD activity around other hippocampal oscillatory patterns, namely, the high-gamma episodes and mixed gamma/ripple oscillations. High-gamma oscillations are another prominent pattern of the hippocampal population activity that typically occurs during alert behaviors (Colgin and Moser, 2010), but also during low arousal states including NREM sleep (Csicsvari et al., 1999; Sullivan et al., 2011). We found that the MD suppression was much weaker or absent around high-gamma oscillations. Furthermore, although MD suppression was systematically present around gamma/ripple events, the modulation magnitude was lower than around pure ripples. The latter result is in agreement with existing evidence that although ripples and high-gamma oscillations share similar mechanisms, the network effects of gamma oscillations are more local (Sullivan et al., 2011). Overall, our present study provides new evidence for coordinated activity

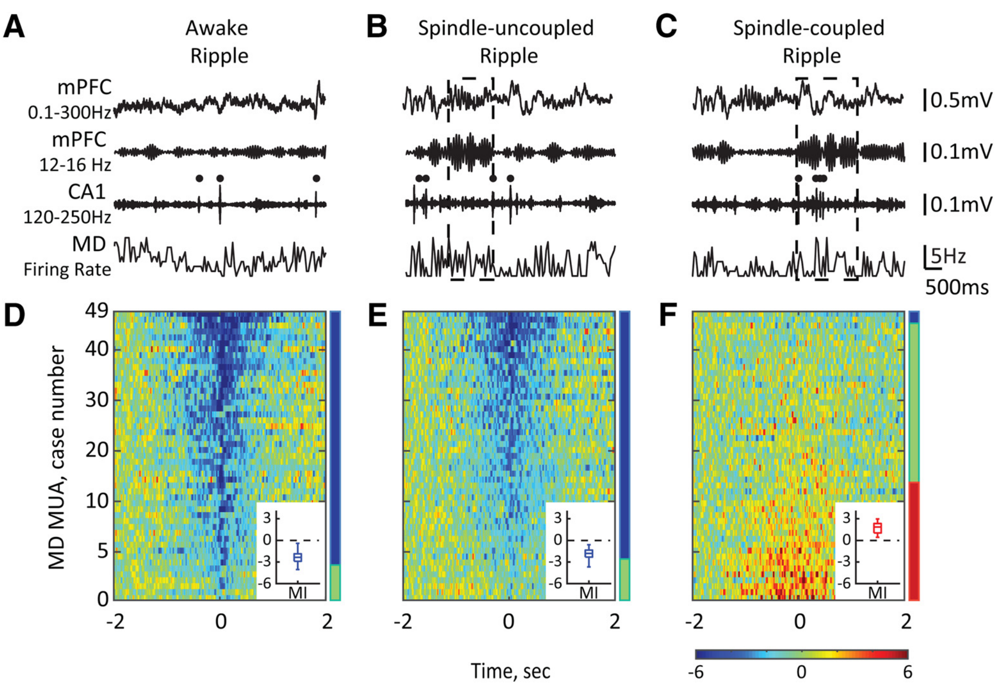

Figure 7. The MD activity is not suppressed around ripples co-occurring with sleep spindles. ***A–C***, Top traces show the broad-band-filtered (0.1–300 Hz) and bandpass-filtered (12–16 Hz) LFPs recorded from the mPFC and the bandpass-filtered (120 –250 Hz) LFPs recorded from the CA1 subfield of the dHPC during awake state (left) and NREM sleep (middle, right). Bottom traces show the corresponding MD firing rates. Black dots mark ripples, dashed-lined rectangles mark sleep spindles. ***D–F***, Normalized firing rates of all MD MUA cases are plotted around ripple onset and sorted according to the MI value. The horizontal color bar shows *z* scores. Vertical color bars show the proportions of MD cases with significant decrease (blue), increase (red), or no change (green) in the firing rate. Insets, Box plots show the MIs distribution across MD MUA cases with significant firing rate modulation. Note that during NREM sleep, ripples may (right) or may not (middle) coincide with sleep spindles, and that periripple MD modulation depends on the ripple/spindle coupling.

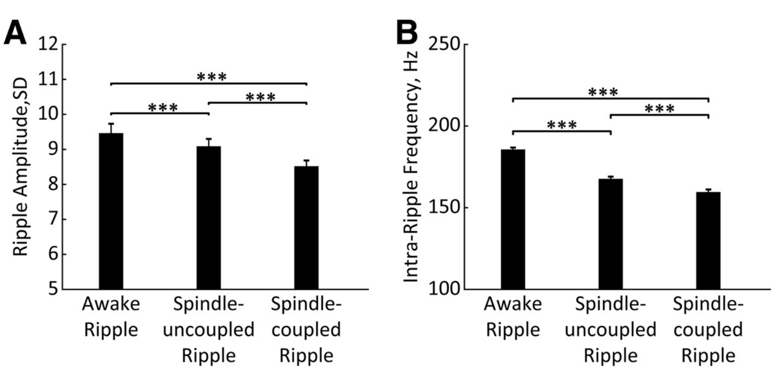

Figure 8. Intrinsic properties of different ripple types. ***A***, ***B***, Bars represent ripple amplitude (***A***) and intraripple frequency (***B***) for awake, spindle-uncoupled, and spindle-coupled ripples. $^{***}p < 0.001$ (Bonferroni corrected). Error bars indicate SE.

Table 1. MI of the MD MUA and MI correlation (*r*) with different subsets of ripples

	First quartile	Second quartile	Third quartile	Fourth quartile	Correlation coefficient
MI, all ripples	-1.11 ± 0.10	-1.57 ± 0.11	-1.80 ± 0.17	-1.81 ± 0.15	$r = -0.28^{***}$
MI, awake ripples	-0.94 ± 0.10	-1.26 ± 0.13	-1.35 ± 0.11	-1.30 ± 0.11	$r = -0.23^{***}$
MI, spindle-uncoupled ripples	-0.93 ± 0.09	-1.30 ± 0.13	-1.20 ± 0.11	-1.20 ± 0.06	$r = -0.12^{*}$
MI, spindle-coupled ripples	0.58 ± 0.10	0.46 ± 0.10	0.41 ± 0.09	0.45 ± 0.05	$r = -0.06$

$^{*}p < 0.05$; $^{***}p < 0.001$.

between the associative thalamus and the dHPC during off-line states and raises further questions about causality of these interactions and the functional significance of the ripple-associated modulation of MD neural activity.

Brain-wide activity pattern associated with hippocampal ripples

By now, it is well established that many cortical regions show coordinated firing with hippocampal population bursts (Sirota et al., 2003; Ji and Wilson, 2007; Peyrache et al., 2009; Wierzynski et al., 2009; Wang and Ikemoto, 2016; Rothschild et al., 2017; Wilber et al., 2017). Inhibition of mPFC neurons was documented around awake ripples (Jadhav et al., 2016). Bidirectional modulation of prefrontal neurons during memory replay is well suited for selectivity of information transfer and triggering synaptic plasticity within memory trace–specific cell assemblies (Peyrache et al., 2011; Jadhav et al., 2016). Ripple-associated neuron firing was also shown in the ventral striatum (Lansink et al., 2008). Both excitatory and inhibitory responses during ripples were observed in the VTA (Gomperts et al., 2015) and BLA neurons (Girardeau et al., 2017). Our previous study combining electrophysiological recordings in the HPC with fMRI-based whole-brain activity mapping provided the first evidence for inverse relationships between thalamic and hippocampal activity during ripples (Logothetis et al., 2012). The ripple-associated spiking suppression was subsequently demonstrated in the lateral geniculate nucleus in nonhuman primates (Logothetis, 2015). Similar findings have been reported previously in rats for the midline thalamus (Lara-Vásquez et al., 2016) and the median raphe nucleus (Wang et al., 2015). Together, these observations reflect a widespread activation/inhibition pattern of brain activity associated with presumed memory replay as indicated by hippocampal ripples. At present, the specificity of such distributed brain activity and its relevance to memory consolidation remains poorly understood.

Bidirectional modulation of ripple-associated thalamic activity

The main finding of the present study is differential engagement of the MD during spindle-coupled versus spindle-uncoupled ripples. The elevated firing rate of MD neurons during spindle-coupled ripples is not surprising. It is well established that sleep spindles emerge due to coordinated interactions within the thalamocortical circuit (Contreras et al., 1996; Steriade, 2006). It has also been demonstrated that ripples tend to occur during periods of enhanced cortical excitability, or up states (Sirota et al., 2003; Battaglia et al., 2004; Mölle et al., 2006), and coincide with sleep spindles (Siapas and Wilson, 1998). In our recordings, about 20% of ripples were temporally coupled with sleep spindles. Expectedly, the MD activity was enhanced during spindles, regardless of whether spindles coincided with ripples or not. A reduced inhibitory input from the limbic-projecting thalamic reticular nucleus (TRN) during sleep spindles (Halassa et al., 2014) is likely the key component regulating this spindle-associated MD activation. On the other hand, one-half of sleep ripples and all awake ripples were not temporally coupled with spindles, and those spindle-uncoupled ripples (~80% of all ripples) were consistently associated with pronounced MD suppression. Thus, we observed a synergistic activity within the thalamic–hippocampal–cortical network during time windows of ripple/spindle coupling, yet a memory-specific relevance of the MD coactivation is currently unknown.

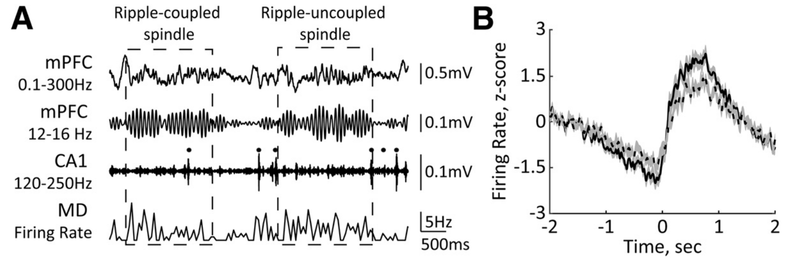

Figure 9. The MD firing rate is elevated around sleep spindles. ***A***, Representative traces of simultaneously recorded neural activity in the mPFC, dHPC-CA1, and MD during NREM sleep. Black dots mark ripples. The dashed rectangles mark ripple-coupled (left) and ripple-uncoupled (right) spindles. ***B***, The MD firing rate is plotted around sleep spindles (solid line) and a subset of ripple-coupled spindles (dashed line). Spindle onset is at $t = 0$. Averages from 42 recording sessions ($n = 8$ rats) are shown; 4409 (43.82%) ripple-coupled spindles were isolated from total of 10,062 detected sleep spindles.

Spindle–ripple coupling has been suggested to be critical for memory consolidation (Diekelmann and Born, 2010). Indeed, an experimentally induced increase of spindle–ripple coupling during postlearning sleep improved memory (Maingret et al., 2016; Latchoumane et al., 2017), while its disturbance impaired memory (Novitskaya et al., 2016). Hippocampal ripples tend to precede sleep spindles (Siapas and Wilson, 1998; Wierzynski et al., 2009; Peyrache et al., 2011); therefore, memory trace reactivation during ripples may trigger synaptic modifications in the cortex during subsequent spindles (Johnson et al., 2010; Timofeev and Chauvette, 2017). It was hypothesized that the hippocampal output during replay may selectively recruit thalamocortical cells into thalamocortical rhythmic interactions reflected as spindles (Peyrache et al., 2011). A strong engagement of cortical inhibition during spindles may permit activation of cortical cell assemblies representing specific memory traces and may therefore reinforce synaptic plasticity within a selective network (Peyrache et al., 2011; Jadhav et al., 2016). The MD coactivation during ripple-spindle coupling may thus facilitate long-range network interactions (Nakajima and Halassa, 2017).

The thalamic suppression during spindle-uncoupled ripples may be favorable for memory processing, as it appears to reduce the thalamocortical relay of sensory information. Indeed, mPFC neurons appear more responsive to hippocampal input during spindle-uncoupled ripples, that is, during periods when the recurrent thalamocortical circuit is not engaged (Peyrache et al., 2011). In this context, a source of MD inhibition presents an interesting question. The ripple-associated MD modulation does not appear to simply reflect global fluctuations of thalamocortical activity that is largely controlled by the TRN (Steriade et al., 1993). Extrathalamic inhibitory control of the thalamic activity is thought to be more selective and therefore more effective for state-dependent gating of thalamocortical information transfer (Bokor et al., 2005; Halassa and Acsády, 2016). For example, cholinergic inputs from the midbrain parabrachial region cause hyperpolarization in the thalamocortical neurons in auditory thalamus (Mooney et al., 2004). Another candidate is the GABAergic input from the zona incerta that selectively targets higher-order thalamic relays (Bokor et al., 2005). The precise temporal dynamics of these interactions would shed light on the neurophysiological mechanisms controlling coordinated activation/deactivation of competing large-scale networks.

The strength of long-range interactions may depend on the behavioral state and cognitive context. For example, a previous study reported differential modulation of activity in the anterior cingulate cortex (ACC) around awake and sleep ripples (Wang and Ikemoto, 2016). Wang and Ikemoto (2016) proposed that the absence of ACC activation during awake ripples may protect freshly acquired information from alteration and, in turn, facilitate intrahippocampal information processing. Furthermore, a type of MD interaction with the hippocampal–cortical network may gate the direction of information transfer. It has been shown that during time windows of spindle–ripple coupling (and MD coactivation), the cortex is less responsive to hippocampal input (Peyrache et al., 2011); therefore, cortical signaling to the HPC may prevail. In turn, during spindle-uncoupled ripples (and MD inhibition), input from the HPC to the cortex is prevalent. Evidence accumulates that awake ripples may additionally support cognitive functions, such as behavioral planning and decision making (Diba and Buzsáki, 2007; Yu and Frank, 2015). Therefore, the MD suppression around awake ripples may also favor memory retrieval from cortex or other nonmnemonic functions requiring cortical–hippocampal interactions. Thus, the functional state of the thalamic–hippocampal–cortical network as well as the content of neural replay and directionality of information transfer may differ during awake, spindle-coupled, and spindle-uncoupled ripples, and these intriguing possibilities shall be further explored.

Possible role of the MD for declarative memory

The anatomical connectivity of the MD supports its involvement in processing and integration of diverse information and mediating it to the mPFC (Mitchell, 2015; Wolff et al., 2015). Consequently, the MD may present a key element within the executive control circuit (Van Der Werf et al., 2003; Ketz et al., 2015), which in the case of declarative memory includes the HPC. Through its connectivity with the hippocampal input and output structures (Groenewegen, 1988; Burwell, 2000), the MD can mediate the bidirectional information flow between the HPC and mPFC (Floresco and Grace, 2003; Peyrache et al., 2011). Consistent with the thalamic control of sensory selection (Saalmann and Kastner, 2011), the MD neuronal populations may coordinate selective engagement of functionally diverse neural circuits in particular oscillatory dynamics (Ketz et al., 2015). Indeed, the MD–PFC synchronization within the β (13–30 Hz) frequency range accompanied performance of a spatial memory task (Parnaudeau et al., 2013). Moreover, the MD inactivation reduced MD–PFC β synchronization and also impaired the task performance (Parnaudeau et al., 2013). Furthermore, sustained activity within the MD–PFC network has been implicated in maintaining information in working memory (Bolkan et al., 2017; Schmitt et al., 2017). Thus, the MD may enhance functional connectivity within a specific brain network (Nakajima and Halassa, 2017).

MD involvement in memory consolidation has been suggested (Squire, 1986; Lee et al., 2011; Tu et al., 2014; Lara-Vásquez et al., 2016), yet this hypothesis requires further experimental validation. The fact that a decrease in MD firing rate systematically preceded the ripple onset suggests that a decreased spiking in the MD may be related to reorganization of the network activity and a shift to a brain state permitting ripple generation, which in turn promotes the hippocampal–cortical communication mediating declarative memory consolidation. Apart from the MD, the midline thalamic nuclei have also been considered to play a role for memory processes (Pereira de Vasconcelos and Cassel, 2015). For example, based on anatomical connectivity, the nucleus reuniens could mediate the prefrontal–hippocampal interactions (Varela et al., 2014). A previous study by Lara-Vásquez et al. (2016) correlated the activity of midline thalamic neurons with different oscillations in the HPC and observed a functional heterogeneity among different cell types. Specifically, calcium-binding protein calretinin (CR)-negative neurons were modulated by theta oscillations, while CR-positive neurons were inhibited during hippocampal ripples. In our study, we sampled a relatively small number of MD single units and did not observe differential modulation. However, heterogeneity of MD responses may be revealed in the future by examining a larger population of MD single units.

The thalamoprefrontal and hippocampal–prefrontal pathways appear to participate in different types of information processing (Ketz et al., 2015; Eichenbaum, 2017), and, therefore, coactivation of these functionally distinct networks may lead to interference. If, indeed, the MD belongs to a competing (e.g., sensory-mediating) network, its activation during ripples would likely interfere with the stabilization of recent memory traces. Thus, a decrease in MD activity may reflect inactivation of a competing network, which would in turn facilitate the hippocampal–cortical communication mediating declarative memory consolidation. Consistent with this view, we showed previously (Novitskaya et al., 2016) that thalamic activation produced by ripple-triggered Locus Coeruleus stimulation impaired consolidation of spatial memory in rats. Our present findings provide evidence that a transient suppression of MD neural activity that precedes hippocampal ripples may possibly play an active role in coordinating activity within large-scale networks involved in different aspects of information processing taking place off-line.

Thus, the activity pattern within a given brain region may reflect its engagement or disengagement within a functionally distinct and distributed network enabling specific types of information processing. Bidirectional modulation of MD activity around ripples was linked to different dynamic states of the thalamic–hippocampal–cortical network differing by topography, the directionality of information transfer, and the brain functions they support. Possibly, spindle-uncoupled ripples combined with thalamic activity suppression presents a brain state that is favorable for memory replay and information transfer from the HPC to the cortex, while the thalamic input at times of hippocampal–cortical communication, indicated by spindle/ripple coupling, may contribute to the neural assembly selection for promoting synaptic plasticity in the cortex. Our present findings open questions about the neurophysiological mechanisms regulating these fine-tuned, thalamic–hippocampal–cortical interactions and their functional significance.

References

Battaglia FP, Sutherland GR, McNaughton BL (2004) Hippocampal sharp wave bursts coincide with neocortical "up-state" transitions. Learn Memory 11:697–704. CrossRef

Bokor H, Frère SG, Eyre MD, Slézia A, Ulbert I, Lüthi A, Acsády L (2005) Selective GABAergic control of higher-order thalamic relays. Neuron 45: 929–940. CrossRef Medline

Bolkan SS, Stujenske JM, Parnaudeau S, Spellman TJ, Rauffenbart C, Abbas AI, Harris AZ, Gordon JA, Kellendonk C (2017) Thalamic projections sustain prefrontal activity during working memory maintenance. Nat Neurosci 20:987–996. CrossRef Medline

Burwell RD (2000) The parahippocampal region: corticocortical connectivity. Ann N Y Acad Sci 911:25–42. Medline

Buzsáki G (1989) Two-stage model of memory trace formation: a role for "noisy" brain states. Neuroscience 31:551–570. CrossRef Medline

Buzsáki G (2004) Large-scale recording of neuronal ensembles. Nat Neurosci 7:446–451. CrossRef Medline

Chrobak JJ, Buzsáki G (1996) High-frequency oscillations in the output networks of the hippocampal-entorhinal axis of the freely behaving rat. J Neurosci 16:3056–3066. CrossRef Medline

Colgin LL, Moser EI (2010) Gamma oscillations in the hippocampus. Physiology 25:319–329. CrossRef Medline

Contreras D, Steriade M (1997) Synchronization of low-frequency rhythms in corticothalamic networks. Neuroscience 76:11–24. Medline

Contreras D, Destexhe A, Sejnowski TJ, Steriade M (1996) Control of spatiotemporal coherence of a thalamic oscillation by corticothalamic feedback. Science 274:771–774. CrossRef Medline

Csicsvari J, Hirase H, Czurkó A, Mamiya A, Buzsáki G (1999) Fast network oscillations in the hippocampal CA1 region of the behaving rat. J Neurosci 19:RC20. CrossRef Medline

Diba K, Buzsáki G (2007) Forward and reverse hippocampal place-cell sequences during ripples. Nat Neurosci 10:1241–1242. CrossRef Medline

Diekelmann S, Born J (2010) The memory function of sleep. Nat Rev 11: 114–126. CrossRef

Eichenbaum H (2017) Prefrontal-hippocampal interactions in episodic memory. Nat Revi 18:547–558. CrossRef

Floresco SB, Grace AA (2003) Gating of hippocampal-evoked activity in prefrontal cortical neurons by inputs from the mediodorsal thalamus and ventral tegmental area. J Neurosci 23:3930–3943. CrossRef Medline

Girardeau G, Inema I, Buzsáki G (2017) Reactivations of emotional memory in the hippocampus-amygdala system during sleep. Nat Neurosci 20:1634–1642. CrossRef Medline

Gomperts SN, Kloosterman F, Wilson MA (2015) VTA neurons coordinate with the hippocampal reactivation of spatial experience. Elife 4:e05360. CrossRef Medline

Groenewegen HJ (1988) Organization of the afferent connections of the mediodorsal thalamic nucleus in the rat, related to the mediodorsal-prefrontal topography. Neuroscience 24:379–431. CrossRef Medline

Halassa MM, Acsády L (2016) Thalamic inhibition: diverse sources, Diverse Scales. Trends Neurosci 39:680–693. CrossRef Medline

Halassa MM, Chen Z, Wimmer RD, Brunetti PM, Zhao S, Zikopoulos B, Wang F, Brown EN, Wilson MA (2014) State-dependent architecture of thalamic reticular subnetworks. Cell 158:808–821. CrossRef Medline

Jadhav SP, Rothschild G, Roumis DK, Frank LM (2016) Coordinated excitation and inhibition of prefrontal ensembles during awake hippocampal sharp-wave ripple events. Neuron 90:113–127. CrossRef Medline

Jay TM, Thierry AM, Wiklund L, Glowinski J (1992) Excitatory amino acid pathway from the hippocampus to the prefrontal cortex. contribution of

AMPA receptors in hippocampo-prefrontal cortex transmission. Eur J Neurosci 4:1285–1295. CrossRef Medline
Ji D, Wilson MA (2007) Coordinated memory replay in the visual cortex and hippocampus during sleep. Nat Neurosci 10:100–107. CrossRef Medline
Johnson LA, Euston DR, Tatsuno M, McNaughton BL (2010) Stored-trace reactivation in rat prefrontal cortex is correlated with down-to-up state fluctuation density. J Neurosci 30:2650–2661. CrossRef Medline
Kapoor V, Krampe E, Klug A, Logothetis NK, Panagiotaropoulos TI (2013) Development of tube tetrodes and a multi-tetrode drive for deep structure electrophysiological recordings in the macaque brain. J Neurosci Methods 216:43–48. CrossRef Medline
Ketz NA, Jensen O, O'Reilly RC (2015) Thalamic pathways underlying prefrontal cortex–medial temporal lobe oscillatory interactions. Trends Neurosci 38:3–12. CrossRef Medline
Lansink CS, Goltstein PM, Lankelma JV, Joosten RN, McNaughton BL, Pennartz CM (2008) Preferential reactivation of motivationally relevant information in the ventral striatum. J Neurosci 28:6372–6382. CrossRef Medline
Lara-Vásquez A, Espinosa N, Durán E, Stockle M, Fuentealba P (2016) Midline thalamic neurons are differentially engaged during hippocampus network oscillations. Sci Rep 6:29807. CrossRef Medline
Latchoumane CV, Ngo HV, Born J, Shin HS (2017) Thalamic spindles promote memory formation during sleep through triple phase-locking of cortical, thalamic, and hippocampal rhythms. Neuron 95:424–435.e6. CrossRef Medline
Lee S, Ahmed T, Lee S, Kim H, Choi S, Kim DS, Kim SJ, Cho J, Shin HS (2011) Bidirectional modulation of fear extinction by mediodorsal thalamic firing in mice. Nat Neurosci 15:308–314. Medline
Llinás RR, Steriade M (2006) Bursting of thalamic neurons and states of vigilance. J Neurophysiol 95:3297–3308. CrossRef Medline
Logothetis NK (2015) Neural-event-triggered fMRI of large-scale neural networks. Curr Opin Neurobiol 31:214–222. CrossRef Medline
Logothetis NK, Eschenko O, Murayama Y, Augath M, Steudel T, Evrard HC, Besserve M, Oeltermann A (2012) Hippocampal-cortical interaction during periods of subcortical silence. Nature 491:547–553. CrossRef Medline
Maingret N, Girardeau G, Todorova R, Goutierre M, Zugaro M (2016) Hippocampo-cortical coupling mediates memory consolidation during sleep. Nat Neurosci 19:959–964. CrossRef Medline
Markowitsch HJ (1982) Thalamic mediodorsal nucleus and memory: a critical evaluation of studies in animals and man. Neurosci Biobehav Rev 6:351–380. CrossRef Medline
Mitchell AS (2015) The mediodorsal thalamus as a higher order thalamic relay nucleus important for learning and decision-making. Neurosci Biobehav Rev 54:76–88. CrossRef Medline
Mölle M, Yeshenko O, Marshall L, Sara SJ, Born J (2006) Hippocampal sharp wave-ripples linked to slow oscillations in rat slow-wave sleep. J Neurophysiol 96:62–70. CrossRef Medline
Mooney DM, Zhang L, Basile C, Senatorov VV, Ngsee J, Omar A, Hu B (2004) Distinct forms of cholinergic modulation in parallel thalamic sensory pathways. Proc Natl Acad Sci U S A 101:320–324. CrossRef Medline
Nakajima M, Halassa MM (2017) Thalamic control of functional cortical connectivity. Curr Opin Neurobiol 44:127–131. CrossRef Medline
Novitskaya Y, Sara SJ, Logothetis NK, Eschenko O (2016) Ripple-triggered stimulation of the locus coeruleus during post-learning sleep disrupts ripple/spindle coupling and impairs memory consolidation. Learn Memory 23:238–248. CrossRef
Parnaudeau S, O'Neill PK, Bolkan SS, Ward RD, Abbas AI, Roth BL, Balsam PD, Gordon JA, Kellendonk C (2013) Inhibition of mediodorsal thalamus disrupts thalamofrontal connectivity and cognition. Neuron 77: 1151–1162. CrossRef Medline
Pereira de Vasconcelos A, Cassel J-C (2015) The nonspecific thalamus: A place in a wedding bed for making memories last? Neuroscience & Biobehavioral Reviews 54:175–196. CrossRef Medline
Peyrache A, Khamassi M, Benchenane K, Wiener SI, Battaglia FP (2009) Replay of rule-learning related neural patterns in the prefrontal cortex during sleep. Nat Neurosci 12:919–926. CrossRef Medline
Peyrache A, Battaglia FP, Destexhe A (2011) Inhibition recruitment in prefrontal cortex during sleep spindles and gating of hippocampal inputs. Proc Natl Acad Sci U S A 108:17207–17212. CrossRef Medline
Ramirez-Villegas JF, Logothetis NK, Besserve M (2015) Diversity of sharp-wave-ripple LFP signatures reveals differentiated brain-wide dynamical events. Proc Natl Acad Sci U S A 112:E6379–E6387. CrossRef Medline
Rothschild G, Eban E, Frank LM (2017) A cortical–hippocampal–cortical loop of information processing during memory consolidation. Nat Neurosci 20:251–259. Medline
Saalmann YB, Kastner S (2011) Cognitive and perceptual functions of the visual thalamus. Neuron 71:209–223. CrossRef Medline
Schmitt LI, Wimmer RD, Nakajima M, Happ M, Mofakham S, Halassa MM (2017) Thalamic amplification of cortical connectivity sustains attentional control. Nature 545:219–223. CrossRef Medline
Selinger JV, Kulagina NV, O'Shaughnessy TJ, Ma W, Pancrazio JJ (2007) Methods for characterizing interspike intervals and identifying bursts in neuronal activity. J Neurosci Methods 162:64–71. CrossRef Medline
Siapas AG, Wilson MA (1998) Coordinated interactions between hippocampal ripples and cortical spindles during slow-wave sleep. Neuron 21:1123–1128. CrossRef Medline
Sirota A, Csicsvari J, Buhl D, Buzsáki G (2003) Communication between neocortex and hippocampus during sleep in rodents. Proc Natl Acad Sci U S A 100:2065–2069. CrossRef Medline
Skelin I, Kilianski S, McNaughton BL (2018) Hippocampal coupling with cortical and subcortical structures in the context of memory consolidation. Neurobiol Learn Memory. Advance online publication. Retrieved April 13, 2018. doi: 10.1016/j.nlm.2018.04.004.
Squire LR (1986) Mechanisms of memory. Science 232:1612–1619. CrossRef Medline
Steriade M (2006) Grouping of brain rhythms in corticothalamic systems. Neuroscience 137:1087–1106. CrossRef Medline
Steriade M, McCormick DA, Sejnowski TJ (1993) Thalamocortical oscillations in the sleeping and aroused brain. Science 262:679–685. CrossRef Medline
Sullivan D, Csicsvari J, Mizuseki K, Montgomery S, Diba K, Buzsáki G (2011) Relationships between hippocampal sharp waves, ripples, and fast gamma oscillation: influence of dentate and entorhinal cortical activity. J Neurosci 31:8605–8616. CrossRef Medline
Timofeev I, Chauvette S (2017) Sleep slow oscillation and plasticity. Curr Opin Neurobiol 44:116–126. CrossRef Medline
Tu S, Miller L, Piguet O, Hornberger M (2014) Accelerated forgetting of contextual details due to focal medio-dorsal thalamic lesion. Front Behav Neurosci 8:320. Medline
Van Der Werf YD, Jolles J, Witter MP, Uylings HBM (2003) Contributions of thalamic nuclei to declarative memory functioning. Cortex 39:1047–1062. CrossRef Medline
Varela C, Kumar S, Yang JY, Wilson MA (2014) Anatomical substrates for direct interactions between hippocampus, medial prefrontal cortex, and the thalamic nucleus reuniens. Brain Struct Funct 219:911–929. CrossRef Medline
Wang DV, Ikemoto S (2016) Coordinated interaction between hippocampal sharp-wave ripples and anterior cingulate unit activity. J Neurosci 36:10663–10672. CrossRef Medline
Wang DV, Yau HJ, Broker CJ, Tsou JH, Bonci A, Ikemoto S (2015) Mesopontine median raphe regulates hippocampal ripple oscillation and memory consolidation. Nat Neurosci 18:728–735. Medline
Wang SH, Morris RG (2010) Hippocampal-neocortical interactions in memory formation, consolidation, and reconsolidation. Annual review of psychology 61:49–79, C1–C4. CrossRef Medline
Wierzynski CM, Lubenov EV, Gu M, Siapas AG (2009) State-dependent spike-timing relationships between hippocampal and prefrontal circuits during sleep. Neuron 61:587–596. CrossRef Medline
Wilber AA, Skelin I, Wu W, McNaughton BL (2017) Laminar organization of encoding and memory reactivation in the parietal cortex. Neuron 95: 1406–1419.e5. CrossRef Medline
Wolff M, Alcaraz F, Marchand AR, Coutureau E (2015) Functional heterogeneity of the limbic thalamus: from hippocampal to cortical functions. Neurosci Biobehav Rev 54:120–130. CrossRef Medline
Ylinen A, Bragin A, Nádasdy Z, Jandó G, Szabó I, Sik A, Buzsáki G (1995) Sharp wave-associated high-frequency oscillation (200 Hz) in the intact hippocampus: network and intracellular mechanisms. J Neurosci 15:30–46. CrossRef Medline
Yu JY, Frank LM (2015) Hippocampal–cortical interaction in decision making. Neurobiol Learn Memory 117:34–41. CrossRef